Classical and Quantum Aspects of Anisotropic Cosmology

Dissertation zur Erlangung des
naturwissenschaftlichen Doktorgrades
der Bayerischen Julius-Maximilians-Universität Würzburg

vorgelegt von

Julian Adamek

aus Würzburg

Würzburg 2011

Eingereicht am: 4. Juli 2011
bei der Fakultät für Physik und Astronomie

1. Gutachter: Prof. Dr. Jens C. Niemeyer[*]
2. Gutachter: Prof. Dr. Haye Hinrichsen
3. Gutachter: —
der Dissertation

1. Prüfer: Prof. Dr. Jens C. Niemeyer[*]
2. Prüfer: Prof. Dr. Haye Hinrichsen
3. Prüfer: Prof. Dr. Thomas Trefzger
im Promotionskolloquium

Tag des Promotionskolloquiums: 27. Oktober 2011

Doktorurkunde ausgehändigt am:

---

[*]seit 2009 an der Georg-August-Universität Göttingen

Classical and Quantum Aspects of Anisotropic Cosmology

Julian Adamek

Preface

This work represents the dissertation which I submit in partial satisfaction of the requirements for the doctoral degree in physics (Dr. rer. nat.) at the University of Würzburg. It is intended to be a comprehensive statement of my research as a doctoral student. As such, it reviews several results which have already been published in [1, 2, 3], but contains additional material as well as a detailed presentation of the context. The following abstract will be given in English and German in order to meet formal requirements.

Abstract The idea that our observable Universe may have originated from a quantum tunneling event out of an eternally inflating false vacuum state is a cornerstone of the multiverse paradigm. Modern theories that are considered as an approach towards the ultraviolet-complete fundamental theory of particles and gravity, such as the various types of string theory, even suggest that a vast *landscape* of different vacuum configurations exists, and that gravitational tunneling is an important mechanism with which the Universe can explore this landscape. The tunneling scenario also presents a unique framework to address the initial conditions of our observable Universe. In particular, it allows to introduce deviations from the cosmological concordance model in a controlled and well-motivated way. These deviations are a central topic of this work.

An important feature in most of the theories mentioned above is the presumed existence of additional space dimensions in excess of the three which we observe in our every-day experience. It was realized that these extra dimensions could avoid our detection if they are compactified to microscopic length scales far beyond the reach of current experiments. There also seem to be natural mechanisms available for dynamical compactification in those theories. These typically lead to a vast landscape of different vacuum configurations which also may differ in the number of macroscopic dimensions, only the total number of dimensions being determined by the theory. Transitions between these vacuum configurations may hence open up new directions which were previously compact, spontaneously compactify some previously macroscopic directions, or otherwise re-arrange the configuration of compact and macroscopic dimensions in a more general way. From within the bubble Universe, such a process may be perceived as an anisotropic background spacetime - intuitively, the dimensions which open up may give rise to preferred directions.

If our $3 + 1$ dimensional observable Universe was born in a process as described above, one may expect to find traces of a preferred direction in cosmological observations. For instance, two directions could be curved like on a sphere, while the third space direction is flat. Using a scenario of gravitational tunneling to fix the initial conditions, I show how the primordial signatures in such an anisotropic Universe can be obtained in principle and work out a particular example in more detail.

A small deviation from isotropy also has phenomenological consequences for the later evolution of the Universe. I discuss the most important effects and show that backreaction can be dynamically important. In particular, under certain conditions, a buildup of anisotropic stress in different components of the cosmic fluid can lead to a dynamical isotropization of the total stress-energy tensor. The mechanism is again demonstrated with the help of a physical example.

Zusammenfassung   Die Vorstellung von einem Multiversum baut unter anderem auf dem Gedanken auf, dass unser beobachtbares Universum in einem Tunnelprozess entstanden sein könnte. Demzufolge hätte es sich dabei von einem ewig währenden, inflationären Vakuumzustand abgekoppelt. Die so entstehende Blase gleicht einer bewohnbaren Insel inmitten eines gewaltigen Ozeans. Moderne Theorien, die als gute Ansätze bezüglich einer fundamentalen und ultraviolett-vollständigen Beschreibung von Elementarteilchen und Gravitation angesehen werden, wie etwa die verschiedenen Ausprägungen der Stringtheorie, legen sogar nahe, dass eine ganze "Landschaft" (im Englischen *landscape*) verschiedener Vakuumzustände existiert, und dass Tunnelprozesse einen wichtigen Mechanismus darstellen, mit dem das Universum die Vielzahl an Möglichkeiten erforschen und realisieren kann. Das Tunnelszenario stellt auch einen einzigartigen Rahmen zur Verfügung, um die Anfangsbedingungen unseres beobachtbaren Universums zu untersuchen. Insbesondere besteht damit die Möglichkeit, geringfügige Abweichungen vom kosmologischen Standardmodell in kontrollierter und gut motivierter Art und Weise zu realisieren. Solche Abweichungen stellen eines der zentralen Themen dieser Arbeit dar.

Eine wichtige Besonderheit der eben erwähnten Theorien ist die Annahme, dass neben den drei uns bekannten Raumdimensionen eine Vielzahl weiterer existieren könnte. Diese Zusatzdimensionen könnten vor uns verborgen sein, wenn sie kompakt sind und nur extrem mikroskopische Ausmaße haben, so dass sie sich weit unterhalb des Auflösungsvermögens heutiger Experimente befinden. Mechanismen, welche eine solche mikroskopische Gestalt dynamisch erklären könnten, sind in den gängigen Theorien auf ganz natürliche Weise verfügbar. Typischerweise ergibt sich daraus das eben gezeichnete Bild einer ausgedehnten "Landschaft" verschiedener Konfigurationen. Die Vakuumzustände können sich nun auch in der Anzahl und Gestalt der mikroskopischen Dimensionen unterscheiden, da nur die Gesamtzahl an Raumdimensionen von der Theorie vorgegeben wird. Übergänge zwischen diesen Zuständen können also dazu führen, dass neue Raumrichtungen entstehen, indem mikroskopische Dimensionen sich plötzlich aufblähen, alte Raumrichtungen verschwinden, indem sie sich spontan ins Mikroskopische zusammenziehen, oder dass die Konfiguration der Raumdimensionen auf eine noch kompliziertere Art und Weise verändert wird. Aus Sicht des neu entstehenden "Universums" in der Blase führt ein solcher Prozess effektiv zu einem anisotropen Hintergrund – vereinfacht ausgedrückt können die neu entstehenden Raumrichtungen eine Vorzugsrichtung ausweisen.

Wenn unser 3+1 dimensionales beobachtbares Universum in einem solchen Prozess entstanden ist, kann man vermuten, dass sich in kosmologischen Beobachtungen Hinweise auf eine Vorzugsrichtung finden lassen müssten. Zum Beispiel könnten zwei Raumrichtungen gekrümmt wie eine Kugeloberfläche sein, während die dritte Richtung keinerlei Krümmung aufweist. Indem ich ein Tunnelszenario benutze, um die Anfangsbedingungen festzulegen, gelingt es mir zu zeigen wie die primordialen Spuren eines solchen anisotropen Universums prinzipiell auszusehen haben und führe eine Berechnung anhand eines speziellen Beispiels explizit vor.

Eine geringfügige Abweichung von Isotropie hat ebenfalls phänomenologische Auswirkungen auf die spätere Entwicklung des Universums. Ich gehe auf die wichtigsten Effekte ein und zeige außerdem, dass Rückkopplung dynamisch relevant sein kann. Insbesondere kann sich unter gewissen Voraussetzungen ein Ungleichgewicht der Druckkräfte in verschiedenen Komponenten der "kosmischen Flüssigkeit" aufbauen, das insgesamt zu einer dynamischen Isotropisierung des kollektiven Energie-Impuls-Tensors führt. Dieser Mechanismus wird ebenfalls anhand eines konkreten Beispiels beleuchtet.

Contents

Notation and Conventions

In this work, manifolds with Lorentzian and Euclidean metric will both appear. On a four-dimensional Lorentzian manifold, the spacetime indices are denoted with Greek letters $\mu, \nu, \ldots$ and take values $0, 1, 2, 3$, where 0 corresponds to the time coordinate. Latin indices from the middle of the alphabet, $i, j, k, \ldots$ take values $1, 2, 3$ only, corresponding to space coordinates. Capital letters from the Latin alphabet are used when the number of dimensions d is arbitrary. Letters from the beginning of the alphabet, $A, B, \ldots$ are used when indices take values $0, 1, \ldots, d-1$, whereas letters from the middle of the alphabet, $I, J, K, \ldots$ are used when indices take values $1, 2, \ldots, d-1$ only. The Lorentzian metric tensor has signature $(-+\ldots+)$.

The indices on a Euclidean manifold are denoted with letters from the beginning of the Latin alphabet, $a, b, \ldots$ and may take values $0, 1, \ldots$. The Euclidean metric tensor has signature $(+\ldots+)$.

If not indicated otherwise, summation over repeated indices is implied (Einstein's summation convention).

Bold face symbols like $\mathbf{k}$ are used to denote elements of $\mathbb{R}^3$. The product of two such quantities should be understood as the usual scalar product. If the same symbol appears in slanted shape instead of bold face, it usually refers to the modulus, $e.g.$, $k = |\mathbf{k}|$.

Units are usually chosen such that $\hbar = c = k_B = G = 1$. Outside of index notation, i is always the imaginary unit.

Quantum states are sometimes denoted with the use of the "bra-ket" notation. The shorthand $\langle Q \rangle \equiv \langle 0|Q|0 \rangle$ denotes the vacuum expectation value of a quantity Q. Furthermore,
$$[A, B] \equiv AB - BA$$
denotes the commutator of A and B.

Chapter 1

Concordance Cosmology – A Success Story

Our current understanding of the Universe is strongly tied to Albert Einstein's theory of gravity, commonly known as General Relativity (GR). In this theory, space and time are no absolute concepts, but are tightly interwoven to yield an inseparable new entity called *spacetime*, conveniently identified with a four-dimensional manifold equipped with a Lorentzian metric which describes its geometry. Einstein's theory of gravity essentially describes how geometry (that is spacetime) and its "material content" (that is particles and fields) mutually depend on one another. The advent of GR gave a whole new perspective on our Universe: what else is our Universe than spacetime and all of its content?

The premise that our Universe does not just exist in some kind of steady-state but is instead highly dynamical was first brought up by Edwin Hubble's groundbreaking observation [4] that all space around us appears to be uniformly expanding. Hubble used a relationship between period and luminosity of Cepheids discovered by Henrietta Swan Leavitt in order to derive the luminosity distance of several galaxies and found that it was related to the redshift of their spectra.

The past decades have brought a wealth of very precise observations about both the geometry of spacetime in which we live and the material it contains. Interpreting these observations in the context of GR so far appears to give a consistent picture which can be boiled down to a *concordance model* of cosmology. This model, called Lambda Cold Dark Matter (ΛCDM) model for reasons that will become apparent, is arguably one of the greatest successes of Einstein's theory.

One of the premier observations in cosmology was the discovery [5] and examination [6, 7] of the Cosmic Microwave Background (CMB). This almost perfectly uniform blackbody radiation at a temperature today of 2.725 K is believed to fill the entire Universe as the afterglow of a very hot and dense state known as the Big Bang, located some 13 billion years to our past. Anisotropies in the CMB are of the order of 10^{-5} only, suggesting that the Universe is (or was) isotropic to a very good approximation. The properties of these tiny anisotropies carry important information about the material content of our Universe as well as about its geometry, and therefore they are still the subject of scrutiny of ongoing campaigns like the European PLANCK mission.

The existence of the CMB supports the idea that our Universe is uniformly expanding under the influence of gravity. Furthermore, the Cosmological Principle is realized in a statistical sense, meaning that the early Universe was homogeneous with only small random fluctuations. This is also supported by the observed distribution of galaxies which, on scales larger than 100 Mpc, appears fairly homogeneous without a sign that the underlying statistical process should break homogeneity or isotropy. It is believed that all the structure we see in the Universe developed from tiny fluctuations in the distribution of material –

fluctuations we can still observe in the CMB – under the influence (mainly) of gravity, and that inhomogeneities and correlations on small scales (below roughly 100 Mpc) are the result of nonlinear structure growth. Observational evidence for homogeneity and isotropy, in the statistical sense, is overwhelming and leaves only little room for possible deviations. However, it should be said that some observations seem to indicate that statistical isotropy and homogeneity may not be an exact symmetry of our Universe. I shall come back to this point in section 1.3 of this chapter.

Observations of the CMB and galaxy distribution are complemented by measurements of luminosity-redshift relations of *standard candles*[1] like Cepheids and Type Ia Supernovae, which can be interpreted in terms of the ΛCDM model in order to reconstruct our recent expansion history. The observation of the abundances of light elements, on the other hand, together with a scenario called *primordial nucleosynthesis* which is well motivated by our knowledge of nuclear physics, can be used to infer the expansion rate shortly after the Big Bang when these elements where produced.

The amazing success of the ΛCDM model is that all these different pieces of evidence seem to fit almost perfectly together under a set of very few simple assumptions. Let me explain the main features of this model. More details, also on the observational foundations of the model, can be found in any contemporary cosmology textbook, for instance [8, 9].

1.1   Basics

The spacetime of the ΛCDM model is a very simple geometry known as the flat Friedmann model. Alexander Friedmann studied geometries with a high degree of symmetry, namely those which can be foliated into *homogeneous and isotropic* spatial hypersurfaces. The term "foliation" refers to a judicious decomposition of the spacetime manifold into spatial submanifolds labeled with a continuous time-analogous parameter. This is not always possible for general spacetimes, and in effect this means that the spacetime manifold is topologically a product $\mathbb{R}_{(\text{time})} \times \Sigma_{(\text{space})}$, a property which is equivalent to *global hyperbolicity*. Physically this means that we are dealing with a situation where the Universe evolves in a causal and predictable manner from some initial conditions which are specified on some spatial hypersurface. If one now imposes an additional symmetry on the spatial submanifolds, namely homogeneity and isotropy, then one arrives at the Friedmann models. As stated above, these symmetries are strongly supported by observational evidence.

The line element on a homogeneous and isotropic spatial submanifold can always be written in a very simple form,

$$g_{ij}dx^i dx^j = \frac{dr^2}{1 - Kr^2} + r^2\left(d\theta^2 + \sin^2\theta d\phi^2\right) \ , \tag{1.1}$$

where the three-metric g_{ij} is defined only up to a total factor because of the invariance under $r \to ar$, $K \to K/a^2$, $g_{ij} \to a^2 g_{ij}$. The only free parameter of this geometry is its constant *scalar curvature*, which is $6K$. If K is positive, the hypersurface locally looks like a three-sphere with curvature radius $K^{-1/2}$ and is called spatially *closed*. If K is negative, the hypersurface is hyperbolic with curvature "radius" $|K|^{-1/2}$ and is called spatially *open*. The case when K is zero corresponds to Euclidean geometry and is therefore called spatially *flat*.

With these simple types of spatial hypersurfaces, the entire four-dimensional metric has only one additional degree of freedom: the metric of eq. (1.1) can be rescaled by a time-dependent *scale factor* $a(t)$. This leads to the familiar Friedmann-Robertson-Walker

---

[1]The term "standard candle" usually refers to an astrophysical object of some kind for which the true luminosity is known and therefore one can infer its distance from its apparent luminosity.

(FRW) line element

$$g_{\mu\nu}dx^\mu dx^\nu = -dt^2 + a^2(t)\left[\frac{dr^2}{1-Kr^2} + r^2\left(d\theta^2 + \sin^2\theta d\phi^2\right)\right] . \qquad (1.2)$$

In this type of spacetime there exists a family of *ideal observers* who remain stationary at constant coordinates (r, θ, ϕ). An ideal observer is a sort of test particle in inertial motion. She travels on a timelike geodesic but her mass is assumed to be negligible such that the geometry of spacetime is not distorted by her presence. Each observer carries her own clock, measuring her individual proper time. Observers who remain stationary in the coordinate frame (r, θ, ϕ) are called *comoving*, and the time coordinate t used in eq. (1.2) is their proper time.

Using the homogeneous and isotropic FRW metric as an *ansatz* for the spacetime geometry, and assuming a distribution of "material" which is, to leading order, likewise homogeneous and isotropic on the spatial hypersurfaces, GR yields a set of evolution equations for the scale factor known as the Friedmann equations. Let me assume for a moment that the material content of the Universe is an ideal fluid (or a mixture of several components behaving as such) which can fully be described by a total (homogeneous) energy density ρ and a total (homogeneous and isotropic) pressure P. The first Friedmann equation relates the expansion rate $H \equiv \partial_t a/a$, also called *Hubble rate*, to the total energy density,

$$H^2 \equiv \left(\frac{\partial_t a}{a}\right)^2 = \frac{8\pi}{3}\rho - \frac{K}{a^2} + \frac{\Lambda}{3} . \qquad (1.3)$$

The new parameter Λ which appears in this equation is Einstein's cosmological constant. It can be interpreted as the energy density of the vacuum, and therefore one sometimes includes it in ρ. Let me keep it for the time being.

The second Friedmann equation relates *acceleration* to the total energy density and pressure,

$$\frac{\partial_t^2 a}{a} = -\frac{4\pi}{3}\left(\rho + 3P\right) + \frac{\Lambda}{3} . \qquad (1.4)$$

These two equations also imply the continuity equation

$$\partial_t \rho = -3H\left(\rho + P\right) , \qquad (1.5)$$

which expresses the conservation of mass-energy.

The system of equations is closed once one adds the equation(s) of state for the fluid(s). Let me make the simplistic assumption that each fluid has a barotropic equation of state of the type

$$P = w\rho , \qquad (1.6)$$

with a constant *barotropic index* w. This simple type of equation covers many important examples, including *dust* (vanishing pressure, $w = 0$), *radiation* (any type of ultra-relativistic particles, $w = 1/3$) and also vacuum energy, which has $w = -1$.

Using eq. (1.6) with eq. (1.5) one can see how the energy density scales with the scale factor:

$$\rho \propto a^{-3(1+w)} . \qquad (1.7)$$

As expected, the energy density of dust scales inversely with the volume, whereas the energy density of radiation decreases with an additional power of the scale factor due to cosmic redshift. Vacuum energy, by definition, does not dilute at all.

Cosmologists commonly use dimensionless *density parameters* instead of physical energy densities. These parameters are obtained by dividing eq. (1.3) by the left-hand side. A fluid X with physical energy density ρ_X has a density parameter Ω_X associated with it, defined as

$$\Omega_X \equiv \frac{8\pi\rho_X}{3H^2} . \qquad (1.8)$$

Equivalently, one defines density parameters for vacuum energy,

$$\Omega_\Lambda \equiv \frac{\Lambda}{3H^2} \ , \tag{1.9}$$

and for curvature,

$$\Omega_K \equiv \frac{K}{a^2 H^2} \ . \tag{1.10}$$

The first Friedmann equation then simply is

$$\sum_X \Omega_X - \Omega_K + \Omega_\Lambda = 1 \ . \tag{1.11}$$

Assuming that we live in a Universe which is, to leading order, well approximated by the Friedmann model, we can interpret observations in order to infer the various parameters of the model. For instance, observation of Cepheids, Type Ia Supernovae and other standard candles with the Hubble Space Telescope [10] gave a fairly accurate measurement of the Hubble rate at which our Universe currently expands. A detailed analysis of the anisotropies in the CMB [7] indicates that our Universe is spatially flat, or nearly flat – the density parameter associated with curvature, Ω_K, is constrained to be of the order of one per cent at most today.

We also have some good observations about the material content of our Universe. The energy density in electromagnetic radiation is dominated by the CMB photons, and is orders of magnitude smaller today than the one of non-relativistic matter. However, since radiation energy density scales with an additional power of the scale factor, it was more important in the past and even dominated the Universe at some early time. From observations of galaxies and clusters we know that most of the non-relativistic matter is not made of atoms or particles we know, but of some "dark" material. The presence of this material reveals itself to us only through its gravitational effect. Galaxies and clusters can be used to trace this dark substance to some extent, and therefore we know something about its abundance and clustering properties. The hypothesis of a non-relativistic (cold), non-interacting (dark) fluid is in good agreement with observational data. This hypothetical fluid, known as *cold dark matter* (CDM), makes up roughly a quarter of the present energy density of our Universe, $\Omega_{CDM} \simeq 0.25$, as data seems to imply [11].

In the recent years, strong evidence was borne out that our Universe is currently accelerating. This is particularly suggested by the luminosity-redshift relation of distant supernovae [12, 13]. The simplest way to achieve this within the Friedmann model is to allow for a positive cosmological constant making up roughly 70% of the energy budget of the Universe today, $\Omega_\Lambda \simeq 0.7$. Cold dark matter and the cosmological constant Λ are the two important ingredients of the ΛCDM concordance model.

The great success of the ΛCDM model is that it is in general agreement with most observed phenomena and is at the same time very simple. However, it has a number of parameters whose values are not explained by the model itself. Most notably, the apparent value of Λ is of the order of 10^{-120}, and it has become one of the greatest challenges of theoretical physics to understand how this number should come about [14]. Some ideas will be discussed in chapter 3.

Several features of the ΛCDM model appear plausible only under an additional assumption, namely that there was a period of *accelerated expansion*, called *inflation*, preceding the Big Bang[2]. In particular, the high degree of flatness (the smallness of Ω_K) and homogeneity, as well as the properties of the CMB anisotropies appear to be a consequence of such a period. The paradigm of cosmic inflation therefore has become one of the hallmark

---

[2]Some authors use the term "Big Bang" when they refer to the beginning of time (if such a thing exists). In this case, of course, it would make no sense to talk about a preceding period. However, throughout this work the term "Big Bang" simply refers to a very hot and dense state of the early Universe. Some people like to use the term "hot Big Bang" in order to distinguish from the other use.

features of the concordance model. Since it is so important, I shall give a short overview of this subject in the following section.

1.2 Inflation

The idea of cosmic inflation was motivated by some obvious problems of the standard Big Bang scenario. From the definition of the curvature parameter, eq. (1.10), it is evident that $|\Omega_K| \propto (\partial_t a)^{-2}$ increases when $\partial_t^2 a < 0$, *i.e.* whenever the Universe decelerates. This was the case for all the time between the Big Bang when radiation was the dominant form of energy in the Universe and the instant when vacuum energy became dominant, which happened only recently in cosmic history. Therefore, since $|\Omega_K|$ is still very small today, one can conclude that it had to be *exponentially small* at the time of the Big Bang. This is known as the *flatness problem*.

Another problem is related to the existence of a *particle horizon*, which is the largest comoving distance which a particle could have traveled since some initial time t_*. This distance can be computed as

$$d_{\mathrm{hor}}(t) \equiv \int_{t_*}^{t} \frac{dt'}{a(t')} \; . \tag{1.12}$$

If one assumes that the initial time t_* lies within the radiation dominated era, for instance at the hot Big Bang, then one can show that the particle horizon at the time of photon last scattering, *i.e.* at the time when the CMB was emitted, is much smaller than the comoving distance the CMB photons have traveled since then. In other words, the region we observe with the CMB is much larger than any region which was in causal contact between t_* and the time of photon last scattering[3]. However, the high degree of isotropy of the CMB suggests that the entire observed region was in causal contact, which raises the question about a t_* which is *earlier* than the hot Big Bang. This is known as the *horizon problem*.

It was realized by Alan Guth that a period of accelerated expansion preceding the Big Bang solves the two problems simultaneously [15]. Firstly, if $\partial_t^2 a > 0$ then $|\Omega_K|$ decreases. Therefore, if accelerated expansion continued for a long enough period, then it is easy to obtain an $|\Omega_K|$ which is exponentially small. One can convince oneself that a long enough period of inflation also allows an arbitrarily large particle horizon.

It is evident from eq. (1.4) that accelerated expansion can only be achieved if the Universe is dominated by a form of energy which makes the right-hand side positive. The simplest solution is a cosmological constant (vacuum energy). However, if the Universe was dominated by the energy density of vacuum, how did the hot and dense state of the Big Bang arise? The only known solution of this problem is to allow the energy density driving inflation to decay into radiation. Therefore, cosmic inflation is assumed to be driven by a form of energy which behaves somewhat similar to vacuum energy, but is in fact some dynamical field and not just a constant.

A simple example for such a form of energy is a homogeneous scalar field which slowly evolves in a potential. For definiteness, let me assume that the scalar field action takes the form

$$\mathcal{S}_\phi = \int d^4 x \sqrt{-g} \left[-\frac{1}{2} \partial^\mu \phi \partial_\mu \phi - V(\phi) \right] \; . \tag{1.13}$$

The homogeneous mode behaves as a perfect fluid source with

$$\rho = \frac{1}{2} (\partial_t \phi)^2 + V(\phi) \; , \tag{1.14}$$

$$P = \frac{1}{2} (\partial_t \phi)^2 - V(\phi) \; . \tag{1.15}$$

---

[3]This is true although any two points which we observe may have been arbitrarily close to each other in physical units at t_*.

Evidently, if $V(\phi)$ is positive and dominates over $\partial_t \phi$ and all other forms of energy, then one obtains accelerated expansion by virtue of eq. (1.4). The condition that $(\partial_t \phi)^2 \ll V(\phi)$ defines the so-called *slow-roll* regime of inflation. There exist many examples of potentials which allow for a slow-roll regime, and one of the aims of cosmological precision observations is to constrain the vast space of inflationary models.

One of the greatest merits of inflation is its ability to "erase" initial conditions. In cosmology, initial conditions are a very tough problem, because it is completely unclear by which principle they are determined. However, once inflation is active, all information becomes dramatically diluted such that a region as large as our observable Universe can deplete to a state of virtual emptiness[4]. This property has become known as the "cosmic no-hair conjecture" [16]. Moreover, perturbations of the energy density (of the scalar field driving inflation) and the geometry are accounted for entirely by *quantum fluctuations*.

Diffeomorphism invariance of GR makes perturbation theory cumbersome because of the gauge freedom. One has to carefully distinguish between gauge variables and physical observables. For instance, perturbations of the scalar field are coupled to the perturbations of the metric. Their combination gives rise to a physical degree of freedom which is associated with a gauge invariant variable ζ, see chapter 6 of [8] for a definition and more details. If one applies a canonical quantization scheme to this variable, one can compute the *power spectrum* of scalar perturbations, which is essentially the Fourier transform of the two-point function of ζ on a spatial hypersurface. It turns out that a typical power spectrum of slow-roll inflation is exactly what is needed in order to explain most of the properties of the observed CMB anisotropies. Not only does cosmic inflation provide a solution to the flatness and horizon problems, it also offers a mechanism to produce the small perturbations in the matter density which are seen in the CMB. These perturbations are needed as seeds for structure formation, and are therefore responsible for essentially everything we see in our Universe.

1.3   Challenges

The merits of inflation should be issued with a caveat. Namely, one is content with the situation only as long as inflation is able to eliminate the dependence on pre-inflationary conditions *perfectly* in the sense that no real experiment can ever detect them. As soon as a measurement would tell us beyond reasonable doubt that, say, $\Omega_K \neq 0$, or homogeneity and isotropy were not exact at the end of inflation in the statistical sense, or that any other property of the Universe is different than expected, then we are again harshly confronted with the issue of initial conditions. The importance of this remark cannot be overstated – every deviation from flatness, homogeneity and isotropy at the end of inflation calls for a theory of initial conditions which explains the departure from the basic assumptions of the ΛCDM model.

Several observations in this direction have already reached out to challenge the concordance model, and more precise measurements with the next generation of experiments may bring firm evidence. For instance, several indications for the breaking of statistical isotropy have been reported, as well as an unexpected lack of correlation of CMB anisotropies on large scales [17, 18, 19]. Yet, the significance of these findings is still subject of debate [20].

If there is still something to learn about the earliest subsistence of our Universe, then it has to be deciphered from such small departures from the ΛCDM cosmology. Therefore, all the hope for deeper insights about the origin of all things rests upon the ability of future experiments to detect and quantify these deviations if they exist. In some later

---

[4]Of course, this does not solve the problem of initial conditions at all because it is not specified why or how inflation started in the first place. However, I will take an agnostic point of view about this issue: there are many possible scenarios for the conditions at the beginning of inflation, but as long as inflation lasted long enough such that all information about these conditions is sufficiently diluted, we will never be able to determine which scenario is correct.

parts of this work I will indulge in this hope and describe some scenarios going beyond the ΛCDM model which make clear predictions about the deviations and could therefore be tested with such data. Also, if it was not for this hope, the search for a theory of initial conditions would merely be an academic enterprise[5].

In the next chapter I will explain a conceptual approach towards the origin of our Universe and introduce the tools which are used in this approach. In chapter 3 I will take a step further and apply these tools in a framework called *landscape*. In particular, I will put forward a scenario where isotropy is broken in our Universe due to a quantum process. Finally, I will discuss some phenomenology of anisotropic spacetime in chapter 4. I will always assume that our Universe is to leading order well described by the ΛCDM cosmology and focus on the signatures of, *e.g.*, a breaking of statistical isotropy at next-to-leading order.

---

[5]One might object that even if there was a long period of inflation, there is some need for a theory of initial conditions that explains it. However, different such theories can not be tested against each other, and therefore I adhere to my agnostic viewpoint.

Chapter 2

Quantum Cosmology

As I have sketched in the last chapter, it seems that today we understand large stretches of the evolution of our Universe well enough to make predictions – or should I say "postdictions" – which are in good agreement with our observations. What remains unexplained so far are some assumptions about the initial conditions. These are tied to the question of how our Universe came into existence (if it has a beginning) or how it was "prepared" into the presumed initial state. Quantum cosmology is a framework of searches for an answer to these questions within the realm of quantum physics. To put it in a nutshell, it means that the entire Universe is considered as a quantum system.

This idea may occur odd at first sight because one is used to apply quantum mechanics only to microscopic systems, and what is less microscopic than the entire Universe? However, it is a well-established premise that also classical systems have an underlying quantum description, their classical appearance only being due to *decoherence*, that is the quantum entanglement with the environment [21]. If one takes this premise seriously, then one is led to the conclusion that even the entire Universe is a quantum system, albeit a very complex and intricate one. Its quantum nature does not reveal itself to us today, but the situation may have been different at some early time when the entire volume we observe today was indeed contained within a microscopic region.

Of course, if one wants to do cosmology, one has to take gravity into the picture. Unfortunately it has proven to be a very hard problem to unify GR and quantum theory to a consistent *theory of quantum gravity*. In order to make some progress, several heuristic approaches have been pursued. For instance, using a Hamiltonian formulation of GR one can apply a canonical quantization scheme to the metric degrees of freedom. Another approach is inspired by the concept of path integral quantization. These approaches are the topic of the forthcoming section 2.1. After having established the basic ideas I will return to the question of initial conditions in section 2.2. A very powerful tool of quantum cosmology will be introduced in section 2.3. Finally, in section 2.4 I will briefly comment about the issue of interpretation in quantum cosmology.

2.1   A Wavefunction of the Universe

In classical GR, the Universe is a spacetime geometry together with a "material" content. The latter is assumed to consist of matter fields – these are for instance the fields of the standard model of particle physics. On laboratory scales, where the geometry can be well approximated by Minkowski spacetime, quantum field theory (QFT) has proven very successful in describing the matter fields. In this framework, the matter degrees of freedom are represented by a wavefunction, and probabilities for, say, the outcomes of an experiment, are related to the amplitudes of the branches of the wavefunction on the corresponding configurations. Quantum cosmology tries to incorporate the geometry into

this picture, putting the metric field on equal footing with matter fields. The Universe hence can be described by a wavefunction which simultaneously represents the degrees of freedom of both matter and geometry.

In order to find the governing equation of this wavefunction of the Universe, I will apply the successful techniques of conventional QFT in the most straightforward way to GR. This approach has been pioneered by Bryce DeWitt [22] and can be found in many textbook reviews (see, *e.g.*, [23] for a recent one).

2.1.1   The Hamiltonian Approach

The quantization of a Hamiltonian system is a standard exercise of quantum mechanics. The canonical prescription says that the generalized coordinates and momenta have to be promoted to operators which fulfill certain equal-time commutation relations. In order to apply this canonical quantization scheme to GR, one first has to find a Hamiltonian description. A suitable starting point is the Einstein-Hilbert action

$$\mathcal{S}_{\text{grav}} = \frac{1}{16\pi} \int d^4x \sqrt{-g}\, [\mathcal{R} - 2\Lambda] \ , \tag{2.1}$$

where $\mathcal{R}$ is the (Ricci) curvature scalar associated to the metric field. In order to Legendre-transform the Einstein-Hilbert Lagrangean to obtain a Hamiltonian, it it necessary to introduce a time coordinate explicitly. This can be done by employing a foliation of space-time. I have shown in section 1.1 how this can be done in a Friedmann model. The most general way of decomposing a spacetime into spatial hypersurfaces is known as the "ADM decomposition" (after Richard Arnowitt, Stanley Deser and Charles Misner [24]). The line element is rewritten as

$$ds^2 = g_{\mu\nu}dx^\mu dx^\nu = -N^2 dt^2 + h_{ij}\left(dx^i + N^i dt\right)\left(dx^j + N^j dt\right) \ , \tag{2.2}$$

where h_{ij} is the metric field on a three-dimensional spatial hypersurface, and the fields N and N^j are called the *lapse function* and *shift vector*, respectively. The metric h_{ij} contains the information on the geometry of the hypersurface, while the lapse and shift determine how the hypersurfaces are stacked together. A detailed account of this type of decomposition can be found in many textbooks, see [25] for a pedagogical one.
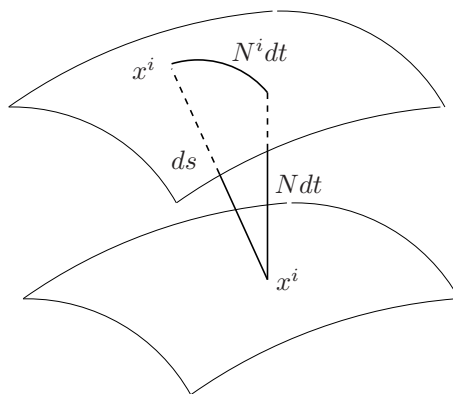

Figure 2.1: A foliation of spacetime in terms of the ADM decomposition.

In these variables, the four-dimensional curvature $\mathcal{R}$ is

$$\mathcal{R} = {}^3\mathcal{R} + K_{ij}K^{ij} - \left(K_i^i\right)^2 \ , \tag{2.3}$$

where $^3\mathcal{R}$ is the three-curvature associated with the metric h_{ij}, and K_{ij} is the *extrinsic curvature tensor* of the spatial submanifold. The extrinsic curvature describes how the hypersurface is embedded into the four-dimensional spacetime. It is defined by

$$K_{ij} \equiv \frac{1}{2N} \left(\partial_t h_{ij} - \nabla_i N_j - \nabla_j N_i \right) , \tag{2.4}$$

where ∇_i denotes *covariant differentiation* with respect to the spatial metric h_{ij}.

The Einstein-Hilbert Lagrangean now reads

$$\mathcal{L}_{\text{grav}} = \frac{N\sqrt{h}}{16\pi} \left[^3\mathcal{R} + K_{ij}K^{ij} - \left(K_i^i \right)^2 - 2\Lambda \right] . \tag{2.5}$$

The ADM variables h_{ij}, N_i, N are the generalized coordinates which carry the geometric degrees of freedom. The corresponding generalized canonical momenta are therefore defined as

$$p \equiv \frac{\delta \mathcal{L}_{\text{grav}}}{\delta \partial_t N} = 0 , \tag{2.6}$$

$$p^i \equiv \frac{\delta \mathcal{L}_{\text{grav}}}{\delta \partial_t N_i} = 0 , \tag{2.7}$$

$$p^{ij} \equiv \frac{\delta \mathcal{L}_{\text{grav}}}{\delta \partial_t h_{ij}} = \frac{\sqrt{h}}{16\pi} \left(K^{ij} - K_k^k h^{ij} \right) . \tag{2.8}$$

The vanishing of the first two lines occurs because the lapse and shift are only Lagrange multipliers. This means that they are not really dynamical degrees of freedom, but they give rise to constraints. The important implications of this fact will become apparent shortly.

The Hamiltonian is obtained from the Einstein-Hilbert Lagrangean by Legendre transform:

$$\begin{aligned} \mathcal{H}_{\text{grav}} &= p^{ij}\partial_t h_{ij} - \mathcal{L}_{\text{grav}} \\ &= N\sqrt{h} \left[16\pi p_{ij}p^{ij} - 16\pi \left(p_i^i \right)^2 - \frac{1}{16\pi} \left(^3\mathcal{R} - 2\Lambda \right) \right] - 2N_i \nabla_j p^{ij} \end{aligned} \tag{2.9}$$

The primary constraints (2.6) and (2.7), together with the Hamiltonian equations of motion, lead to the secondary constraints

$$0 = \partial_t p = \frac{\delta \mathcal{H}_{\text{grav}}}{\delta N} = \sqrt{h} \left[16\pi p_{ij}p^{ij} - 16\pi \left(p_i^i \right)^2 - \frac{1}{16\pi} \left(^3\mathcal{R} - 2\Lambda \right) \right] \equiv \mathcal{H}_\perp , \tag{2.10}$$

$$0 = \partial_t p^i = \frac{\delta \mathcal{H}_{\text{grav}}}{\delta N_i} = -2\nabla_j p^{ij} \equiv \mathcal{H}^i , \tag{2.11}$$

which are called the *Hamiltonian constraint* and *momentum constraint*, respectively. If matter fields are present, the constraints acquire extra terms. For instance, a matter source with stress-energy tensor $T_{\mu\nu}$ enters the Hamiltonian constraint as

$$\mathcal{H}_\perp = \sqrt{h} \left[16\pi p_{ij}p^{ij} - 16\pi \left(p_i^i \right)^2 - \frac{1}{16\pi} \left(^3\mathcal{R} - 2\Lambda \right) + \rho \right] = 0 , \tag{2.12}$$

where $\rho \equiv T_{\mu\nu}n^\mu n^\nu$ is the component of the stress-energy tensor that projects onto the timelike unit normal n^μ of the hypersurface.

The canonical quantization prescription is that the Hamiltonian (which is a constraint in this case) is promoted to an operator that acts on the wavefunction. To this end, all canonical momenta are replaced by derivative operators,

$$p^{ij} \rightarrow -i\frac{\delta}{\delta h_{ij}} , \tag{2.13}$$

and similarly for the momenta which appear in the matter part. However, there is no unique way of performing this replacement. While in the original Hamiltonian the factor ordering of products of coordinates and canonical momenta was unimportant, this is no longer the case once the momenta are operators which do not commute with the coordinates. This leaves one with the infamous *operator ordering ambiguity*. The correct factor ordering can only be determined by comparison with experiments – an option one does not have in quantum cosmology (see also section 2.4). However, all the calculations presented later in this work are carried out in the *semiclassical approximation*. This means that, although quantum effects like tunneling are considered, they are treated only to leading order in $\hbar$ (this statement will be made more precise later). Fortunately, the operator ordering affects the results only at subleading order and can therefore be chosen arbitrary for the purposes of all semiclassical calculations.

After the canonical quantization scheme has been applied, one arrives at the Wheeler-DeWitt equation:

$$\hat{\mathcal{H}}_\perp \left[h_{ij}, \frac{\delta}{\delta h_{ij}}, \ldots \right] \Psi \left[h_{ij}, \ldots \right] = 0 \qquad (2.14)$$

The ellipsis stands for matter variables.

The Wheeler-DeWitt equation has several peculiarities. The most striking feature is the absence of time – the state of the Universe does not evolve at all. This, of course, reflects the fact that there obviously is no external time parameter, but time is a concept which is contained in the Universe as well. In order to recover a notion of time, one has to introduce a *physical clock*, which is a collection of matter degrees of freedom. One can then study the wavefunction as a function of the corresponding matter variables. This means, however, that time remains an approximate concept, which emerges only on semiclassical configurations when a physical clock can be sensibly defined. On configurations outside of a semiclassical regime there exists no notion of time whatsoever.

The Wheeler-DeWitt equation is a condition on *physical states*: all states that are physically viable give zero when the constraint operator is acted on their wavefunction. This does, however, not single out a particular state. In fact, there are still infinitely many possible states for our Universe which are physically viable.

Note that the Wheeler-DeWitt equation is usually understood as the quantized version of the Hamiltonian constraint. The momentum constraint gives another condition on physical states, namely it guarantees diffeomorphism invariance on the three-geometry[1]. Loosely speaking, the Hamiltonian constraint (or the Wheeler-DeWitt equation) states that the time parameter chosen in the ADM decomposition has no physical significance, while the momentum constraint makes a similar statement about the coordinates on the hypersurface. In order to recover a notion of position, one has again to introduce a physical device which is constructed out of matter degrees of freedom. Positions of physical entities are therefore defined only relative to each other, and again only in an approximate sense.

It is also noteworthy that the wavefunction is a function on the space of all possible configurations of matter *and* three-geometry. This configuration space is called *superspace*. However, it is generally impracticable to work with the full superspace: the full description of arbitrary configurations contains far too many degrees of freedom. In order to handle this problem, one usually works with a drastically truncated version of superspace (often called *minisuperspace*) which contains only configurations with a high degree of symmetry. For instance, a first cosmological application would be to consider only homogeneous and isotropic configurations. The description of highly symmetric configurations requires only few degrees of freedom. This way of making the problem tractable is therefore called *symmetry reduction*. The imposed symmetry depends on the particular aspects one wants to study.

---

[1] In order to find physical states one often makes an ansatz which incorporates diffeomorphism invariance by construction. Then one only has to care about solving the Wheeler-DeWitt equation.

In order to fix the wavefunction, *i.e.* the state of the Universe, one has to specify boundary conditions on the boundaries of (reduced) configuration space. Unfortunately, it is far from being clear which boundary conditions should be formulated. It is not even sure if this question can be answered one day, because there may be no experiments to test different hypotheses. The hope is, however, that different hypotheses make different predictions for our observations, such that some hypothesis may appear more plausible than another in the face of observational data. For instance, it has been attempted to predict the probability of inflation lasting long enough to solve the flatness and horizon problems based on different assumptions about boundary conditions in quantum cosmology (see [26] for a review). A special prescription of boundary conditions which is motivated from a path-integral approach will be the subject of the forthcoming section.

2.1.2   The No-Boundary Proposal of Hartle and Hawking

Almost three decades ago, James Hartle and Stephen Hawking proposed a wavefunction of the Universe based on a construction of the *ground state*, that is the state of minimum excitation [27]. Their construction based heavily on the ideas of path-integral quantization [28]. Without going into the technical details and the issues concerning a rigorous definition, the ground state wavefunction of Hartle and Hawking can formally be represented as

$$\Psi_{\text{NB}}\left[h_{ij}, \chi_N\right] \propto \int \mathcal{D}g_{ab}\mathcal{D}\phi_N e^{-\mathcal{S}_{\text{E}}[g_{ab},\phi_N]} \ . \tag{2.15}$$

This expression needs some explanation. The symbols χ_N and ϕ_N denote configurations of all matter fields, N being a label that enumerates the fields and not a spacetime index. The configurations occurring as argument in the wavefunction, χ_N, are specified on the three-dimensional hypersurface only, while the configurations ϕ_N live on a four-dimensional geometry. The path-integral on the right-hand side is a sum over all regular four-dimensional compact geometries with a single compact three-dimensional boundary and over all possible regular configurations ϕ_N on them with the condition that the induced metric on the boundary matches h_{ij} and the restriction of ϕ_N to the boundary matches χ_N. The sum is weighted by the exponential of the Euclidean action $\mathcal{S}_{\text{E}}$ of the four-dimensional geometry and matter configuration, see section 2.3.3 for a definition. Since the path-integral contains only geometries with just one boundary, specified by the argument of the wavefunction, and therefore without any "initial" boundary, this state has become known as the *no-boundary state* (hence the subscript "NB" on the left-hand side).

Note that the three-dimensional geometry in the argument of the wavefunction is supposed to be compact. The no-boundary state therefore only admits a closed Universe. This is not a very restrictive assumption once inflation is presumed to take place. It is even possible that the emergent semiclassical spacetime admits both closed and open slicings, and the observed curvature depends on the class of observers one chooses.

The no-boundary wavefunction fulfills both the Wheeler-DeWitt equation and the momentum constraint by construction. It is interesting how the concept of classical spacetime emerges. Classical configurations (those which are consistent with the classical equations of motion) extremize the action and therefore constitute saddlepoints appropriate for approximating the path-integral with the method of steepest descent. Note that the path-integral is formulated in a completely Euclidean way. The Lorentzian nature of semiclassical spacetime is obtained if the saddlepoints are complex [29] – in this case they occur as complex conjugate pairs such that the wavefunction remains real.

The method of steepest descent is a powerful device for obtaining semiclassical approximations of the wavefunction. Some applications of this method will be illustrated in the forthcoming sections. I will leave the presentation of the no-boundary proposal at that superficial level and carry on with a central topic of this work, the quantum mechanical decay of a metastable vacuum configuration. A detailed account of the no-boundary proposal can be found in the literature (see, *e.g.*, [30] for a recent review).

2.2 False Vacuum Decay

The scalar field example presented in section 1.2 illustrates that potential energy can effectively act like a contribution to the cosmological constant. Potentials may appear in the Lagrangean description of a fundamental theory, but more importantly, they are ubiquitous in low-energy *effective* field theory – they typically arise as the result of integrating out some high-energy degrees of freedom. Understood as a function in field space, a potential may have a very complicated structure. In particular, it may have local minima and saddle points. Any local minimum corresponds to a classical ground state configuration of fields. In general, the fields tend to evolve towards these configurations.

Since the potential energy at the minimum acts like vacuum energy, it can drive cosmic inflation. This means that, once the fields in a region of the Universe approach a minimum in such a way that the potential energy comes to dominate, the region inflates and – as a consequence – supercools into the *vacuum configuration* corresponding to the local minimum of the potential. If several local minima exist for a potential, there are correspondingly many different vacuum configurations. The notion of vacuum therefore is not unique, and what is more important, different vacua can have different vacuum energies as a result of the respective contributions from the potential.

It may happen that the effective vacuum energy density at a minimum is negative. In this case, instead of driving cosmic inflation, gravity acts such that the region which contains the negative energy vacuum collapses. Classically, the region encounters a so-called *Big Crunch* singularity. From the viewpoint of quantum cosmology, there will probably be no singularity (the wavefunction remains well-behaved), but the classical description of the configuration will break down. At any rate, the region will become a bad place for physical observations, since the very notion of observation is defined only in a classical sense. Therefore, throughout this section, I will only consider vacuum configurations with non-negative effective vacuum energies.

Classically, once the fields have settled to a minimum, they remain trapped at this configuration forever. However, true quantum fields always fluctuate around the vacuum configuration. Therefore, if the potential has other minima, the configuration is rendered metastable due to the possibility that the fields tunnel through the potential barrier to another minimum. The mechanics of this process, which is called *false vacuum decay*, is the main subject of this section. Although being extremely rare, it is believed that this process is very important, because it allows the Universe to explore the potential and hence to populate all possible vacuum configurations. The dominant decay channel, which I will discuss in much detail in the following, is the spontaneous nucleation of bubbles containing a new and energetically favored phase like in a first-order phase transition. This process has been extensively studied in the literature. The subject was pioneered by Sidney Coleman and collaborators [31, 32, 33]. The inverse process of vacuum decay, which is the population of an energetically disfavored configuration from a lower-lying initial vacuum, was described in [34]. For an overview of the cosmological applications of vacuum transitions, see for instance [35].

The properties of the vacuum inside a bubble are drastically different from the outside, such that one generally speaks of a new-born bubble-*universe*. It is indeed conceivable that our entire observable Universe is contained within such a bubble. Adopting it as a new premise that this is the case leads to new exciting consequences. First of all, by arranging a long enough period of additional inflation taking place inside the bubble, one can always come to agreement with the ΛCDM concordance model up to arbitrary precision. A finite amount of inflation will lead to finite deviations from the concordance model. However, these deviations are not random, but depend on "initial conditions" which are determined by the scenario of false vacuum decay. Therefore, the scenario offers a well-motivated and elegant possibility to introduce deviations from the ΛCDM concordance model in a *controlled way*. This aspect makes the study of false vacuum decay particularly interesting.

2.2.1   Bubble Nucleation on Minkowski Background

In order to give a first intuitive picture of the vacuum decay process, let me set aside gravitational effects for a moment and discuss the problem in the familiar arena of Minkowski space. This is a good approximation if the relevant length scales are small compared to the curvature scale of spacetime, and if all energy densities are likewise small. I will relax these assumptions in the forthcoming sections.

I consider a scenario where the fields have supercooled into a metastable phase, corresponding to a local minimum in field space of the effective potential. The effective potential is assumed to have another local minimum with a lower value of vacuum energy. The present configuration of the fields is therefore called a *false* vacuum, while the configuration corresponding to the lower minimum is called the *true* vacuum. This is just for definiteness – in fact, the lower minimum does not have to be a global minimum of the potential, and there may be other, even lower minima. The terms "false" and "true" vacuum are just used to distinguish between the two configurations which are involved in the particular process under consideration.

The decay of the false vacuum to the true one proceeds as follows. The fields in the false vacuum configuration are subject to quantum fluctuations. By chance, these fluctuations can take the fields in some region of space across the potential barrier to a configuration which is close to the true vacuum. On the boundary of the region, the fields have to connect to the false vacuum configuration and therefore have to spend some parts beneath the barrier. However, since the true vacuum is energetically favored, just by making the region large enough, one can arrange that enough energy becomes available to balance the costs of this boundary layer, such that the virtual quantum fluctuation can become real and classical. It is also intuitively clear that fluctuations of small regions occur with much larger probability than those of large regions. As a consequence, the spontaneous nucleation of true vacuum domains predominantly produces spherical domains, so-called *bubbles*, because these have the optimal proportion between surface and volume.

In fact, the probability of aspherical nucleation is suppressed so dramatically that it is an extremely good approximation to assume that false vacuum decay proceeds *entirely* by nucleation of spherical bubbles, the next-to-leading order being only tiny perturbations about sphericity. The problem can hence be simplified a lot by symmetry reduction: imposing spherical symmetry turns the $3 + 1$ dimensional setup into a $1 + 1$ dimensional one. I will therefore use spherical coordinates of Minkowski space,

$$ds^2 = \eta_{\mu\nu}dx^\mu dx^\nu = -dt^2 + dr^2 + r^2 d\Omega^2 \ , \tag{2.16}$$

and assume that the bubble is centered at the origin $r = 0$.

Let me denote a field configuration with the symbol ϕ, and let ϕ_+, ϕ_- be the configurations at the false and true vacuum, respectively. Furthermore, let me denote the effective potential as $V(\phi)$. The difference on the potential energy of the two phases gives rise to a "latent heat" ϵ,

$$\epsilon = V(\phi_+) - V(\phi_-) \ . \tag{2.17}$$

I will assume that ϵ is a small parameter.

A bubble of true vacuum is circumscribed by a boundary layer in which the field configuration interpolates between ϕ_- and ϕ_+. Since this interpolation runs beneath the potential barrier which separates the two local minima of the potential, the surface layer is characterized by a surface energy density, or "surface tension" σ. Up to corrections of order ϵ, it is given by the integral expression

$$\sigma = \int_{\phi_-}^{\phi_+} d\phi \sqrt{2\left(V(\phi) - V(\phi_+)\right)} \ , \tag{2.18}$$

where the integration path follows the trajectory of "least resistance," *i.e.* the field configuration changes in such a way that a minimum amount of energy has to be spent.

If one assumes that the boundary layer is of negligible thickness, the problem of bubble nucleation can be described with a single degree of freedom: the radial position of the boundary layer. This additional simplification is known as the *thin-wall approximation.*

A justification of eq. (2.18) can be sketched as follows. Consider a scalar field action of the type given in eq. (1.13). In the thin-wall approximation, the contribution from the surface layer comes from a region localized around the *worldsheet* of the bubble wall. Choosing local normal coordinates with a spacelike direction n orthogonal to the worldsheet, the contribution from the bubble wall can be written as

$$\mathcal{S}_{\text{wall}} = \int_{\text{wall}} d^4x \left[-\frac{1}{2} \partial^\mu \phi \partial_\mu \phi - V(\phi) \right] \simeq A_{\text{wall}} \int_{n_-}^{n_+} dn \left[-\frac{1}{2} (\partial_n \phi)^2 - V(\phi) \right] , \qquad (2.19)$$

where A_{wall} is the volume of the worldsheet, and n is integrated over the infinitesimal thickness of the wall, n_- and n_+ being the endpoints of integration on the true and false vacuum side, respectively. Variation of the action gives an equation for $\phi(n)$,

$$\partial_n^2 \phi = \partial_\phi V , \qquad (2.20)$$

which is equivalent to

$$\partial_n \left[\frac{1}{2} (\partial_n \phi)^2 - V(\phi) \right] = 0 . \qquad (2.21)$$

With the boundary condition that ϕ matches ϕ_+ at spatial infinity, this can be directly integrated to yield

$$\frac{1}{2} (\partial_n \phi)^2 = V(\phi) - V(\phi_+) . \qquad (2.22)$$

Inserting back into eq. (2.19) and changing the integration variable, one finds

$$\int_{n_-}^{n_+} dn \left[-\frac{1}{2} (\partial_n \phi)^2 - V(\phi) \right] = \int_{\phi_-}^{\phi_+} d\phi \sqrt{2 \left(V(\phi) - V(\phi_+) \right)} - \left(n_+ - n_- \right) V(\phi_+) . \quad (2.23)$$

In the thin-wall approximation, however, the last term can be dropped, and one arrives at the expression (2.18).

When the thin-wall approximation applies, the properties of the scalar potential are entirely encoded in the two parameters ϵ and σ. One can now write down an effective action that contains only a single degree of freedom, the position $r(t)$ of the bubble wall:

$$\mathcal{S}_{\text{eff}} = \int dt \left[\frac{4\pi}{3} \epsilon r^3(t) - 4\pi \sigma r^2(t) \sqrt{1 - (\partial_t r)^2} \right] . \qquad (2.24)$$

The square root arises from the timelike line element on the worldsheet of the bubble wall, $-d\tau^2 = -dt^2 + dr^2 \Rightarrow d\tau = dt \sqrt{1 - (dr/dt)^2}$.

As a first step, I will examine the classical system. Introducing $p \equiv \partial \mathcal{L}_{\text{eff}} / \partial \partial_t r$, the canonical momentum conjugate to r, a classical Hamiltonian of the system is given by

$$\mathcal{H}(r, p) = p \partial_t r - \mathcal{L}_{\text{eff}} = \sqrt{p^2 + 16\pi^2 \sigma^2 r^4} - \frac{4\pi}{3} \epsilon r^3 . \qquad (2.25)$$

The false vacuum configuration corresponds to the solution $p = r = 0$, which means that there is no bubble. For this configuration, the total energy of the system is zero. Squaring the zero-energy equation yields

$$p^2 + 16\pi^2 \sigma^2 r^4 - \frac{16\pi^2}{9} \epsilon^2 r^6 = 0 , \qquad (2.26)$$

which is the equation of a particle of unit mass moving in the potential

$$U(r) = 8\pi^2 \sigma^2 r^4 - \frac{8\pi^2}{9} \epsilon^2 r^6 . \qquad (2.27)$$

Apart from the solution $p = r = 0$, there obviously exists a second solution with zero total energy where the particle approaches from infinity until it reaches the point $r = 3\sigma/\epsilon$, where it is reflected at the potential barrier and subsequently recedes to infinity again.

Quantum mechanically, the two solutions can be connected by a tunneling process in which the particle spontaneously relocates itself to the other side of the barrier[2] which separates the two classical trajectories.

In order to estimate the tunneling rate, recall that the wavefunction of a point particle under a potential barrier, in the WKB approximation, behaves roughly as

$$\psi_{\text{WKB}}(r) \sim e^{-\int^r \sqrt{2U(r')}dr'} \ . \tag{2.28}$$

Although this treatment is not seriously justified since I have not quantized the system yet, integrating across the barrier from $r = 0$ to $r = 3\sigma/\epsilon \equiv r_0$ and comparing the squared WKB amplitudes yields a *tunneling rate* of

$$\Gamma \simeq \frac{|\psi_{\text{WKB}}(r_0)|^2}{|\psi_{\text{WKB}}(0)|^2} \simeq e^{-27\pi^2\sigma^4/2\epsilon^3} \ . \tag{2.29}$$

Despite this very crude derivation, this final result coincides with the one which is obtained in a rigorous calculation, as will be shown in later sections.

2.2.2   Constructing the Wavefunction in Thin-Wall Approximation

A difficulty arises when one wants to quantize the system because of the appearance of a square root in the action integral, see eq. (2.24), which reappears also in the Hamiltonian, eq. (2.25). In order to deal with this problem, I will follow an approach which is widely used in string models and reparametrize the worldline of the wall position. For a modern textbook introduction on this technique, see for instance chapter 2.1 of [36]. To my knowledge, it has not been applied to the problem of bubble nucleation in this way before. Let me first rewrite eq. (2.24) such that it is explicitly invariant under time reparametrizations:

$$\mathcal{S}_{\text{eff}} = \int d\lambda \left[\frac{4\pi}{3}\epsilon r^3 \partial_\lambda t - 4\pi\sigma r^2 \sqrt{(\partial_\lambda t)^2 - (\partial_\lambda r)^2} \right] \ . \tag{2.30}$$

The worldline (r, t) of the bubble wall is now parametrized by an arbitrary parametrization λ. Now, in order to avoid the square root, one may replace the action equivalently by

$$\mathcal{S}_{\text{eff}} = \int d\lambda \left[\frac{4\pi}{3}\epsilon r^3 \partial_\lambda t + 2\pi\sigma r^2 \left(\frac{(\partial_\lambda r)^2 - (\partial_\lambda t)^2}{\nu} - \nu \right) \right] \ . \tag{2.31}$$

On the classical level, this action is completely equivalent to (2.24) or (2.30). This can be seen by solving the Euler-Lagrange equation of ν, which yields $\nu = \sqrt{(\partial_\lambda t)^2 - (\partial_\lambda r)^2}$, and inserting this back into eq. (2.31). The advantage of eq. (2.31) is that it is much more convenient for quantization due to the absence of square roots.

I now introduce the canonical momenta

$$p \equiv \frac{\partial \mathcal{L}}{\partial \partial_\lambda r} \ , \qquad\qquad q \equiv \frac{\partial \mathcal{L}}{\partial \partial_\lambda t} \ , \tag{2.32}$$

and perform the Legendre transformation to obtain the Hamiltonian

$$\mathcal{H} = \nu \left(\frac{p^2 - q^2}{8\pi\sigma r^2} + \frac{\epsilon r q}{3\sigma} - \frac{2\pi\epsilon^2 r^4}{9\sigma} + 2\pi\sigma r^2 \right) \ . \tag{2.33}$$

---

[2]Note that in this picture, the tunneling of the fields ϕ in the potential $V(\phi)$ is replaced by an effective description where a single degree of freedom r tunnels through an effective potential $U(r)$. The two potentials $V(\phi)$ and $U(r)$ should not be confused!

Since ν is only a Lagrange multiplier and no dynamical degree of freedom, which can be seen from $\partial \mathcal{L} / \partial \partial_\lambda \nu \equiv 0$, one concludes that $\partial \mathcal{H} / \partial \nu = 0$. This forces the Hamiltonian itself to zero, which can be interpreted in terms of a *Hamiltonian constraint*

$$H_\nu \equiv p^2 - \left(q - \frac{4\pi}{3} \epsilon r^3 \right)^2 + 16\pi^2 \sigma^2 r^4 = 0 \ . \tag{2.34}$$

The Lagrange multiplier ν plays a similar role as the lapse function in the ADM formalism. Applying the canonical quantization prescription

$$p \to -i\partial_r \ , \qquad q \to -i\partial_t \ , \tag{2.35}$$

to the Hamiltonian constraint, one arrives at a Wheeler-DeWitt type of equation

$$\hat{H} \left[r, \partial_r, t, \partial_t \right] \psi(r, t) = 0 \ . \tag{2.36}$$

The motion of a bubble has a conserved energy E associated with it. This follows directly from the fact that the Hamiltonian is independent of t and therefore q is a conserved quantity. In fact, q is just the quantum mechanical energy with the wrong sign, *cf.* eq. (2.35). For energy eigenstates, I make the usual *product ansatz*

$$\psi(r, t) = e^{-iEt} \psi_E(r) \ . \tag{2.37}$$

with this *ansatz*, ψ_E obeys an ordinary differential equation. Specializing to a certain form of operator ordering, this equation reads

$$\left[-\partial_r^2 + \frac{n}{r} \partial_r - E^2 - \frac{8\pi}{3} \epsilon E r^3 - \frac{16\pi^2}{9} \epsilon^2 r^6 + 16\pi^2 \sigma^2 r^4 \right] \psi_E(r) = 0 \ , \tag{2.38}$$

where n parametrizes a residual freedom in choosing the operator ordering which I keep for later convenience.

The state appropriate for describing spontaneous bubble nucleation corresponds to a solution with zero energy. Setting $E = 0$ one arrives at an equation which is very similar to the stationary Schrödinger type of equation which would be obtained naively from eq. (2.26). This should not come as a big surprise. However, the derivation presented here is more rigorous and allows to treat also arbitrary states. The choice of the state remains somewhat *ad hoc* though.

The zero-energy equation can be cast into dimensionless form by defining $x \equiv r/r_0$ and $Z \equiv \pi \sigma r_0^3 / 2$:

$$\left[-\partial_x^2 + \frac{n}{x} \partial_x - 64 Z^2 \left(x^6 - x^4 \right) \right] \psi_{E=0}(x) = 0 \ . \tag{2.39}$$

It turns out that it is useful to write $\psi_{E=0}(x) \equiv \varphi(x^2)$. Since x is restricted to the positive real axis, this may be done without ambiguity. The equation for φ becomes particularly simple if one chooses the operator ordering corresponding to $n = 1$. Defining $s \equiv x^2$ one then has

$$\partial_s^2 \varphi + 16 Z^2 (s^2 - s) \varphi(s) = 0 \ . \tag{2.40}$$

By completing the square, this can be brought to a canonical form known as the Weber differential equation. Its solutions are the parabolic cylinder functions D_ν, which are characterized *e.g.* in [37]. In terms of these, two independent solutions are

$$\begin{aligned}
\psi_{E=0}^+(x) &\propto D_{-\frac{1}{2} - \frac{i}{2} Z} \left(-(i-1)\sqrt{Z} \left(2x^2 - 1 \right) \right) \ , \\
\psi_{E=0}^-(x) &\propto D_{-\frac{1}{2} + \frac{i}{2} Z} \left(-(i+1)\sqrt{Z} \left(2x^2 - 1 \right) \right) \ .
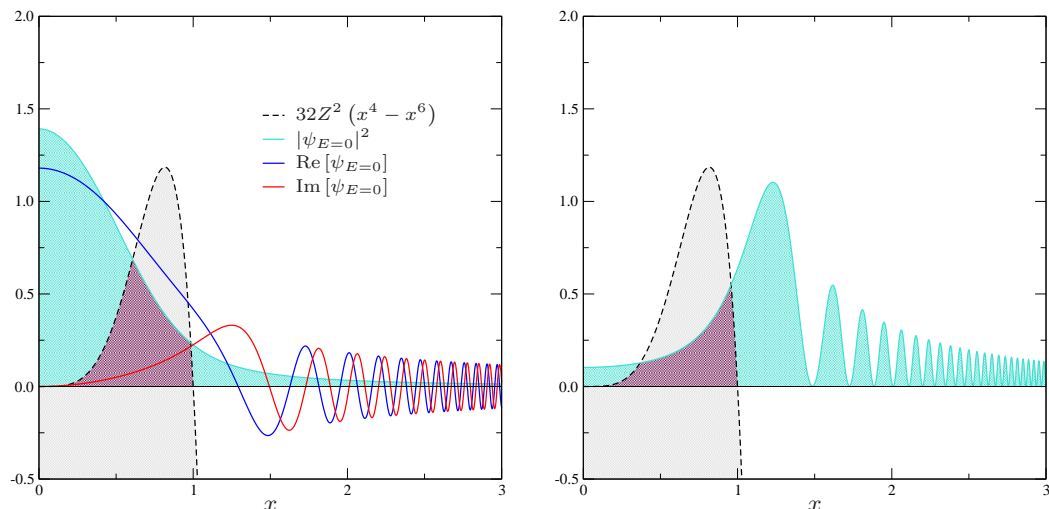\end{aligned} \tag{2.41}$$

Figure 2.2: Wavefunction $\psi_{E=0}$ with boundary conditions corresponding to a tunneling bubble (left panel) and a "bouncing" bubble (right panel). Real and imaginary part of the former are shown in blue and red, respectively – the arbitrary phase was chosen such that $\mathrm{Im}\,[\psi_{E=0}(0)] = 0$. In order to get a visible appearance to the right of the barrier, I have chosen $Z = 0.5$, which corresponds to a tunneling rate of order unity. For small tunneling rates, $Z \gg 1$, the wavefunction to the right of the barrier is exponentially small. The probability amplitude of the "bouncing" bubble shows a clear interference pattern (standing wave) to the right of the barrier, since the incoming bubble is largely reflected at the potential. Also in this case the probability for the radius to penetrate through the barrier is small and quickly approaches zero as Z becomes large.

The boundary condition of having an outgoing wave[3] at $x \to \infty$ selects the first solution. This is the physically significant case of having no "incoming bubble." A plot of this solution is shown in fig. 2.2 (left panel), from which it is evident that the probability is high for the bubble radius to be trapped inside the potential $U(r)$, but also that an exponentially small tail of the wavefunction leaks out beyond the *classical turning point* at $x = 1$. An asymptotic expansion for large Z shows that

$$\frac{\left|\psi_{E=0}^{+}(1)\right|^{2}}{\left|\psi_{E=0}^{+}(0)\right|^{2}} \sim e^{-\pi Z} \qquad \text{as} \qquad Z \to \infty\ . \tag{2.42}$$

This confirms the result of the WKB estimate given in eq. (2.29).

The second solution, $\psi_{E=0}^{-}$, is shown in fig. 2.2 (right panel). It can be interpreted as a pre-existing bubble that approaches the classical turning point from infinity, "bounces," and reexpands indefinitely. Most of the wavefunction is reflected at the barrier, producing the usual standing wave pattern. However, a small fraction is allowed to tunnel to $x = 0$, which is in a sense the reversed process of spontaneous nucleation – the bubble spontaneously disappears and the false vacuum configuration is restored.

2.2.3 Tunneling in Time-dependent Settings

Having understood the basic features of bubble nucleation in Minkowski space, let me now move on to a slightly more general setup in which the background is allowed to have some dynamics[4]. I will still assume that the nucleation process does not disturb the background,

---

[3]The notion of an "outgoing wave" is somewhat arbitrary. I take a heuristic definition and simply pick the solution which has the asymptotic property that $\hat{p}\psi = -i\partial_r\psi \sim \sqrt{-2U(r)}\psi$, *i.e.* the solution which asymptotes to the "outgoing" WKB mode.

[4]This section closely rephrases some parts of [1], in which the work presented here has been published.

but the background dynamics shall be allowed to have some effect on the bubbles. Having a cosmological scenario in mind, I will consider the case where the ambient spacetime is well approximated by a flat Friedmann universe. It is convenient to work in conformal time τ, in which the FRW line element of eq. (1.2) reads

$$ds^2 \equiv g_{\mu\nu}dx^\mu dx^\nu = a^2(\tau)\left[-d\tau^2 + dr^2 + r^2 d\Omega^2\right] \ . \tag{2.43}$$

I have set $K = 0$ for simplicity. The conformal time is related to the proper time by $dt = ad\tau$.

On this type of background, the effective action (2.24) which governs the radial motion of a bubble wall generalizes to

$$\mathcal{S}_{\text{eff}} = \int d\tau \left[\frac{4\pi}{3}\epsilon a^4 r^3 - 4\pi\sigma a^3 r^2 \sqrt{1 - (\partial_\tau r)^2}\right] \ . \tag{2.44}$$

In this expression, $a(\tau)$ is an external "source" with a given time-dependence. In cosmology, the time evolution of the scale factor is governed by the Friedmann equations, as outlined in section 1.1. Due to this explicit time-dependence introduced by the background, the nucleation rate will in general be time-dependent as well. A formalism to calculate tunneling rates in such settings has been presented by Esko Keski-Vakkuri and Per Kraus [38]. In their approach, the tunneling rates are obtained in a semiclassical calculation directly from the classical equations of motion, thereby avoiding the quantization of the system and all the issues it would entail. The classical equation which governs the motion of the bubble wall reads

$$4\pi\epsilon a^4 r^2 - 8\pi\sigma a^3 r\sqrt{1 - (\partial_\tau r)^2} = \frac{d}{d\tau}\left[4\pi\sigma\frac{a^3 r^2 \partial_\tau r}{\sqrt{1 - (\partial_\tau r)^2}}\right] \ . \tag{2.45}$$

It is clear by intuition that the classical trajectory after tunneling emanates from a classical turning point where the canonical momentum

$$p \equiv \frac{\partial\mathcal{L}}{\partial\partial_\tau r} = 4\pi\sigma\frac{a^3 r^2 \partial_\tau r}{\sqrt{1 - (\partial_\tau r)^2}} \tag{2.46}$$

vanishes. It has been pointed out in [38] that by analytic continuation to complex τ one can find a classical trajectory (in the complex τ plane) that smoothly shrinks the bubble to zero size. To this end, it is useful to rewrite eq. (2.45) as an equation for $\tau(r)$:

$$4\pi\epsilon a^4 r^2 \partial_r\tau - 8\pi\sigma a^3 r\sqrt{(\partial_r\tau)^2 - 1} = \frac{d}{dr}\left[4\pi\sigma\frac{a^3 r^2}{\sqrt{(\partial_r\tau)^2 - 1}}\right] \ . \tag{2.47}$$

I am looking for the solution with the boundary conditions

$$p(\tau_0) = 4\pi\sigma\frac{a^3 r^2}{\sqrt{(\partial_r\tau)^2 - 1}}\Bigg|_{\tau=\tau_0} = 0 \ , \qquad \partial_r\tau\Big|_{r=0} = 0 \ , \tag{2.48}$$

where τ_0 is a free parameter, the *nucleation time*. The *nucleation radius*, *i.e.* the coordinate radius of the bubble at the classical turning point, will be denoted as r_0 as before, and fulfills $\tau(r_0) = \tau_0$. The first condition matches the solution to the turning point, from which on it remains on the real axis. In order to understand where the second condition comes from, consider the full spherically symmetric worldsheet of the bubble traced out by the trajectory $(r, \tau(r))$. The trajectory is simply extended into the classically forbidden region $r < r_0$ by analytic continuation. The second condition then guarantees that the worldsheet

remains regular at the origin. This is precisely what is meant by *smoothly* shrinking the bubble to zero size. These two boundary conditions characterize a one-parameter family of solutions labeled by their individual nucleation times.

After some algebra, eq. (2.47) simplifies to

$$\frac{\epsilon}{\sigma} a \sqrt{(\partial_r \tau)^2 - 1} = 2 \frac{\partial_r \tau}{r} + 3 \frac{\partial_\tau a}{a} - \frac{\partial_r^2 \tau}{(\partial_r \tau)^2 - 1} \ . \tag{2.49}$$

Since τ will depart from the real axis for $r < r_0$, it is clear that one also has to continue the time-dependent scale factor a to the complex plane. In some cases a is given in terms of elementary functions and the continuation is straightforward.

With a solution to eq. (2.49) which obeys the boundary conditions (2.48), the semiclassical tunneling rate is determined by the imaginary part of its action:

$$\Gamma \sim e^{-2\mathrm{Im}[\mathcal{S}_{\mathrm{eff}}]} \ . \tag{2.50}$$

This semiclassical formula is analogous to the WKB estimate of eq. (2.29) and follows from a similar reasoning. A rigorous justification for this approach follows from the methods explained in section 2.3. It is again useful to write $\mathcal{S}_{\mathrm{eff}}$ in terms of $\tau(\tau_0; r)$:

$$\mathrm{Im}\left[\mathcal{S}_{\mathrm{eff}}\right] = \mathrm{Im}\left[\int_0^{r_0} dr \left(\frac{4\pi}{3} \epsilon a^4 r^3 \partial_r \tau - 4\pi \sigma a^3 r^2 \sqrt{(\partial_r \tau)^2 - 1}\right)\right] \ . \tag{2.51}$$

One should keep in mind that each solution is labeled with an individual nucleation time τ_0, and that the value of the above integral can in general depend on this parameter. This is what is meant by a time-dependent tunneling rate.

In order to illustrate the whole approach, let me apply it to several examples. Before turning to time-dependent backgrounds, it is useful to review the situation in Minkowski space. In this case, one can set $a = 1$, and conformal time is equivalent to proper time. The trajectory is a hyperbola,

$$r^2 - (\tau - \tau_0)^2 = r_0^2 \ , \tag{2.52}$$

which means

$$\tau(r) = \tau_0 + \sqrt{r^2 - r_0^2} \ . \tag{2.53}$$

The sign for the square root is chosen corresponding to an expanding bubble. One can check that this trajectory fulfills the boundary conditions (2.48), and furthermore, with eq. (2.49) one infers $r_0 = 3\sigma/\epsilon$. The imaginary part of the action can be found readily from eq. (2.51),

$$\mathrm{Im}\left[\mathcal{S}_{\mathrm{eff}}\right] = \frac{27\pi^2 \sigma^4}{4\epsilon^3} \ , \qquad \text{(Minkowski)} \tag{2.54}$$

which gives the same semiclassical decay rate as the WKB estimate (2.29).

As a first example for an expanding background, I shall now consider de Sitter space. Although it can actually be written in static coordinates, the FRW metric with *flat* spatial sections has a scale factor which grows exponentially with proper time, $a = e^{Ht}$. Written in conformal time this becomes $a = -1/(H\tau)$, where τ runs from $-\infty$ to 0 as t runs from $-\infty$ to $+\infty$. With this form of scale factor, eq. (2.49) reads

$$-\frac{\epsilon}{\sigma H \tau} \sqrt{(\partial_r \tau)^2 - 1} = \frac{\partial_r \tau}{r} - \frac{3}{\tau} - \frac{\partial_r^2 \tau}{(\partial_r \tau)^2 - 1} \ . \tag{2.55}$$

While looking for the complete set of solutions to this problem does not seem promising, it turns out that one can guess the relevant solution by sensibly generalizing the one of Minkowski space. Since de Sitter space (in flat coordinates) has a constant expansion

rate H, one should expect that the *proper* nucleation radius is independent of τ_0, the time of nucleation. However, r_0 is the nucleation radius in *comoving* coordinates, *i.e.* the proper nucleation radius divided by the scale factor. A first guess would therefore be $r_0 = -3H\tau_0\sigma/\epsilon$. As one may easily check, it turns out that this redefinition, together with eq. (2.53), gives the correct solution to eq. (2.55) with the boundary conditions (2.48).

With this input, the integral of eq. (2.51) is still solvable, and its imaginary part is found to be

$$\text{Im}\left[\mathcal{S}_{\text{eff}}\right] = \frac{4\pi^2\epsilon}{3H^4}\sinh^2\frac{1}{4}\ln\left(1 + (3H\sigma/\epsilon)^2\right) \ , \qquad \text{(de Sitter)} \qquad (2.56)$$

which is independent of the choice τ_0 for the time of nucleation. Therefore, the decay rate in de Sitter space is time-independent, which is just a reflection of the fact that the spacetime has no true dynamics.

The above expression contains the result of Minkowski space, eq. (2.54), as a limiting case for $H \to 0$. The first correction is of order H^2 and complies with an expansion found in [39].

Another interesting limit is $\epsilon \to 0$, which corresponds to the nucleation of a domain wall separating two degenerate vacua. For energetic reasons, this process is forbidden in Minkowski space, but it is allowed in de Sitter space – the "energy" necessary for the nucleation is supplied by the background. The nucleation rate obtained from eq. (2.56) corresponds to

$$\lim_{\epsilon \to 0}\text{Im}\left[\mathcal{S}_{\text{eff}}\right] = \frac{\pi^2\sigma}{H^3} \ . \qquad \text{(de Sitter)} \qquad (2.57)$$

This is in complete agreement with a result found in [40]. Despite the appearance of limiting cases in the literature, to my knowledge, the full expression (2.56) has first been published in [1].

Thus far I have only considered static spacetimes in order to demonstrate the new tools. Let me finally turn to a more general case where the expansion rate is not assumed to be constant. A simple deformation of de Sitter expansion is given by power law inflation, where the scale factor grows as $a = (\tau_1/\tau)^{1+\alpha}$. This kind of inflationary evolution can be obtained as exact solution if the *inflaton field* – that is, the scalar field driving inflation as explained in section 1.2 – has an exponential potential. For small deformation parameters α, the first slow-roll parameter is simply $-\partial_t H/H^2 \approx \alpha$. The instant τ_1 denotes an arbitrary point in time where the scale factor is normalized to unity. I want to study the effect of a time-varying cosmological expansion rate on the tunneling probability. For power law inflation, eq. (2.49) reads

$$\frac{\epsilon}{\sigma}\left(\frac{\tau_1}{\tau}\right)^{1+\alpha}\sqrt{(\partial_r\tau)^2 - 1} = 2\frac{\partial_r\tau}{r} - 3\frac{1+\alpha}{\tau} - \frac{\partial_r^2\tau}{(\partial_r\tau)^2 - 1} \ . \qquad (2.58)$$

I was unable to find an analytic solution to this equation and therefore decided to treat it numerically. A parameter study of the numerical tunneling rates reveals the following picture. There are now three different time scales in the problem. The background has two characteristic time scales, given by the inverse of the expansion rate, H^{-1}, and the inverse rate of *change* of the expansion rate, $|\partial_t H/H|^{-1}$. These two time scales have to be compared to a characteristic time scale of the tunneling process, which can be defined as the nucleation radius divided by the speed of light – roughly $3\sigma/\epsilon$.

If the characteristic time scale of the tunneling process is the smallest time scale of the problem, then the tunneling rate is well approximated by the result in Minkowski space, eq. (2.54). However, if the tunneling time scale at the instant of nucleation τ_0 is not much smaller than the inverse of the expansion rate, there are two possibilities. Either, the characteristic time scale of the change of the expansion rate, $|\partial_t H/H|^{-1}$, is still much larger than the one of the tunneling process – then a *quasistatic approximation* is valid

Figure 2.3: Numerical values for the imaginary part of the action $\mathcal{S}_{\text{eff}}$ for tunneling solutions with proper nucleation radius $3\sigma/\epsilon = 2H^{-1}(\tau_0)$, as a function of the slow roll parameter $\partial_t H/H^2$. The values are normalized to the *quasistatic approximation*, which is obtained from eq. (2.56) by setting $H = H(\tau_0)$. Thus, in this approximation only instantaneous dynamical parameters are taken into account. The tunneling process, however, has a characteristic time scale given by the light-travel time across the bubble. Hence it is more appropriate to take into account some *average* dynamics of the background. In a crude way, this can be accomplished by using an averaged expansion rate to evaluate the tunneling probability in the quasistatic approximation. The dashed red line is obtained from a *proper time average* of H taken over an interval $\Delta t = 3\sigma/\epsilon$ prior to nucleation.
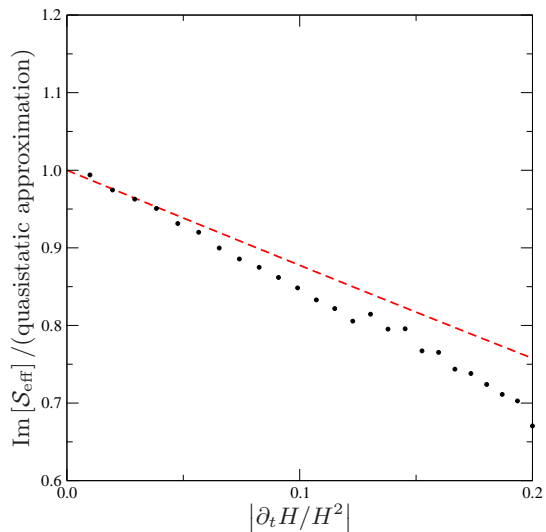
such that a good estimate for the tunneling probability can be obtained from eq. (2.56) by setting $H = H(\tau_0)$. Or the characteristic time scale of the tunneling process cannot be regarded as small with respect to either of the other two time scales. In this case, the tunneling process "feels" the changing of the expansion rate and the tunneling probability is modified significantly.

It turns out that a quite accurate estimate of the tunneling probability can still be obtained if one first *averages* the expansion rate over an interval $\Delta t = 3\sigma/\epsilon$, corresponding to the time scale of the tunneling process. If one then plugs this averaged expansion rate into eq. (2.56), one obtains an estimate that is still accurate to leading order in α, *cf.* fig. 2.3.

2.2.4 Bubble Dynamics in General Relativity

Thus far I have looked upon the problem of bubble formation and propagation without taking into account gravitational effects induced by the bubble itself. Of course, a bubble has stress-energy and therefore the geometry, which was treated as a fixed background up to this point, will in fact respond according to the laws of GR. A relativistic treatment of vacuum decay introduces new difficulties. Many of these are related to the role of time and will be addressed to some extent in the forthcoming sections. In this section, I first want to discuss the *classical dynamics* of vacuum bubbles in GR. In the limit where the thin-wall approximation holds, there is an elegant way to treat this problem. Detailed accounts can be found in the literature, *e.g.* in [41, 42].

In the thin-wall approximation, the geometry of a false vacuum configuration which contains a bubble of true vacuum can still be split into two domains – the *interior* and the *exterior* of the bubble. The geometry in each domain has to be a vacuum solution to Einstein's equations. Furthermore, *Birkhoff's theorem* already guarantees that the geometry has to be that of Schwarzschild-de Sitter (SdS) spacetime, because of spherical symmetry. The Schwarzschild-de Sitter metric can be written as

$$ds^2 \equiv g_{\mu\nu}dx^\mu dx^\nu = -\left(1 - \frac{2M}{r} - \frac{\Lambda}{3}r^2\right)dt^2 + \left(1 - \frac{2M}{r} - \frac{\Lambda}{3}r^2\right)^{-1}dr^2 + r^2 d\Omega^2 \ . \quad (2.59)$$

It has two parameters: the cosmological constant Λ which arises from the energy density of the vacuum, and the so-called Misner-Sharp mass M, which is the mass parameter of

a black hole centered at the origin. However, the interior of a bubble does not contain a singularity at $r \to 0$, and therefore the mass parameter of the interior SdS solution is zero. The corresponding spacetime is, of course, de Sitter space (dS).

Assuming that the bubble spontaneously nucleated from the vacuum given by the exterior vacuum configuration, it is clear that the bubble does not generate a non-zero mass parameter for the exterior region either. One is therefore confronted with a situation where interior and exterior spacetime are both described by the de Sitter geometry, the only difference being the respective vacuum energy density.

The problem of bubble dynamics can therefore be rephrased as the question of how the two geometries, which are the respective vacuum solutions of Einstein's equations, have to be joined together at the common boundary, the worldsheet of the bubble wall. An analogous problem arises in electrodynamics if one wants to match the solutions in two different media across a common interface. Recall that in this problem there arise two matching conditions: one says that the electric field projected onto the interface has to be continuous, and the other guarantees that the discontinuity of the perpendicular component is proportional to the surface charge density on the interface, *i.e.* that Maxwell's equations are satisfied.

The junction conditions for two spacetime geometries are completely analogous. A first junction condition states that the metric projected onto the interface has to be continuous. This, of course, means that the worldsheet of the bubble has a well-defined geometry at all. A second junction condition guarantees that a discontinuity in the *extrinsic curvature*, which is essentially the part of the metric orthogonal to the interface, is proportional to the surface stress-energy of the bubble wall. In other words, the second junction takes care that Einstein's equations are satisfied.

These conditions have become known as Israel's junction conditions due to the work by Werner Israel [43]. Nice introductions can be found in many textbooks, see *e.g.* [44]. The junction conditions completely determine the dynamics of the bubble wall. Let me denote the worldsheet of the bubble wall as Σ. Furthermore, quantities defined in the interior domain shall be denoted with a lower bar, like $\underline{g}_{\mu\nu}$, $\underline{\Lambda}$, *etc.*, and those defined in the exterior domain with an upper bar, like $\overline{g}_{\mu\nu}$, $\overline{\Lambda}$, *etc.* The line element on the worldsheet Σ can be written as

$$ds_\Sigma^2 = -dT^2 + R^2 d\Omega^2 \ , \tag{2.60}$$

where T is the proper time measured along the wall trajectory. Let me use the flat FRW metric of de Sitter space for the two vacuum domains,

$$d\overline{s}^2 \equiv \overline{g}_{\mu\nu} d\overline{x}^\mu d\overline{x}^\nu = \frac{1}{\overline{H}^2 \overline{\tau}^2} \left[-d\overline{\tau}^2 + d\overline{r}^2 + \overline{r}^2 d\Omega^2 \right] \ , \tag{2.61}$$

and similarly for all bars lowered. I use conformal time which runs from $-\infty$ to 0 as should be familiar from last section. Note that I identify angular coordinates in the two domains and on the interface, and therefore do not distinguish between $d\overline{\Omega}$, $d\Omega$ and $d\underline{\Omega}$.

With these definitions, the first junction condition reads

$$-\frac{\overline{r}}{\overline{H}\overline{\tau}} = R = -\frac{\underline{r}}{\underline{H}\underline{\tau}} \ , \qquad\qquad \frac{d\overline{\tau}^2 - d\overline{r}^2}{\overline{H}^2 \overline{\tau}^2} = dT^2 = \frac{d\underline{\tau}^2 - d\underline{r}^2}{\underline{H}^2 \underline{\tau}^2} \ . \tag{2.62}$$

The latter can be rearranged to show that

$$(\partial_T \overline{\tau})^2 = \frac{\overline{H}^2 \overline{\tau}^2}{1 - \left(\partial_\tau r\right)^2} \ , \tag{2.63}$$

and similarly for all bars lowered.

Working out the second junction condition yields the equation[5]

$$\sqrt{(\partial_T R)^2 - \underline{H}^2 R^2 + 1} - \sqrt{(\partial_T R)^2 - \overline{H}^2 R^2 + 1} = 4\pi\sigma R \ . \tag{2.64}$$

For a derivation of this relation, see [1] and the references therein, in particular [41]. It can be solved for the kinetic term,

$$(\partial_T R)^2 = \left[\underline{H}^2 + \left(\frac{\epsilon}{3\sigma} + 2\pi\sigma \right)^2 \right] R^2 - 1 \ . \tag{2.65}$$

Here, ϵ denotes again the difference in the vacuum energy density between false and true vacuum, $\epsilon \equiv 3(\overline{H}^2 - \underline{H}^2)/(8\pi)$, and σ is the surface energy density as in eq. (2.18). Using the first junction condition, the left-hand side can be rewritten as

$$(\partial_T R)^2 = \frac{1}{1 - \left(\overline{\partial_\tau r} \right)^2} \left(\frac{\overline{r}}{\overline{\tau}} - \overline{\partial_\tau r} \right)^2 \ , \tag{2.66}$$

or, equivalently, with all bars lowered. This allows one to write the junction conditions as a first-order differential equation for $\overline{r}(\overline{\tau})$ or $\underline{r}(\underline{\tau})$, the trajectory of the bubble wall in exterior or interior coordinates, respectively.

One may check that a hyperbolic trajectory of the form (2.52) solves this equation if one chooses

$$\frac{\overline{r}_0^2}{\overline{H}^2 \overline{\tau}_0^2} = \left(\frac{\epsilon}{3\sigma} - 2\pi\sigma \right)^{-2} \ , \qquad \frac{\underline{r}_0^2}{\underline{H}^2 \underline{\tau}_0^2} = \left(\frac{\epsilon}{3\sigma} + 2\pi\sigma \right)^{-2} \ . \tag{2.67}$$

Evidently, the proper nucleation radius in the false vacuum background is somewhat larger than $3\sigma/\epsilon$, which was the result obtained in the previous section. The new result takes gravitational effects fully into account. The difference with respect to the previous result has an intuitive explanation if one considers the gravitational energy of the bubble and the distortion of the geometric volume, see [33] for a discussion. The bottom line of this consideration is that the effective volume of the bubble is reduced[6] and therefore the volume energy is is smaller even despite a positive contribution from the gravitational binding energy. Being a purely gravitational effect, the difference between the relativistic formula (2.67) and the result of the previous section vanishes in the limit where the Planck mass goes to infinity.

Note that one can see from an inspection of eq. (2.64) that the surface tension has to satisfy the inequality

$$2\pi\sigma \leq \frac{\epsilon}{3\sigma} \ . \tag{2.68}$$

The bound is saturated if the bubble needs an entire horizon volume of the false vacuum in order to nucleate. Creation of larger bubbles is forbidden by causality. One could also say that larger bubbles do not "fit" into the false vacuum de Sitter spacetime.

In order to obtain the semiclassical tunneling rate, one needs to follow the trajectory into the classically forbidden region. In the previous section, this was accomplished by analytic continuation of the global time parameter. Such a parameter is not available in the full

---

[5]The signs of the square roots are fixed by the requirement that the radial coordinate decreases as one moves away from the interface into the interior domain and increases as one moves into the exterior domain. With a certain interpretation in mind, namely the decay of a false vacuum by bubble nucleation, this seems to be a suitable choice. Other choices could be appropriate in other situations. For instance, a positive sign of both square roots corresponds to a situation where both domains appear to be *interior* regions, *i.e.* an observer on either side of the interface would perceive herself as being enclosed within a bubble.

[6]Note that the proper nucleation radius as seen from the *interior* of the bubble, according to eq. (2.67), is somewhat *smaller* than $3\sigma/\epsilon$.

relativistic picture. However, it is quite clear what happens: at the configuration which corresponds to the classical turning point, the bubble trajectory together with *the entire geometry* has to be continued analytically into a classically forbidden part of configuration space. This, in fact, is the basic idea behind the concept of gravitational *instantons*. The construction of the analytic continuation and the calculation of semiclassical tunneling rates will be the subject of the corresponding section 2.3.3.

Another possible route, which is somewhat less powerful and elegant than the instanton method but nonetheless very instructive, is the construction of a wavefunction in the Hamiltonian framework outlined in section 2.1.1. A detailed account on this approach can be found in [45].

## 2.2.5   Desynchronization of the Bubble Universe and its Environment

Before I shall carry on with a general introduction to instanton methods in the next section, let me comment a bit on the issue of time in the relativistic picture. I have already argued that the notion of time is a semiclassical one and breaks down on some occasions within the full framework of quantum cosmology. However, even if a classical description is valid, such as the one discussed in the previous section, the notion of time in GR is ambiguous by virtue of the very principle of *relativity*. Only in very special situations there exists a *preferred* family of ideal observers who can be used to define a *preferred* frame of reference. For instance, in an FRW geometry, the family of comoving observers can be defined as the only observers who are at rest with respect to the cosmic fluid. Of course, this definition is only appropriate if the cosmic fluid has a unique rest frame; in case the fluid is pure vacuum, the notion of comoving observers remains ambiguous. Recall that de Sitter space can equally well be foliated as open, flat, or closed FRW geometry.

Defining a preferred family of observers, and thus, a preferred notion of time, becomes even more arbitrary in the case of false vacuum decay. I will explain in the next sections that the symmetry of the geometry which contains a single bubble – hereafter called a *one-bubble spacetime* – allows to define a family of preferred observers. As is evident from eq. (2.52), which holds as a fully relativistic solution if the parameters comply with eq. (2.67), the worldsheet of the bubble wall is a hyperboloid, and is therefore invariant under Lorentz boosts. This boost symmetry of one-bubble spacetime also pertains if the thin-wall approximation breaks down. Within the past and future lightcones of the nucleation point, the boost-invariant hypersurfaces are two-sheeted hyperboloids. These hypersurfaces are spacelike and can be used to foliate the interior of the lightcones as open FRW spacetimes with the usual notion of comoving observers. However, this leaves the entire region outside of the lightcones, and in particular, all of the false vacuum domain, void of observers.

In the thin-wall limit, the exterior domain is well approximated by a patch of de Sitter space, and it may therefore appear natural to choose a family of comoving observers corresponding to some convenient foliation. In fact, if the tunneling probability is exponentially small as is usually assumed, then one expects that inflation takes place in the false vacuum phase for an exponentially long period of time before the tunneling event occurs. On physical reasons it then seems natural to define a family of observers which perceives a *flat* inflationary FRW geometry in the exterior. Remember that inflation effectively dilutes curvature, and therefore the worldlines of observers in an arbitrary foliation of de Sitter space asymptotically converge towards the worldlines of observers who are comoving in the spatially flat foliation.

Let me therefore consider this family of comoving observers in the exterior domain. The worldlines of at least some observers will intersect the worldsheet of the bubble wall and enter the interior domain. Therefore, the eigentime of these observers can be used to carry the notion of cosmic time from the exterior domain into the bubble. Moreover, one

Figure 2.4: Conformal diagram of the interior de Sitter patch of a vacuum bubble nucleating with a proper nucleation radius of $0.1\overline{H}^{-1}$. The vacuum energy densities of true and false vacuum were chosen such that $\overline{\Lambda} = 4\underline{\Lambda}$, or, equivalently, $\overline{H} = 2\underline{H}$. The solid grid shows the foliation carried into the bubble by exterior comoving observers. More precisely, the timelike lines are geodesics of such observers, and the spacelike lines are surfaces of constant eigentime as indicated by their clocks, which have been synchronized on a spatial hypersurface of the exterior spacetime in the flat foliation. The dashed grid indicates the coordinate system of an open foliation applied to the interior of the future lightcone of the nucleation event.
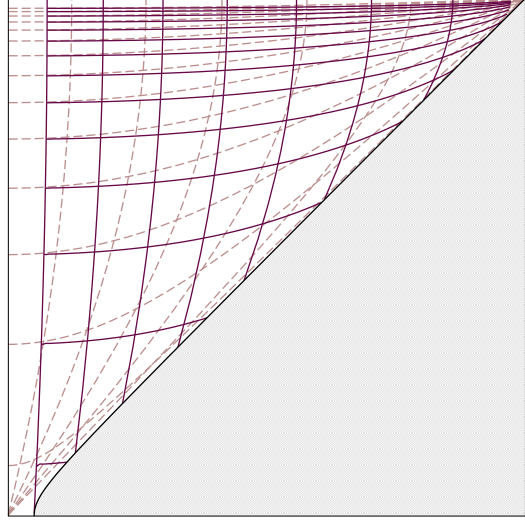
can imagine a foliation of the entire one-bubble spacetime, including the interior of the bubble, using the eigentime of this family of *exterior comoving observers*.

In order to construct this foliation, one has to consider the geodesics on the one-bubble spacetime. In any local coordinate system, a geodesic is a solution to the geodesic equation

$$\partial_t^2 x^\mu + \Gamma^\mu_{\kappa\lambda}\partial_t x^\kappa \partial_t x^\lambda = 0 \; , \tag{2.69}$$

where $\Gamma^\mu_{\kappa\lambda}$ are the Christoffel symbols and t is the eigentime parameter of the geodesic. This equation can be solved in the exterior and interior domains separately, such that the only interesting thing happens when a geodesic hits the junction hypersurface Σ.

Let me consider a geodesic passing from the exterior domain into the bubble. At the point of intersection with Σ, hereafter denoted as p, the geodesic has a tangent vector $\overline{u}^\mu = \partial_t \overline{x}^\mu|_p$, expressed in exterior coordinates $\overline{x}^\mu$. I shall perform the following change of coordinate system. The vector $\overline{u}^\mu$ will be decomposed into two components by projecting it once into the hypersurface Σ and once onto the surface unit normal n^μ in point p. This corresponds to Gaussian normal coordinates in p. The advantage of these coordinates is the fact that the basis vectors coincide on either side of Σ, and so do the components of the tangent vector of the geodesic in this basis. In other words, in order to continue the geodesic through the junction hypersurface, I first compute the components of $\overline{u}^\mu$ in Gaussian normal coordinates at p, and then make another transformation from Gaussian normal coordinates to the coordinate system $\underline{x}^\mu$ on the other side of Σ to obtain $\underline{u}^\mu$. This defines the initial conditions for the geodesic in the interior. In this construction, it is assumed that ideal observers do not interact with any sources of stress-energy except gravitationally, such that there is no additional momentum transfer from the bubble wall. A realistic observer, made up of physical matter, may not be so lucky. She would probably be disintegrated by the highly energetic impact.

A comoving observer in the exterior has no velocity in the angular part, and the problem reduces to a $1 + 1$ dimensional one. I will therefore simplify notation by dropping the angular coordinates from the equations. In terms of exterior coordinates (2.61), the velocity components of a comoving observer read $\overline{u}^\mu = (-\overline{H}\overline{\tau}, 0)$, and one may check that $\overline{u}^\mu \overline{u}_\mu = -1$ as desired.

At the point of intersection with Σ, I define the unit tangent vector t^μ in direction T, and the unit normal vector n^μ of the hypersurface. Again, in terms of the exterior

coordinates, one has, respectively,

$$\overline{t}^{\mu} \;\; = \;\; -\frac{\overline{H}\overline{\tau}}{\sqrt{1 - \left(\overline{\partial_{\tau}r}\right)^2}} \left(1, \overline{\partial_{\tau}r}\right) \;, \tag{2.70}$$

$$\overline{n}^{\mu} \;\; = \;\; -\frac{\overline{H}\overline{\tau}}{\sqrt{1 - \left(\overline{\partial_{\tau}r}\right)^2}} \left(\overline{\partial_{\tau}r}, 1\right) \;, \tag{2.71}$$

and one may check that $\overline{t}^{\mu}\overline{t}_{\mu} = -1$, $\overline{n}^{\mu}\overline{n}_{\mu} = 1$, $\overline{t}^{\mu}\overline{n}_{\mu} = 0$. A similar construction applies on the interior side of Σ.

The vectors t^{μ} and n^{μ} are the unit vectors of the Gaussian normal coordinate system at the point of intersection. The projections of u^{μ} onto these are

$$u^{\mu}t_{\mu} = \;\; \overline{u}^{\mu}\overline{t}_{\mu} \;\; = -\frac{1}{\sqrt{1 - \left(\overline{\partial_{\tau}r}\right)^2}} \;, \tag{2.72}$$

$$u^{\mu}n_{\mu} = \;\; \overline{u}^{\mu}\overline{n}_{\mu} \;\; = -\frac{\overline{\partial_{\tau}r}}{\sqrt{1 - \left(\overline{\partial_{\tau}r}\right)^2}} \;. \tag{2.73}$$

Finally, the components of u^{μ} in terms of the interior coordinates $(\underline{\tau}, \underline{r})$ are

$$\begin{aligned}
\underline{u}^{\mu} &= \;\; \frac{1}{\sqrt{1 - \left(\overline{\partial_{\tau}r}\right)^2}}\underline{t}^{\mu} - \frac{\overline{\partial_{\tau}r}}{\sqrt{1 - \left(\overline{\partial_{\tau}r}\right)^2}}\underline{n}^{\mu} \\
&= \;\; -\frac{\underline{H}\underline{\tau}}{\sqrt{1 - \left(\overline{\partial_{\tau}r}\right)^2}\sqrt{1 - \left(\underline{\partial_{\tau}r}\right)^2}} \left(1 - \overline{\partial_{\tau}r}\underline{\partial_{\tau}r}, \underline{\partial_{\tau}r} - \overline{\partial_{\tau}r}\right) \;.
\end{aligned} \tag{2.74}$$

Using this transformation rule and the first junction condition (2.62), which relates the interior and exterior coordinates at the bubble wall, one can determine the geodesics of external comoving observers which collide with the bubble and enter the interior region. A plot of their trajectories, as seen from the interior de Sitter piece, is shown in fig. 2.4. It is evident that the foliation obtained from the exterior proper time, carried into the interior of the bubble by the exterior comoving observers traveling on free-fall trajectories, does not coincide with any of the usual foliations of de Sitter space. In particular, it does not coincide with the open foliation which is favored by the symmetry of the one-bubble spacetime, and which is the one that is *physically* realized in certain scenarios like, *e.g.*, open inflation[7] [46]. Neither does it coincide with the flat or closed foliations. Therefore, what one considers as a good notion of cosmic time depends on the perspective. An exterior observer may consider the construction carried out above as a suitable definition of cosmic time. However, an observer living inside the bubble may find other definitions more natural, like the one related to the open foliation.

2.3   Instanton Methods

In this section I want to present a general introduction to *instantons*, which are a powerful concept of QFT and, furthermore, very useful for quantum cosmology and the semiclassical description of false vacuum decay. This introduction is strongly influenced by Sidney Coleman's inspired lectures on this topic [47].

---

[7]As will be explained in later sections, one can consider a scenario where our observable Universe is located inside a bubble which experienced a certain amount of slow-roll inflation after it was nucleated. The symmetry of one-bubble spacetime then dictates that, *e.g.*, the temperature of the CMB is homogeneous on *open* slices contained within the interior of the future lightcone of the nucleation point. Therefore, observers at rest with respect to the CMB are comoving in an open FRW geometry.

I have shown in the last sections that a phenomenon similar to quantum tunneling exists in QFT. However, in order to describe this phenomenon, the system had to be truncated drastically: using spherical symmetry and the thin-wall approximation, the underlying field-theoretic problem could be reduced to a quantum mechanical one with only one single degree of freedom. From this perspective, the instanton methods will present an interesting (and very elegant) alternative because they allow to treat the problem entirely within the framework of QFT. In particular, the methods allow to go beyond the thin-wall approximation.

2.3.1   Instantons in Particle Quantum Mechanics

In order to give a first taste of this method, I will follow Coleman's pedagogical approach and discuss it in the familiar context of particle quantum mechanics. In this context, the method of instantons is not particularly useful, because it is actually more cumbersome and less intuitive than other techniques. The exercise should serve to demonstrate some basic ideas without obscuring the calculations by the complexity of a more general setup. After the basics have been illustrated, I will proceed with a generalization to QFT in the next section.

The simple quantum system I want to consider here is a particle of unit mass in a one-dimensional potential $V(x)$. The classical Hamiltonian takes the form

$$H = \frac{1}{2}\left(\partial_t x\right)^2 + V(x) \ . \tag{2.75}$$

As starting point, let me recall the path-integral formulation of a transition amplitude,

$$\langle x_1, 0 | x_2, t \rangle = \int \mathcal{D}x\, e^{i\mathcal{S}[x]/\hbar} \ , \tag{2.76}$$

where I have restored $\hbar$ for the time being. This formula expresses the probability amplitude for a single particle which was found in position x_1 to travel to position x_2 within a specified time t. The right-hand side is a sum over all possible trajectories with these boundary conditions, each "weighted" by a phase factor determined by the action functional

$$\mathcal{S} = \int_0^t dt' \left[\frac{1}{2}\left(\partial_{t'}x\right)^2 - V(x)\right] \ . \tag{2.77}$$

The idea now is to evaluate the path-integral in a *stationary phase approximation*. As is well known, in the classical limit $\hbar \to 0$, the path-integral is dominated by the stationary points of the action. The stationary phase approximation is therefore tantamount to a *semiclassical* approximation.

In order to see how tunneling probabilities can be computed with such an approximation, let me consider a potential $V(x)$ as is shown in fig. 2.5 (left panel). I can always shift the potential by a constant such that $V(x_0) = 0$ at the local minimum x_0. Such a shift only gives a constant contribution to the action and therefore results in a trivial factor in eq. (2.76) which can be taken out of the path-integral[8]. I assume that the ground state ψ_0 of the harmonic oscillator obtained by expanding the potential up to quadratic order around the local minimum x_0 is an approximate ground state for small $\hbar$,

$$\psi_0(x) = \left(\frac{\omega}{\pi\hbar}\right)^{1/4} e^{-\omega(x-x_0)^2/(2\hbar)} \ , \qquad \omega^2 \equiv \partial_x^2 V\big|_{x=x_0} \ . \tag{2.78}$$

This actually becomes an exact ground state in the limit $\hbar \to 0$. Preparing the particle in this approximate ground state initially, I want to compute the probability to find it in the vicinity of x_0 after some finite time. Quantum tunneling out of the minimum into the
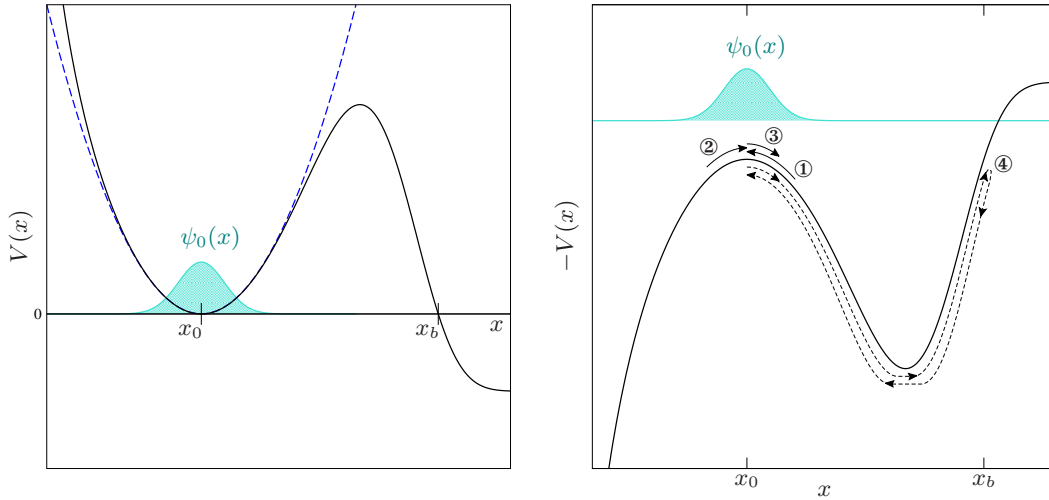
Figure 2.5: Example for a particle in a potential $V(x)$ with a local minimum x_0 which allows for a metastable quasi-groundstate whose spatial wavefunction can be well approximated by a Gaussian wave packet ψ_0 centered around x_0. If x_0 were a global minimum, like for the harmonic oscillator indicated as blue dashed line (left panel), then ψ_0 would be the true ground state – the eigenstate of the lowest-lying energy level. The state is rendered metastable by the possibility for the particle to tunnel to x_b in order to reach a region where the potential is even lower. The semiclassical trajectories can be analyzed in the Euclidean picture, where the system is that of a particle in the *inverted* potential (right panel). If the particle starts in the vicinity of x_0 and is found after a long period of (Euclidean) time again close to x_0, then the semiclassical path initially has to bring the particle up to the "hilltop" x_0, like *e.g.* on ① or ②, where it then loiters for most of the time until it eventually rolls to its final position, like *e.g.* on ③, to arrive there just in time. Summing over these semiclassical paths gives the leading contribution in the absence of tunneling. In the semiclassical limit, the correction due to tunneling arises from paths where the particle sporadically leaves its loitering position at the hilltop, rolls across the inverted barrier to x_b and back again on path ④, just to continue loitering as before.

region beyond x_b will lead to a gradual decay of this probability. Moreover, the rate of decay, by definition, corresponds to the tunneling rate.

Since the evolution of the state is *analytic* in t, one can make a "Wick rotation" and compute the path-integral in the Euclidean picture. That is, one makes a substitution $t_E \equiv it$, where t_E is called the *Euclidean time*. This can be regarded merely as a mathematical trick in order to simplify calculations. In particular, the semiclassical paths which dominate the path-integral can be analyzed more conveniently under this transformation. These are now the stationary points of the *Euclidean action*

$$\mathcal{S}_E = \int dt'_E \left[\frac{1}{2} \left(\partial_{t'_E} x \right)^2 + V(x) \right] , \qquad (2.79)$$

which is defined as $\mathcal{S}_E \equiv -i\mathcal{S}$. Evidently, with this redefinition, the oscillatory behavior of the integrand in eq. (2.76) is converted into exponential decay in the asymptotic regions where the Euclidean action becomes large, making the path-integral strongly convergent in these directions. In this context, the stationary phase approximation is usually called *saddle point approximation* or *method of steepest descent*, which are all similar concepts. After the path-integral has been evaluated, the Wick rotation will eventually be revoked for the final results.

---

[8]This is no longer true if gravity is included in the picture, as I will show in section 2.3.3.

In the path-integral formulation, the evolution of the state follows from

$$\psi_{t_{\mathrm{E}}}(x_2) = \int dx_1 \psi_0(x_1) \int\limits_{x(0)=x_1}^{x(t_{\mathrm{E}})=x_2} \mathcal{D}x \; e^{-\mathcal{S}_{\mathrm{E}}[x]/\hbar} \; . \tag{2.80}$$

The initial state, for small $\hbar$, is strongly localized around x_0. In order to obtain the wavefunction in the vicinity of x_0 after some time, the path integral has to be evaluated with initial and final positions x_1, x_2 both very close to x_0. Let me therefore consider all stationary points of the Euclidean action with such boundary conditions.

A stationary point of $\mathcal{S}_{\mathrm{E}}$ corresponds to a classical solution of the equations of motion for a particle moving in the *inverted* potential $-V(x)$. Let me denote such a solution by $\bar{x}$. Demanding the Euclidean action to be stationary at $\bar{x}$ means that $\bar{x}$ solves the corresponding Euler-Lagrange equation

$$\partial_{t'_{\mathrm{E}}}^2 \bar{x} - \partial_{\bar{x}} V = 0 \; . \tag{2.81}$$

This can be written as

$$\frac{d}{dt'_{\mathrm{E}}}\left[\frac{1}{2}\left(\partial_{t'_{\mathrm{E}}}\bar{x}\right)^2 - V(\bar{x})\right] = 0 \; . \tag{2.82}$$

To begin with, let me consider a case where the potential minimum at x_0 is the global minimum and therefore no tunneling can occur out of the ground state. The classical paths with endpoints in the vicinity of x_0 have a property which can be understood by the following argument. Consider a particle starting close to x_0, which is the "hilltop" of the inverted potential. After a very long time t_{E}, the particle will have rolled away to large distances except for the case when the initial velocity was extremely fine-tuned such that the particle (almost) reaches the hilltop with nearly vanishing velocity. Then the particle can remain there, barely moving, for a very long time, until it finally rolls off in one or the other direction to reach a final position still in the vicinity of x_0 "just in time." Classical paths which connect two points in the vicinity of x_0, in the limit of very long times, can therefore be separated in three segments. An initial segment of short duration brings the particle very close to x_0 and its velocity very close to zero. Examples are indicated as ① and ② in fig. 2.5 (right panel). Then an intermediate segment taking up most of the time but nearly giving no contribution to the action has $x \approx x_0$. The particle just loiters at the hilltop. Finally, the last segment, which has again only short duration, brings it to its final position. An example is indicated as ③ in fig. 2.5 (right panel).

Evidently, such paths are solutions to eq. (2.82) with

$$\frac{1}{2}\left(\partial_{t'_{\mathrm{E}}}\bar{x}\right)^2 - V(\bar{x}) \approx -V(x_0) \equiv 0 \; . \tag{2.83}$$

In the case where there is no tunneling, the path-integral, for each set of initial and final positions x_1 and x_2, is dominated by a unique path of this type. In the path-integral, one takes a sum over all perturbations of the path. Let me therefore expand the Euclidean action around the classical path. That is, I write

$$x(t'_{\mathrm{E}}) = \bar{x}(t'_{\mathrm{E}}) + y(t'_{\mathrm{E}}) \; , \tag{2.84}$$

and make a Taylor series expansion in y:

$$\mathcal{S}_{\mathrm{E}} = \int dt'_{\mathrm{E}} \left[\frac{1}{2}\left(\partial_{t'_{\mathrm{E}}}\bar{x} + \partial_{t'_{\mathrm{E}}}y\right)^2 + V(\bar{x}) + y\partial_{\bar{x}}V + \frac{1}{2}y^2\partial_{\bar{x}}^2 V + \ldots\right] \; . \tag{2.85}$$

Since all perturbations y of the path have to vanish at the boundary, one can integrate by parts in order to obtain

$$\mathcal{S}_{\mathrm{E}} = \int dt'_{\mathrm{E}} \left[\frac{1}{2}\left(\partial_{t'_{\mathrm{E}}}\bar{x}\right)^2 + V(\bar{x}) - y\left(\partial_{t'_{\mathrm{E}}}^2\bar{x} - \partial_{\bar{x}}V\right) + \frac{1}{2}y\left(-\partial_{t'_{\mathrm{E}}}^2 + \partial_{\bar{x}}^2 V\right)y + \ldots\right] \; . \tag{2.86}$$

The first two terms in the integrand yield the Euclidean action of $\bar{x}$, *i.e.* the contribution from the stationary point. The next term vanishes by virtue of eq. (2.81) – this is expected because it is the first variation of the action. The remaining term is the second variation of the action, and the ellipsis stands for higher variations which are dropped in the saddle point approximation.

One can write the variation y in terms of a complete set of real orthonormal functions which vanish at the boundaries. A possible choice would be the eigenfunctions of the second variational derivative of $\mathcal{S}_{\mathrm{E}}$ at $\bar{x}$, which are the solutions to the eigenvalue problem

$$\left(-\partial_{t_{\mathrm{E}}'}^2 + \partial_{\bar{x}}^2 V\right) y_n = \lambda_n y_n \; . \tag{2.87}$$

If one writes $y = \sum_n c_n y_n$, then the integral measure $\mathcal{D}x$ of the path-integral, up to normalization (the Jacobians are constants), can be understood as $\prod_n dc_n$. In the stationary phase approximation, the path-integral becomes a product of Gaussians, and one finds

$$\int\limits_{x(0)=x_1}^{x(t_{\mathrm{E}})=x_2} \mathcal{D}x \; e^{-\mathcal{S}_{\mathrm{E}}[x]/\hbar} \simeq N e^{-\mathcal{S}_{\mathrm{E}}[\bar{x}]/\hbar} \prod_n \lambda_n^{-1/2} = N e^{-\mathcal{S}_{\mathrm{E}}[\bar{x}]/\hbar} \left[\det\left(-\partial_{t_{\mathrm{E}}'}^2 + \partial_{\bar{x}}^2 V\right)\right]^{-1/2} \; , \tag{2.88}$$

where N is a normalization constant which will disappear in the final result. The action of the classical path can readily be evaluated as the sum of the contributions from each segment,

$$\mathcal{S}_{\mathrm{E}}\left[\bar{x}\right] \simeq \left|\int_{x_0}^{x_1} dx \sqrt{2V(x)}\right| + \left|\int_{x_0}^{x_2} dx \sqrt{2V(x)}\right| \simeq \frac{\omega}{2}\left(x_1 - x_0\right)^2 + \frac{\omega}{2}\left(x_2 - x_0\right)^2 \; , \tag{2.89}$$

where the actions of the initial and final segment were computed with the use of eq. (2.83) and under the assumption that the quadratic expansion of V holds up to x_1 and x_2. Under this assumption, the determinantal factor in eq. (2.88) becomes independent of x_1 and x_2, since one can simply replace $\partial_{\bar{x}}^2 V \simeq \omega^2$. Therefore, the wavefunction factorizes to

$$\psi_{t_{\mathrm{E}}}(x_2) = \psi_0(x_2)\sqrt{\frac{\pi\hbar}{\omega}} N \left[\det\left(-\partial_{t_{\mathrm{E}}'}^2 + \omega^2\right)\right]^{-1/2} \; . \qquad \text{(no tunneling)} \tag{2.90}$$

At this point, it should be noted that the first factor, up to a constant, is independent of the initial state. In fact, by taking the limit of very large times, I have projected the initial state onto the approximate ground state, as can be seen from the integral over x_1 which had to be carried out in order to arrive at the above equation. This can be understood as follows. In the Schrödinger picture, the state evolves as

$$|\psi\rangle_t = e^{-i\hat{H}t/\hbar}|\psi\rangle_0 \; . \tag{2.91}$$

Now, expanding the initial state in the energy basis and making the analytic continuation to Euclidean time, this can be written as

$$|\psi\rangle_{t_{\mathrm{E}}} = \sum_n \langle n|\psi\rangle_0 e^{-E_n t_{\mathrm{E}}/\hbar}|n\rangle \; . \tag{2.92}$$

Thus, for large Euclidean time, only the projection onto the state of lowest energy survives. This, however, is precisely the state which I am interested in. One should only keep in mind that the following analysis is not suitable for general initial states, meaning that more work would be required because one needs to keep track of the exponentially suppressed terms in above expansion.

The determinantal factor in eq. (2.90) can be evaluated as follows. First, I choose the Fourier sine series

$$y_n(t_{\mathrm{E}}') = \sqrt{\frac{2}{t_{\mathrm{E}}}} \sin\frac{n\pi t_{\mathrm{E}}'}{t_{\mathrm{E}}} \tag{2.93}$$

for the decomposition of the variation. One may check that these form an orthonormal eigenbasis for the operator $(-\partial_{t_{\mathrm{E}}'}^2 + \omega^2)$. The corresponding eigenvalues are

$$\lambda_n = \omega^2 + \frac{n^2\pi^2}{t_{\mathrm{E}}^2} \; . \tag{2.94}$$

The product of all eigenvalues is divergent. However, the divergence is canceled by factors which I have collectively absorbed into the normalization constant N. Let me separate off the divergent part of the product and write

$$\prod_n \lambda_n^{-1/2} = \prod_n \left(1 + \frac{\omega^2 t_{\mathrm{E}}^2}{n^2\pi^2}\right)^{-1/2} \prod_n \left(\frac{t_{\mathrm{E}}^2}{n^2\pi^2}\right)^{1/2} = \sqrt{\frac{\omega t_{\mathrm{E}}}{\sinh\left(\omega t_{\mathrm{E}}\right)}} \prod_n \left(\frac{t_{\mathrm{E}}^2}{n^2\pi^2}\right)^{1/2} \; . \tag{2.95}$$

The remaining product, as well as N, are independent of ω. Therefore a comparison with the case of the free particle, which is obtained for the limit $\omega \to 0$, allows one to fix

$$N \prod_n \left(\frac{t_{\mathrm{E}}^2}{n^2\pi^2}\right)^{1/2} = (2\pi\hbar t_{\mathrm{E}})^{-1/2} \; , \tag{2.96}$$

see, for instance, [48]. For large t_{E}, one obtains

$$\sqrt{\frac{\pi\hbar}{\omega}} N \left[\det\left(-\partial_{t_{\mathrm{E}}'}^2 + \omega^2\right)\right]^{-1/2} \simeq e^{-\omega t_{\mathrm{E}}/2} \; . \tag{2.97}$$

An alternative derivation of this formula is found in [47]. As expected,

$$\psi_{t_{\mathrm{E}}}(x_2) = \psi_0(x_2) e^{-\omega t_{\mathrm{E}}/2} \; , \qquad \text{(no tunneling)} \tag{2.98}$$

and under the analytic change back to $t = t_{\mathrm{E}}/i$ the state behaves exactly like the harmonic oscillator ground state. This is as yet not surprising, because I have so far assumed that the quadratic expansion of the potential is appropriate for *all purposes*, and therefore the tunneling can of course not be seen.

If I now consider the case of the full potential V as shown in fig. 2.5, then the classical paths described above are no longer the *unique* classical trajectories which connect the two points x_1 and x_2. Consider for instance a particle sitting on the "hilltop" x_0 of the inverted potential. If the particle rolls off to the right, it does not run away to very large distances. It will climb up on the other side of the inverted barrier only until it reaches x_b. Then it returns on a reverse trajectory and comes back to x_0. This semiclassical path is called the *bounce*.

With the use of the bounce, new approximate[9] stationary points of the action can be constructed. For instance, starting from a path as used in the previous discussion, one can insert a bounce anywhere along the intermediate segment, where the particle loiters at the hilltop. In fact, one can insert any number of bounces, placed at random locations on the time axis. All these possibilities have to be summed over in the path-integral. Note that a single bounce only has a short duration compared to the long period of time which the particle spends at the hilltop. The summation can therefore be done in a *dilute gas approximation* as follows. For each bounce it contains, the action of a path has to be increased by the action of a single bounce $\mathcal{S}_{\mathrm{E}}^{(\mathrm{b})}$. Also the determinantal factor in eq. (2.88) has to be corrected. Following Coleman [47], let me assume that the correction can be written as

$$\left[\det\left(-\partial_{t_{\mathrm{E}}'}^2 + \partial_{\bar{x}}^2 V\right)\right]_{(n \text{ bounces})}^{-1/2} = \left[\det\left(-\partial_{t_{\mathrm{E}}'}^2 + \omega^2\right)\right]^{-1/2} K^n \; , \tag{2.99}$$

---

[9] For an explanation concerning the appearance of approximate stationary points, please refer to Coleman's writings [47].

where K can be defined by demanding that this formula is correct for the case of a single bounce. For n bounces centered at $t_{\mathrm{E}}^{(1)}, \ldots, t_{\mathrm{E}}^{(n)}$, one has to integrate over their locations within the time interval t_{E}:

$$
\int_0^{t_{\mathrm{E}}} dt_{\mathrm{E}}^{(1)} \int_0^{t_{\mathrm{E}}^{(1)}} dt_{\mathrm{E}}^{(2)} \ldots \int_0^{t_{\mathrm{E}}^{(n-1)}} dt_{\mathrm{E}}^{(n)} = \frac{t_{\mathrm{E}}^n}{n!} \ . \tag{2.100}
$$

Having said this, it should be noted that the time translations of the bounces are associated with a solution of eq. (2.87) with zero eigenvalue. This seems to be a problem because the corresponding Gaussian integral would diverge. However, the integral of eq. (2.100) is the correct way of treating this variation of the path, and therefore the zero eigenvalue should be omitted from the determinant. A more careful consideration, see *e.g.* [47], shows that one has to include a factor of $(\mathcal{S}_{\mathrm{E}}^{(\mathrm{b})}/2\pi\hbar)^{1/2}$ coming from the Jacobian associated with the change of variables from an integration over dc_0 to an integration over dt_{E}, *i.e.* one should replace

$$
\left[\det\left(-\partial_{t_{\mathrm{E}}'}^2 + \partial_{\bar{x}}^2 V\right)\right]^{-1/2} \rightarrow \left(\frac{\mathcal{S}_{\mathrm{E}}^{(\mathrm{b})}}{2\pi\hbar}\right)^{1/2} \left[\det'\left(-\partial_{t_{\mathrm{E}}'}^2 + \partial_{\bar{x}}^2 V\right)\right]^{-1/2} \ , \tag{2.101}
$$

where $\det'$ denotes the determinant with the zero eigenvalue omitted. Therefore

$$
K = \left(\frac{\mathcal{S}_{\mathrm{E}}^{(\mathrm{b})}}{2\pi\hbar}\right)^{1/2} \left[\frac{\det\left(-\partial_{t_{\mathrm{E}}'}^2 + \omega^2\right)}{\det'\left(-\partial_{t_{\mathrm{E}}'}^2 + \partial_{\bar{x}}^2 V\right)}\right]^{1/2} \ . \tag{2.102}
$$

The evolution of the state finally follows as

$$
\psi_{t_{\mathrm{E}}}(x_2) \simeq \psi_0(x_2) e^{-\omega t_{\mathrm{E}}/2} \sum_n \frac{K^n e^{-n\mathcal{S}_{\mathrm{E}}^{(\mathrm{b})}/\hbar} t_{\mathrm{E}}^n}{n!} = \psi_0(x_2) \exp\left[\left(K e^{-\mathcal{S}_{\mathrm{E}}^{(\mathrm{b})}/\hbar} - \frac{\omega}{2}\right) t_{\mathrm{E}}\right] \ . \tag{2.103}
$$

At this point, the reader may be puzzled about the significance of this result, because the correction due to bounces goes to zero faster than any power of $\hbar$, and is therefore smaller than the terms of order $\hbar$ which have been neglected in the semiclassical approximation throughout. However, as I will show now, it turns out that K in this formula is imaginary. Reverting back to $t = t_{\mathrm{E}}/i$, this means that the wavefunction is decaying, and the correction I have computed is the leading order of the decay.

To see that K is imaginary, consider first the eigenfunction of zero eigenvalue in the spectrum of $(-\partial_{t_{\mathrm{E}}'}^2 + \partial_{\bar{x}}^2 V)$, where $\bar{x}$ now is a solution which contains a single bounce. As said before, the variations of the path associated with the zero eigenvalue correspond to translations of the bounce along the time axis, since such translations leave the action unchanged. The eigenfunction therefore is proportional to $\partial_{t_{\mathrm{E}}'}\bar{x}$, the generator of translations. Simply by inspecting the trajectory of the bounce, *cf.* ④ in fig. 2.5, it is clear that this eigenfunction has a single node. Therefore, as Coleman also points out in [47], there has to be a nodeless eigenfunction with lower eigenvalue. That is, there is a single negative eigenvalue.

It looks as if this should be a problem, since a negative eigenvalue should give a diverging Gaussian integral in the derivation of eq. (2.88). In order to make the path-integral convergent, one has to make an analytic continuation. Following again Coleman's approach, let me consider a path in function space parametrized by a real variable z. The path is chosen such that it goes through two stationary points of the action: at $z = 0$, it goes through the stationary point $x(t_{\mathrm{E}}) = x_0$, while at $z = 1$ it goes through the bounce. Moreover, the tangent vector to the path at $z = 1$ is proportional to y_0, the eigenfunction associated with the negative eigenvalue. Therefore, the path goes through the bounce in
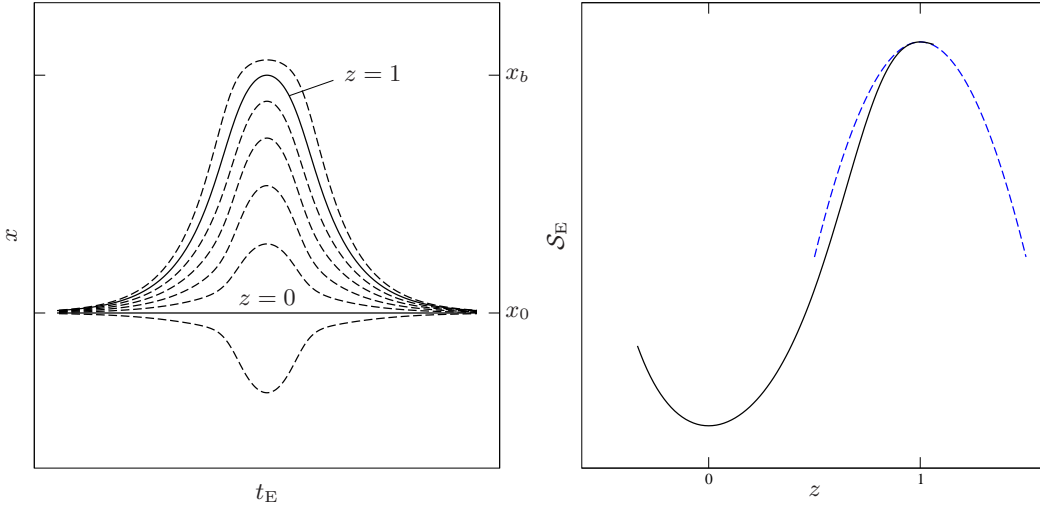
Figure 2.6: Sketch of a path through function space parametrized by a real variable z (left panel). The path goes through the stationary points $x(t_\mathrm{E}) \equiv x_0$ at $z = 0$ and the bounce at $z = 1$. The Euclidean action has a saddle point at $z = 1$, and the path goes through this saddle point in the "dangerous" direction where the sectional curve has negative curvature (right panel). The dashed blue line shows the parabolic fit to the sectional curve at the saddle point, which is used to compute the contour integral in the saddle point approximation. In order to make the integral convergent, the contour has to be deformed into the complex z plane.

the most dangerous direction, and $z = 1$ is a maximum of $\mathcal{S}_\mathrm{E}$. The situation is illustrated in fig. 2.6.

In order to make the integral over this contour in function space convergent, one has to deform the contour into the complex plane – that is, one has to make an analytic continuation to complex z. For instance, one can lead the contour along the real line from $-\infty$ to $z = 1$, the saddle point, and then out into the imaginary direction. The fact that one sums over complex trajectories should not be given too much physical meaning, this is merely another analytic method of computation. The integral is now convergent, and one can close the contour in the upper half-plane. Clearly, the integral now has an imaginary part, and in the saddle point approximation one obtains

$$\mathrm{Im} K = \frac{1}{2} \left(\frac{\mathcal{S}_\mathrm{E}^{(\mathrm{b})}}{2\pi\hbar} \right)^{1/2} \left| \frac{\det\left(-\partial_{t_\mathrm{E}'}^2 + \omega^2\right)}{\det'\left(-\partial_{t_\mathrm{E}'}^2 + \partial_{\bar{x}}^2 V\right)} \right|^{1/2} . \tag{2.104}$$

The factor $1/2$ arises because the integration is only over half of a Gaussian. Of course, in order to obtain the above result, one also has to integrate over all variations orthogonal to the contour. At the stationary points, these directions only involve positive (or zero) eigenvalues and can therefore be treated as before.

Finally, putting everything together and making the analytic change back to $t = t_\mathrm{E}/i$, one finds following semiclassical approximation for the decay rate[10]:

$$\Gamma \equiv -\left. \frac{\partial_t \left|\psi_t(x)\right|^2}{\left|\psi_t(x)\right|^2} \right|_{x \approx x_0} = \left(\frac{\mathcal{S}_\mathrm{E}^{(\mathrm{b})}}{2\pi\hbar} \right)^{1/2} \left| \frac{\det\left(-\partial_{t_\mathrm{E}'}^2 + \omega^2\right)}{\det'\left(-\partial_{t_\mathrm{E}'}^2 + \partial_{\bar{x}}^2 V\right)} \right|^{1/2} e^{-\mathcal{S}_\mathrm{E}^{(\mathrm{b})}/\hbar} . \tag{2.105}$$

The determinantal factor is usually very hard to compute even in the simplest scenarios. One therefore often is content with an estimate for the exponential factor. Using eq. (2.83),

---

[10]The derivation of this formula finally also gives a justification for eq. (2.50).

the Euclidean action of the bounce can be expressed as

$$\mathcal{S}_{\mathrm{E}}^{(\mathrm{b})} = 2 \int_{x_0}^{x_b} d\bar{x} \sqrt{2V(\bar{x})} \ . \tag{2.106}$$

Reassuringly, the exponential factor which governs the semiclassical decay rate is the same as the one obtained from the WKB estimate given in eq. (2.28).

Let me finally comment on some properties of the bounce. First of all, it is a mathematical object which has the structure of a localized excitation, similar to a "particle" if one reinterprets x as some direction in field space instead of position space. On this account, and because they are actually structures in (Euclidean) time, such solutions are called *instantons*. Being a solution of the Euclidean equations of motion, it is actually the *analytic continuation* of a classical path into the classically forbidden region. For instance, consider eq. (2.83). Going back to "Lorentzian" time t, one sees that the bounce is still a solution of the classical equations of motion, yet with an *imaginary momentum*. Furthermore, as the bounce reaches x_b, it can be smoothly connected to the classical trajectory of a particle emerging from x_b, which is the classical turning point. This property, and the interpretation that the bounce is the analytic continuation of the classical path through the forbidden region, will be very useful in the following sections.

2.3.2 Instantons in Quantum Field Theory

The power of the method to compute semiclassical decay rates with the use of instantons is that it can straightforwardly be generalized to QFT. Its application to the problem of false vacuum decay was pioneered by Sidney Coleman himself in a seminal paper [31]. I will just report on the main aspects here.

The field-theoretic problem is the one presented in section 2.2.1. For definiteness, let me consider the theory of a single scalar field ϕ with action (1.13), where the potential has a shape as shown in fig. 2.7. Furthermore, let me assume that the field is initially in a homogeneous configuration with $\phi(x) = \phi_+$. I want to compute the semiclassical decay rate into a state where a bubble of true vacuum has spontaneously appeared. Gravitational effects shall be ignored for the time being, such that I will work in Minkowski space and its Euclidean version, which is simply $\mathbb{R}^4$ with the Euclidean metric.

As before, the decay process is governed by a stationary point of the Euclidean action

$$\mathcal{S}_{\mathrm{E}} = \int d^3x \, dt_{\mathrm{E}} \left[\frac{1}{2} \partial_a \phi \partial^a \phi + V(\phi) \right] \ . \tag{2.107}$$

Note that the use of Euclidean time changes the metric signature, such that the Minkowski metric $\eta_{\mu\nu}$ is replaced by the metric δ_{ab} of four-dimensional Euclidean space. The trivial false vacuum solution $\phi \equiv \phi_+$ has vanishing action and is the dominant stationary point if one starts in this configuration. The decay into a state with a bubble of true vacuum is governed by non-trivial stationary points which contain some region where ϕ is close to the true vacuum value ϕ_-. The dominant stationary point is the one with the smallest action – contributions of stationary points with larger Euclidean action are exponentially suppressed. At least in the thin-wall limit, where the true and false vacuum domains are separated by a thin surface layer, it is quite clear that the smallest action is obtained for a configuration which is spherically symmetric. It can actually be shown that this is generally the case in single field models [49].

Let me denote the Euclidean distance to the symmetry point with χ,

$$\chi \equiv \sqrt{t_{\mathrm{E}}^2 + \mathbf{x}^2} \ . \tag{2.108}$$

A configuration is spherically symmetric if ϕ is a function only of χ. In addition, if the

Figure 2.7: Scalar field potential with two minima. The field value ϕ_+ at the minimum with the larger value of the potential corresponds to the false vacuum, whereas ϕ_- denotes the true vacuum. The potential has been shifted such that $V(\phi_+) \equiv 0$.
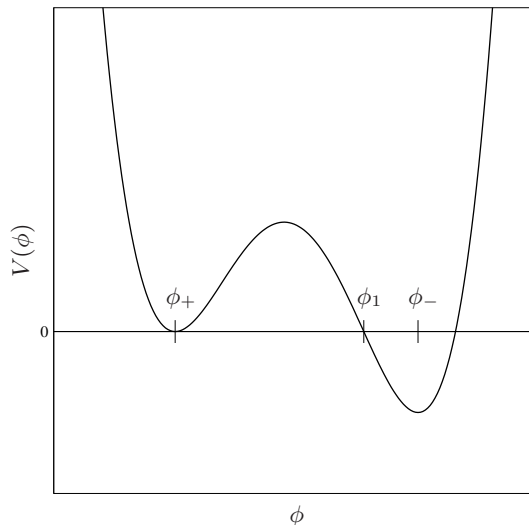
action is to be stationary, then ϕ has to obey the Euler-Lagrange equation

$$\partial_\chi^2 \phi + \frac{3}{\chi} \partial_\chi \phi = \partial_\phi V \ . \tag{2.109}$$

The instanton which is relevant for the decay of the false vacuum is a configuration which is close to the true vacuum at $\chi = 0$ and asymptotes to the false vacuum ϕ_+ as $\chi \to \infty$. A regular solution furthermore has to have

$$\partial_\chi \phi \mid_{\chi=0} = 0 \ . \tag{2.110}$$

In a potential as in fig. 2.7, a solution with these boundary conditions always exists, as can be seen by following argument. Consider the one parameter family of solutions of eq. (2.109) with the boundary conditions (2.110) and $\phi(0) = \phi_0$, where ϕ_0 is the free parameter. If ϕ_0 is chosen far enough to the left of ϕ_- in fig. 2.7, then ϕ will never reach the value ϕ_+ because it does not acquire enough momentum – one says the field *undershoots*. This is definitely true for initial values ϕ_0 somewhat to the left of ϕ_1. On the other hand, by choosing ϕ_0 close enough but still to the left of ϕ_-, one can arrange that ϕ loiters very close to ϕ_- up to an arbitrary large distance χ. Then, however, the friction term in eq. (2.109) can be neglected and the field will finally roll across the inverted barrier without significant loss and reach ϕ_+ with excess momentum – the field *overshoots*. By continuity, there has to be an initial value ϕ_0 between ϕ_1 and ϕ_- for which the field approaches the false vacuum with asymptotically vanishing momentum[11].

As before, the instanton obtained this way is called the *bounce*. In the thin-wall approximation, its Euclidean action can in fact be computed in closed form. With parameters ϵ and σ for the volume and surface energy as in section 2.2.1, a solution with a spherical region of radius χ_{wall} has an action of

$$\mathcal{S}_{\text{E}} = 2\pi^2 \chi_{\text{wall}}^3 \sigma - \frac{1}{2}\pi^2 \chi_{\text{wall}}^4 \epsilon \ . \qquad \text{(thin-wall approximation)} \tag{2.111}$$

Here, the volume and surface integrals are carried out in Euclidean $\mathbb{R}^4$. The action is stationary for $\chi_{\text{wall}} = 3\sigma/\epsilon$. The action of the bounce, in the thin-wall limit, is therefore

$$\mathcal{S}_{\text{E}}[\phi_{\text{bounce}}] = \frac{27\pi^2\sigma^4}{2\epsilon^3} \ . \tag{2.112}$$

---

[11]The original version of this argument was given by Coleman in [31]. Note that it is difficult to find a similar argument in case of a multidimensional field space, and it may be possible that there exist some examples where no instanton can be constructed.

The corresponding decay rate is in perfect agreement with the WKB estimate of eq. (2.29).

The action of the bounce is invariant under the entire group of four-dimensional translations. This corresponds to four variations of the path with zero eigenvalue. The zero eigenvalues have to be treated in the same way as in the case of one-dimensional quantum mechanics explained in the previous section, see [32]. Since now four eigenvalues have to be omitted from the determinant, and the eigenvalues have the dimension of length^{-2}, the decay rate turns out to have the dimension length^{-4} = time^{-1} × length^{-3}. Note that three of the zero eigenvalues are associated to the integrations over the spatial volume. This is actually a good thing, because the probability for a bubble of true vacuum to appear should not only be proportional to the waiting time, but also to the observed volume. The decay rate therefore gives the number of events *per unit time interval* and *per unit volume element*.

The bounce in the field-theoretic context also has some interesting properties, analogous to the ones found in the previous section, which I want to point out now. To begin with, it is a configuration of the field in four-dimensional Euclidean space. One of the dimensions is the result of an analytic continuation to imaginary time. Therefore, slices of constant Euclidean time t_{E} correspond to configurations in the classically forbidden region of configuration space. These configurations, stacked along the Euclidean time direction, smoothly interpolate between the false vacuum configuration and the configuration containing a critical bubble. Indeed, a maximal slice through the bounce corresponds to the configuration at the classical turning point. This can be seen by noting that on the maximal slice, $\partial_{t_{\mathrm{E}}}\phi \equiv 0$, and therefore one can revert back to Lorentzian time to obtain a configuration with zero momentum. The field then propagates according to the classical equations of motion into the classically allowed region of configuration space. However, since the Lorentzian equations of motion are related to the Euclidean ones simply by analytic continuation, and since the bounce is a solution to the Euclidean equations, one can obtain the classical evolution partially from the bounce by continuing $t_{\mathrm{E}} \to it$. Outside the lightcone of the nucleation event ($\mathbf{x} = \mathbf{0}, t = 0$), the evolution is simply given as

$$\phi_{\mathrm{class}}(\mathbf{x}, t) = \phi_{\mathrm{bounce}}(\chi = \sqrt{\mathbf{x}^2 - t^2}) \ . \qquad (2.113)$$

The $O(4)$-symmetry of the bounce therefore continues to an $O(3,1)$-symmetry of the Lorentzian solution. Within the lightcone of the nucleation event, the solution has to be extended to imaginary values of χ. Note that this continuation simply turns eq. (2.109) into its Lorentzian counterpart. The field rolls from ϕ_0 towards the true vacuum and begins to perform damped oscillations around ϕ_- until its kinetic energy has dissipated.

2.3.3   Gravitational Instantons

Let me finally take the effect of gravity into account. Instanton methods have proven to be very useful for this purpose, which underlines once again the power of the concept. Gravitational effects have been studied in the context of vacuum decay again by Sidney Coleman, who published an influential paper on this topic [33] together with Frank De Luccia. Again, I will only summarize the main aspects here.

Basically, to include gravity in the picture, all one has to do is to add the Einstein-Hilbert term to the action and also treat the metric as a dynamical component of the system. At this point, a first important remark is in order. In the previous cases where gravity was ignored, I always had the freedom to make a constant shift of the potential in order to arrange that the potential is zero in the false vacuum. This is no longer the case when gravity is taken into account, because a shift of the potential is equivalent to a redefinition of the cosmological constant in the Einstein-Hilbert term, which, of course, leads to physical consequences. In fact, one can turn the argument around and say that the cosmological constant can actually be absorbed into the potential, but that the absolute scale of the potential is now physically relevant. The value of the potential in a local

minimum can then be interpreted as the effective vacuum energy (the effective cosmological constant) in the corresponding vacuum configuration.

This point of view lies at the heart of some approaches towards an understanding of the cosmological constant. As I have noted already in section 1.1, the apparent vacuum energy density of the ΛCDM concordance model has a very peculiar value, being tiny by all standards of particle physics yet different from zero. In a sufficiently complicated potential *landscape* with a vast number of local minima and, correspondingly, a vast number of possible values of the effective vacuum energy, it seems plausible that a value like the observed one can be accommodated. The question about the value of Λ is then restated as the question of which vacuum configuration an observer is likely to find her cosmic neighborhood in. I will deepen this viewpoint in chapter 3.

In order to discuss the implications of gravity, let me turn back to the simple scenario presented in the last section which shall now be augmented by the Einstein-Hilbert term in the action. If the false vacuum has finite vacuum energy, then the action of the false vacuum configuration itself does not vanish. Let me assume that I know how to compute the Euclidean action in the presence of gravity – I will come to this point shortly. The bounce, being a well-localized object in a "sea" of false vacuum, differs in action from the false vacuum configuration only in a well-localized region. Going once again through the derivation of eq. (2.105), it is obvious that the exponential factor which governs the decay rate has to be replaced by

$$\Gamma \sim e^{-\left(\mathcal{S}_{\mathrm{E}}^{(\mathrm{b})} - \mathcal{S}_{\mathrm{E}}^{(+)}\right)} \ , \tag{2.114}$$

where $\mathcal{S}_{\mathrm{E}}^{(+)}$ is the action of the false vacuum configuration, and I have returned to the convention of setting $\hbar = 1$. The tunneling is suppressed by the *extra* amount of action it costs to go from the false vacuum configuration to the critical bubble.

The Euclidean action for gravity is obtained by making a formal analytic continuation of the metric to Euclidean signature $(++++)$. Recalling that I have defined $\mathcal{S}_{\mathrm{E}} = -i\mathcal{S}$, this leads to

$$\mathcal{S}_{\mathrm{E}} = \int d^4 x_{\mathrm{E}} \sqrt{\gamma} \left[\frac{1}{2} \partial_a \phi \partial^a \phi + V(\phi) - \frac{1}{2\kappa} \mathcal{R} \right] \ , \tag{2.115}$$

where γ is the Euclidean metric, $\mathcal{R}$ is the associated Ricci scalar, and I have introduced $\kappa \equiv 8\pi G$ to keep track of gravitational effects. I have absorbed the cosmological constant into the potential, which now has $V(\phi_+) = \Lambda_+/\kappa$, where Λ_+ is the *effective* cosmological constant in the false vacuum.

I now generalize the construction of $O(4)$-symmetric classical solutions by imposing the $O(4)$-symmetry on both the metric field and the scalar matter. The Euclidean line element therefore takes the form

$$ds_{\mathrm{E}}^2 = \gamma_{ab} dx_{\mathrm{E}}^a dx_{\mathrm{E}}^b = d\chi^2 + \rho^2(\chi) d\Omega_3^2 \ , \tag{2.116}$$

where $d\Omega_3$ is the line element on the unit three-sphere. As before, χ measures the distance from the symmetry point and ϕ, as well as ρ, are assumed to be functions only of χ. Under this symmetry reduction, the scalar field equation reduces to

$$\partial_\chi^2 \phi + 3 \frac{\partial_\chi \rho}{\rho} \partial_\chi \phi = \partial_\phi V \ . \tag{2.117}$$

Furthermore, the $\chi\chi$-component of Einstein's equation reads

$$(\partial_\chi \rho)^2 = 1 + \frac{\kappa}{3} \rho^2 \left[\frac{1}{2} (\partial_\chi \phi)^2 - V(\phi) \right] \ , \tag{2.118}$$

and the remaining components are redundant. The above two equations are a set of coupled ordinary differential equations for the two functions ϕ and ρ.

Consider first the false vacuum solution. In this case, $\phi(\chi) = \phi_+$ is a trivial solution to eq. (2.117). Moreover, eq. (2.118) can readily be solved:

$$\rho(\chi) = H_+^{-1} \sin(H_+\chi) \ , \qquad\qquad (2.119)$$

where $H_+ \equiv \sqrt{\Lambda_+/3}$, and I have assumed that Λ_+ is non-negative. Evidently, the Euclidean geometry is that of a four-sphere with radius H_+^{-1}. It is also evident from the definition of Λ_+ and H_+ that the limit of weak gravity corresponds to the limit of small H_+, and therefore, large radius of the Euclidean geometry. I will now argue that, at least in this limit, it is always possible to construct an $O(4)$ symmetric bounce.

As before, the bounce is a non-trivial solution to the equations of motion with the boundary condition $\partial_\chi\phi|_{\chi=0} = 0$ and $\phi(0) = \phi_0$ somewhere on the true vacuum side of the barrier. The initial condition for ρ is $\rho(0) = 0$ at the symmetry point, which I will call the *south pole* of the Euclidean geometry. If gravity is weak, then the presence of the bounce will only have a mild effect on the geometry, and at the same time, the volume of the geometry will be enormous. However, the geometry closes at some very large $\chi = \chi_{\max} \simeq H_+^{-1}\pi$, which I shall call the *north pole*. In order to obtain a field configuration which is regular on the entire geometry, and in particular at the north pole, one has to meet the new requirement

$$\partial_\chi\phi|_{\chi=\chi_{\max}} = 0 \ , \qquad\qquad (2.120)$$

which now replaces the boundary condition that ϕ has to approach the false vacuum with asymptotically vanishing momentum. Clearly, these two conditions become equivalent in the limit of $\kappa \to 0$ where the geometry becomes infinitely large. Repeating the argument about overshooting and undershooting with some obvious modifications it can be shown that there exists a solution which complies with the boundary conditions also at least for some range of small but non-vanishing κ.

The bounce obtained this way is known as the *Coleman-De Luccia instanton*. Using the thin-wall approximation, Coleman and De Luccia were able to construct explicit solutions and estimate the effect of gravity on the tunneling formula (2.114).

The Coleman-De Luccia instanton has following qualitative structure. Starting at the south pole, the field is initially very close to the true vacuum minimum and remains almost stationary out to some distance χ_{wall}. The geometry inside this region is well approximated by a spherical cap cut from a four-sphere with radius H_-^{-1}, where $H_-^2 \equiv \Lambda_-/3 \equiv \kappa V(\phi_-)/3$ characterizes the effective energy density in the true vacuum. I assume that this is also non-negative. Roughly at χ_{wall}, the field rolls through the inverted barrier and approaches the false vacuum. In the thin-wall approximation, this happens within a fairly short interval $\Delta\chi$. Beyond the wall region, the field is very close to the false vacuum and remains almost stationary until the geometry closes at $\chi_{\max}$, the north pole. The geometry of this region is well approximated by the false vacuum four-sphere, barring the spherical cap replaced at the south pole. A sketch of this geometry is shown in fig. 2.8.

As the gravitational coupling becomes larger, meaning that the energy scale of the scalar potential becomes larger in terms of Planck units, the volume of the false vacuum geometry decreases. Although the critical bubble radius is also subject to gravitational corrections, it is clear that at some point the critical bubble will no longer fit into the geometry. The Coleman-De Luccia instanton then ceases to exist. The decay of the false vacuum is still possible, however, it does no longer occur dominantly in form of bubble nucleation. It has been understood that a new type of instanton then becomes responsible for the transition, known as the *Hawking-Moss instanton* [50]. Roughly speaking, this process corresponds to a *thermal excitation* which takes the field within an entire horizon volume across the barrier. This is possible due to the thermal nature of de Sitter space [51].

Strictly speaking, the tunneling formula (2.114) can only be justified in the way presented here if the thin-wall approximation is valid. Relaxing this approximation, one sees

Figure 2.8: Sketch of the geometry of a four-dimensional Coleman-De Luccia instanton, embedded into flat five-dimensional $\mathbb{R}^5$. The picture shows a three-dimensional maximal section through the embedding, going through the two poles of the instanton – meridians and circles of latitude indicate the three-dimensional shape. At the south pole (left-hand side), the geometry roughly consists of a spherical cap cut from a four-sphere with radius H_-^{-1}. This is the true vacuum region. It is bounded by the "bubble wall," a layer in which the field crosses the potential barrier and approaches the false vacuum (see lower panel). The latter takes ~~up most of the re-~~ maining geometry, which is well approximated by a four-sphere of radius H_+^{-1} from which a spherical cap has been removed. The potential of the scalar field was chosen as in fig. 2.7, with $\Lambda_+ = 3\Lambda_-$. The potential energies were chosen to be relatively large, $\Lambda_- = 1.5 \times 10^{-3}$ (in Planck units), in order to emphasize the gravitational effect.
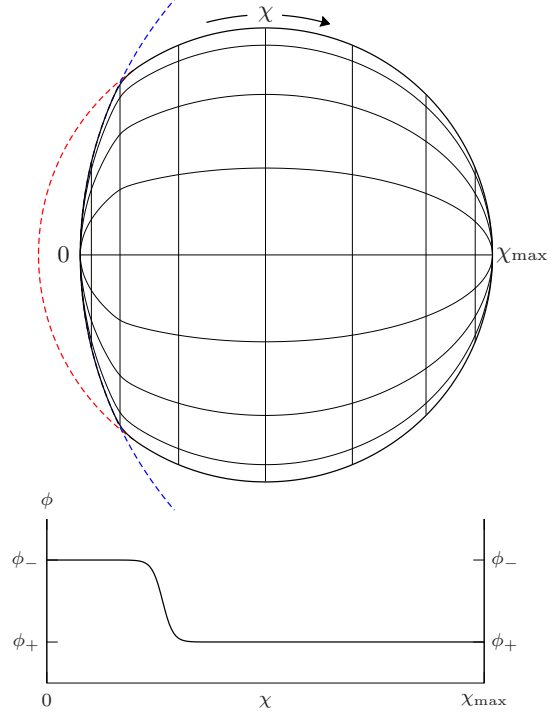
that the bounce is actually *not* localized within some small region of the Euclidean geometry, and that the field on the bounce solution is *nowhere* in the false vacuum configuration. In this case, a more elaborate derivation of eq. (2.114) is required, as has been presented in [52].

Let me finally explain how the one-bubble spacetime is obtained as an analytic continuation of the Coleman-De Luccia instanton, in the region of parameter space where it exists and represents the dominant decay channel. As before, a turning-point configuration can be obtained from a maximal section of the bounce. In this case, this prescription does not only specify the field configuration at the classical turning point, but also the geometry of the spacelike hypersurface. This input can be used as initial data to solve the Cauchy problem in the classically allowed region of configuration space. However, since the classical equations of motion are related to the Euclidean ones by analytic continuation, part of the work has already been done by constructing the Euclidean bounce. In particular, one can obtain the solution outside the lightcones of the nucleation point of the bubble (the south pole) and its antipode (the north pole) simply by replacing the three-sphere factor in eq. (2.116) by its Lorentzian analog, which is a timelike hyperboloid in Minkowski space:

$$ds^2 = d\chi^2 + \rho^2(\chi) \left[-d\tau^2 + \cosh^2\tau \, d\Omega^2 \right] \, . \tag{2.121}$$

Here, as usual, $d\Omega^2$ is the line element on the unit two-sphere.

In order to construct the inside of the lightcone of the nucleation event (or its antipode), one has to make an analytic continuation of χ. As before, this means that one has to solve the Lorentzian versions of eqs. (2.117) and (2.118) with initial conditions $\rho = 0$, $\partial_\chi \phi = 0$ and $\phi = \phi(0)$ ($\phi = \phi(\chi_{max})$ for the antipode). With $\chi = it$, the metric in the lightcone of the nucleation point is

$$ds^2 = -dt^2 + \rho^2(it) \left[dr^2 + \sinh^2 r \, d\Omega^2 \right] \, , \tag{2.122}$$

where the three-sphere now had to be replaced by the spacelike hyperboloid. Note that this is the metric of an open FRW universe with scale factor $a(t) \equiv \rho(it)$. Similarly, the

interior of the antipodal lightcone is covered by

$$ds^2 = -dt^2 + \rho^2(\chi_{\max} + it) \left[dr^2 + \sinh^2 r \; d\Omega^2 \right] \; . \tag{2.123}$$

Note that the entire classical geometry is free of physical singularities since the vanishing of ρ on the lightcones of the nucleation event and its antipode is a pure coordinate singularity. Furthermore, the $O(4)$-symmetry of the Euclidean bounce carries over to an $O(3,1)$-symmetry of the Lorentzian solution[12]. In a potential as the one of fig. 2.7, in particular when the thin-wall approximation is valid, the field inside the bubble is delivered in its new vacuum to very good accuracy. This means that the interior of the bubble is *empty*. However, it is possible to construct potentials for which the field is displaced from the true vacuum by an appreciable amount even at the center of the critical bubble. The evolution equations inside the lightcone then can lead to a period of slow-roll inflation followed by reheating and post-Big-Bang cosmology. In this setting, the symmetry of the one-bubble spacetime leads to an open FRW cosmology within the bubble. One therefore obtains an attractive scenario, known as *open inflation* [46], which could explain some non-vanishing (negative) curvature and at the same time comes with a precise prescription of "initial conditions," which are here determined by the dominant decay channel of the false vacuum. This is a first example where one sees that a deviation from flat ΛCDM cosmology is connected to a theory of initial conditions. In fact, most of the ideas I will present in chapter 3 are extensions of this scenario. The common premise is that our observable Universe is contained within such a bubble. Arranging for a long enough period of slow-roll inflation inside the bubble, one can always come to agreement with the ΛCDM model. As already pointed out in section 2.2, the exciting point is that there is room for introducing deviations in a *controlled way*.

2.4   The Measurement Problem

In this section, I want to make a comment about the interpretation of the tunneling rate Γ in false vacuum decay. A physically meaningful interpretation requires a prescription of how Γ can actually be *measured*. One could, for instance, consider an ensemble of classical measuring devices which somehow can monitor and identify the ambient vacuum configuration without significantly disturbing it. These devices should be distributed widely separated all over space, which is initially in a false vacuum configuration. Each device records the amount of time which elapses until it encounters a bubble of true vacuum. Assuming that a device is not destroyed by an encounter, one can imagine that the devices are read out after a very long time. The readings can be used to infer an average survival probability of the false vacuum along a worldline of a measuring device. Assuming, as additional idealizations, that the measuring devices are ideal observers and that the radius of a critical bubble is negligible, this survival probability can be directly related to the tunneling rate, see [53] for details. In the case of QFT on Minkowski background, this interpretation is equivalent to the one given in section 2.3.2: the decay rate Γ gives the average number of decay events per unit four-volume.

However, this measuring prescription relies on many idealizations. For instance, it is not straightforward to incorporate the effects of extended critical bubbles and extended bubble walls. Furthermore, in an expanding universe, it is impossible even *in principle* to read out a measuring device which is located outside of one's horizon. Therefore, the number of independent measurements is fundamentally limited. Under these conditions, Γ can only be measured to finite accuracy, and in a sense, the interpretation of its theoretic value becomes inherently approximate[13].

---

[12]This shows that the one-bubble solution is invariant under boosts, as was asserted in section 2.2.5.

[13]In order to really measure Γ, which is an exponentially small quantity, one would require exponentially many independent measurements. Clearly, this is in serious conflict with the fundamental limits already in cases of moderate expansion. Hence, Γ is no physical observable for nearly all practical purposes.

The situation is even worse if one takes into account the effect of gravity on the tunneling process itself. For instance, as I have shown, there are situations where the bounce geometry does not contain a false vacuum region at all. In this case, the entire horizon volume is affected by the quantum fluctuation. Since the quantum fluctuation also embraces the geometry itself, it seems impossible to sustain the classical description of a measuring device during the tunneling event. This means that there simply exists no classical device which could observe such a tunneling event, and hence no possibility to measure Γ.

This issue about interpretation is actually ubiquitous in quantum cosmology. In order to apply the usual interpretation schemes of quantum mechanics, one always needs classical measuring devices and the possibility to access an arbitrary large ensemble of identical quantum systems. In quantum cosmology, however, these systems are actually subsystems of a single large quantum system, the Universe. By definition, one always has access to only one single Universe. Furthermore, there are regions of configuration space where the classical description of *all* physical degrees of freedom breaks down, and therefore no measuring device can be defined. Hence, probability, as well as unitarity, become approximate concepts, only available in a semiclassical regime. This point of view has been elaborated in [54].

However, even in situations where the tunneling rate Γ as computed in the previous sections is no meaningful physical observable, because no adequate measurement can be carried out, this does not imply that the decay process itself is not a real physical phenomenon. It may be impossible for an observer living in a bubble universe to measure the rate at which similar universes are produced, but it is still conceivable that she can see some consequences of the tunneling event in her observational data. As said before, deviations from the ΛCDM concordance model can be linked to certain properties of the tunneling scenario, and it may therefore be possible to learn from observations if such a tunneling event is likely to have occurred in our past. The nature of deviations can even inform us about some basic characteristic features of the specific scenario which was physically realized. It is this eventuality which I wish to entertain in the following chapter.

Chapter 3

A Landscape to Discover

I have introduced all the tools which are necessary in order to study gravitational tunneling in the early Universe. Now I want to apply these tools in a framework which is *inspired* by some ideas stemming from string theory and supergravity theory. These theories have been developed as an attempt to unify GR with the quantum theory of particles or, more specifically, with supersymmetry. The primary aim of these approaches is to find a fundamental microscopic description of all interactions which is mathematically complete and consistent. At the current stage of their development, despite decades of strong efforts, these theories still appear to be *too microscopic* for the purpose of making testable predictions[1]. Nevertheless, their appealing mathematical properties still lend support to the hopes that one is somehow "on the right track."

Since even a tentative introduction into the subject of string theory would lead me too far away from the topic of this work, I can give only some heuristic arguments here. The ambitious reader who wants to learn more about the mathematical details has a large body of literature at his disposal. There also exist some textbook introductions, like *e.g.* [36].

One of the striking features of string and supergravity theories is the fact that their consistent formulation requires the introduction of *extra dimensions*. In other words, on top of the three spatial dimensions which are familiar from our every-day experience, the theory is formulated under the assumption that additional "hidden" dimensions exist. For instance, *M-theory* and *maximal supergravity* have a total of eleven dimensions. It can actually be considered as a very appealing feature that the number of dimensions can be fixed by the requirement of mathematical consistency. However, if these theories should have anything to do with reality, one needs to explain why our world appears to be only four dimensional.

In order to achieve this *dimensional reduction*, several approaches have been pursued. For instance, one can try to localize the fields of the standard model somehow on a $3 + 1$ dimensional submanifold, a so-called *brane*[2]. Another alternative is the *compactification* of the extra dimensions. The idea behind this approach is that the extra dimensions only have a very small volume and therefore can not be probed by present-day experiments. Roughly speaking, the Compton-wavelength of any particle which we can produce or measure is still much too large to fit into the extra dimensions, and therefore these directions are invisible to us. They only become "illuminated" at energies well beyond the reach of current technology.

It should not come as a surprise that there is no unique way of compactifying the extra dimensions. On the one hand, several mechanisms to achieve compactification dynamically

---

[1] For instance, in order to make contact with current collider experiments, one would typically have to extrapolate by more than ten orders of magnitude in energy scale.

[2] The term "brane" is derived from the word "membrane" and refers to a higher-dimensional analog thereof.

have been proposed. On the other hand, each proposal comes with a large number of different solutions which are characterized, for instance, by different sizes and shapes of the compact dimensions. From the point of view of the low-energy *effective* theory which should describe our present-day experiments, one can think of the characteristics of the compact dimensions, like sizes and shapes, as some additional fields, so-called *moduli*. The stable configurations of the moduli and any additional fields which may have to be introduced in order to achieve stabilization are called *string vacua*. There typically exists a vast number of such vacua in any string theory scenario with compactifications. In effect, these vacuum solutions are local minima of an *effective potential* for the moduli and stabilizing fields. This situation, where a potential has a complicated structure with many local minima in a high-dimensional field space, is often compared to the topography of a mountainous terrain, and one therefore speaks of the string theory *landscape*[3].

The existence of a vast number of possible vacuum configurations was found to have an upside in the context of understanding the cosmological constant. As I have explained in the last chapter, the potential energy at any local minimum gives rise to an *effective* cosmological constant. The value of vacuum energy can therefore be different in each individual vacuum, giving rise to a vast number of available values for Λ. Furthermore, gravitational tunneling in the landscape leads to the nucleation of bubbles containing new vacuum configurations, typically ones which have a lower vacuum energy than before. It has been argued in [56, 57] that this may lead to a *dynamical neutralization* of the cosmological constant, meaning that eventually some bubbles with nearly vanishing vacuum energy will appear. Anthropic arguments can then be used to give a "plausible explanation" for the observed value of the cosmological constant in our Universe.

Such an argument could be sketched as follows. Given that the Universe at some time is in some arbitrary vacuum state with some "natural" value of the cosmological constant, it will eternally inflate, but does not contain any observers in the inflating region. Sporadically, it will spawn new bubble-universes containing vacua of lower cosmological constant. These regions will also inflate and produce new bubbles, and so on. Now comes the anthropic argument, *cf.* [58, 59]. In order to support observers, that is, lifeforms capable of perceiving their environment and drawing reasonable conclusions from their observations, a bubble universe has to have a long enough era of matter domination to allow these lifeforms to develop. Therefore, lifeforms like ourselves only exist in bubbles where the effective cosmological constant is sufficiently small as not to terminate matter dominantion too early. Hence, any lifeform like ourselves will *inevitably* measure only a very small cosmological constant, despite the fact that a randomly chosen vacuum configuration typically has a cosmological constant vastly different from zero.

It has proven surprisingly hard to find a rigorous formulation of this argument which is scientifically acceptable. The problems are mostly connected to the notion of a "typical" observer within the infinite set which is supposedly realized in the Universe. For instance, many attempts to define a measure on observers run into the problem that they are dominated by so-called *freak observers* or *Boltzmann brains*. These are observers which spontaneously appear "out of thin air" as a result of thermal fluctuations within the eternally inflating regions. Despite being an incredibly rare occurrence, they can easily outweigh the biological lifeforms due to the exponentially replicating volume of the inflationary domain. These issues and some possible solutions are discussed *e.g.* in [60].

Yet, even if the problem of selection of the vacuum remains unsettled, it appears that the landscape paradigm offers such a large variety of possibilities that any value of the cosmological constant, in particular the one we observe in our Universe, can be accommodated. Furthermore, with the tunneling scenarios at hand, it is plausible that all these possibilities can also be realized simultaneously in different regions of the Universe. The global structure of the Universe then appears to be chaotic[4], with huge eternally inflating

---

[3]The term *landscape* was coined by Leonard Susskind, see [55].
[4]The scenario described here was proposed by Andrei Linde in [61] and is now known as *chaotic inflation*.

patches of various vacuum configurations which are continuously spawning new bubble-universes. It has been suggested that this self-replicating process eventually leads to a sort of steady state, where the chaotic structure of the Universe continues to reproduce itself in a self-similar fashion. In some sense, this idea nicely addresses the question about the state of the Universe if the steady state can be reached from quite arbitrary initial conditions. For an overview on the subjects of *eternal* and *chaotic inflation*, see *e.g.* [62] and references therein.

It is interesting to note that the only observational consequences of the landscape paradigm, if any exist at all, are connected to the tunneling scenario. As I have announced already, and I will demonstrate this in detail in the following, a tunneling event in our cosmological history can leave distinct signatures in our observations. In practice the observability depends on the amount of additional inflation which took place after the tunneling event. As pointed out in section 1.2, inflation drastically dilutes the information about its initial conditions, such that after some time the possibility to detect any traces thereof will be lost. Therefore, the scenarios which I will describe in this chapter will only have observable consequences if the period of inflation which ensues the tunneling event is sufficiently short. At this point it should be noted that observations so far seem to be in overall agreement with the ΛCDM model, which means that traces of initial conditions have not yet been conclusively detected. Solid evidence for a tunneling scenario can therefore only be found with the next generation of precision observations if the length of inflation lies within a fairly narrow window[5]. However, for the purpose of this work, I accept it as a plausible possibility that this is the case. Some support can again be found in anthropic reasoning, see for instance [63]. Furthermore, an exploration of the observational prospects in the landscape may also entail some useful lessons of conceptual relevance, *e.g.* for the purpose of model building.

In the following section 3.1, I will briefly explain a mechanism for compactification of extra dimensions. This sets the stage for vacuum transitions which connect string vacua corresponding to different compactification solutions. These transitions are the subject of section 3.2, where several examples will be given. Observational consequences of the tunneling scenarios will finally be discussed in section 3.3, with attention to a specific example.

3.1 Compactification of Extra Dimensions

A simple mechanism of dynamical compactification of extra dimensions was set forth by Peter Freund and Mark Rubin already some thirty years ago [64]. In many variations, this mechanism now generally is referred to as *flux compactification* and is the starting point of many studies in the context of the string landscape. A comprehensive review can be found, *e.g.*, in [65]. The philosophy behind this mechanism can be summarized as follows. As a first step, the high dimensional *fundamental* spacetime is written as a product manifold $\mathcal{ST}_d \times \mathcal{M}_{D-d}$, where D is the total dimensionality of the fundamental spacetime, $\mathcal{ST}_d$ is a d-dimensional spacetime of a lower-dimensional *effective* theory, and $\mathcal{M}_{D-d}$ is a microscopic compact manifold which takes up the "hidden" dimensions. This, however, is not a vacuum solution of the lower-dimensional effective theory if the size and shape of $\mathcal{M}_{D-d}$ is unstable under small perturbations. In order to achieve stabilization, one introduces additional fields, so-called *fluxes*. In a certain configuration, these fields will give rise to a restraining force which stabilize the moduli. Usually, it comes at no cost to assume that appropriate fields are present, as higher dimensional gauge theories can have a large number of gauge fields which are suitable for this purpose.

---

[5]Note that the possibility of a significant detection even has a fundamental limit if one can only probe a finite volume. Therefore, constraints cannot be tightened indefinitely by simply increasing the precision. Several observational probes will come close to their fundamental bound in the forseeable future, some even already with the next generation of experiments.

Let me illustrate this mechanism with a standard example, which is the basis of many simple scenarios as *e.g.* in [66, 67, 68]. The starting point is D-dimensional Einstein-Maxwell theory, which is described by the action

$$\mathcal{S}^{(D)} = \mathcal{S}_{\text{grav}}^{(D)} + \mathcal{S}_{\mathbf{F}}^{(D)} = \frac{1}{16\pi} \int d^D x \sqrt{-g} \left[\mathcal{R} - 2\Lambda - \mathbf{F}^2 \right] \ , \tag{3.1}$$

where Λ is the D-dimensional cosmological constant and $\mathbf{F}$ is a q-form field strength of a generalized Maxwell field. Note that, for $D = 4$ and $q = 2$, the theory reduces to conventional electromagnetism coupled to gravity in four spacetime dimensions.

Making the *ansatz* that the solution manifold has a q-dimensional spherical factor, the line element reads

$$ds_D^2 = g_{AB} dx^A dx^B = \gamma_{AB} dy^A dy^B + R^2(y^A) d\Omega_q^2 \ , \tag{3.2}$$

where γ_{AB} is the metric tensor of a d-dimensional spacetime manifold with coordinates y^A, and the radius of the q-sphere factor, R, may depend on these coordinates. Note that $D = d + q$ by definition. One can now specialize to the case where the q-form field strength is proportional to the volume form of the q-sphere,

$$\mathbf{F} = Q \sin^{q-1}\theta_1 \ldots \sin\theta_{q-1} d\theta_1 \wedge \ldots d\theta_q \ . \tag{3.3}$$

If Q is a constant, then $\mathbf{F}$ solves Maxwell's equations trivially. Furthermore, it is obvious that this solution is compatible with the symmetries of the metric *ansatz*.

Dimensional reduction of the theory is now achieved by integration over all the coordinates of the q-sphere, $\theta_1 \ldots \theta_q$. The action then reads

$$\mathcal{S}^{(d)} = \frac{V_q}{16\pi} \int d^d y \sqrt{-\gamma} R^q \left[\mathcal{R}_d + \frac{q(q-1)}{R^2} \left(1 + \partial_A R \partial^A R \right) - 2\Lambda - q! \frac{Q^2}{R^{2q}} \right] \ , \tag{3.4}$$

where $V_q \equiv \int d\Omega_q = 2\pi^{(q+1)/2}/\Gamma[(q+1)/2]$ is the volume of the unit q-sphere, $\mathcal{R}_d$ is the (Ricci) curvature scalar associated with the d-dimensional metric γ_{AB}, and an integration by parts was performed in order to remove second derivatives on R. Evidently, the theory has a d-dimensional effective description where a new scalar degree of freedom R appears, which is related to the volume modulus of the compact extra dimensions.

If $d > 2$ it is possible to apply a conformal transformation to the metric γ_{AB} in order to cancel the R-dependent factor in front of the curvature term. This transforms the action into the so-called *Einstein frame*. To this end, one writes

$$\gamma_{AB} = R^{-\frac{2q}{d-2}} \tilde{\gamma}_{AB} \ . \tag{3.5}$$

Under this transformation, the action reads

$$\mathcal{S}^{(d)} = \frac{V_q}{16\pi} \int d^d y \sqrt{-\tilde{\gamma}} \left[\tilde{\mathcal{R}}_d - \frac{q}{R^2} \frac{D-2}{d-2} \partial_A R \partial^A R + R^{-\frac{2q}{d-2}} \left(\frac{q(q-1)}{R^2} - 2\Lambda - q! \frac{Q^2}{R^{2q}} \right) \right] \ , \tag{3.6}$$

where $\tilde{\mathcal{R}}_d$ is the transformed (Ricci) curvature scalar, and second derivatives of R were again removed integrating by parts.

The modulus R of the compact manifold (the q-sphere) can take positive values only. It is therefore convenient to consider its logarithm, which can take any real value. Furthermore, with the definition

$$R = e^{\sqrt{\frac{8\pi(d-2)}{q(D-2)V_q}}\phi} \ , \tag{3.7}$$

the kinetic term of the logarithm ϕ is canonically normalized. The action then has the form

$$\mathcal{S}^{(d)} = \int d^d y \sqrt{-\tilde{\gamma}} \left[\frac{V_q}{16\pi} \tilde{\mathcal{R}}_d - \frac{1}{2} \partial_A \phi \partial^A \phi - V(\phi) \right] \ , \tag{3.8}$$

Figure 3.1: Effective potential $V(\phi)$ for the canonically normalized "modulus field" which describes the compactification radius. In the shown example, the compact manifold is a seven-sphere which leads to a dimensional reduction from eleven to four macroscopic dimensions ($q = 7$, $d = 4$, $D = d + q = 11$). The value of the eleven-~~dimensional cosmo~~logical constant was chosen as $\Lambda = 4$ (in eleven-dimensional Planck units). Depending on the quantum number Q of the magnetic flux, the effective potential can have a local minimum with negative or positive potential energy. However, for large values of Q, the local minimum disappears and no stable configuration exists.
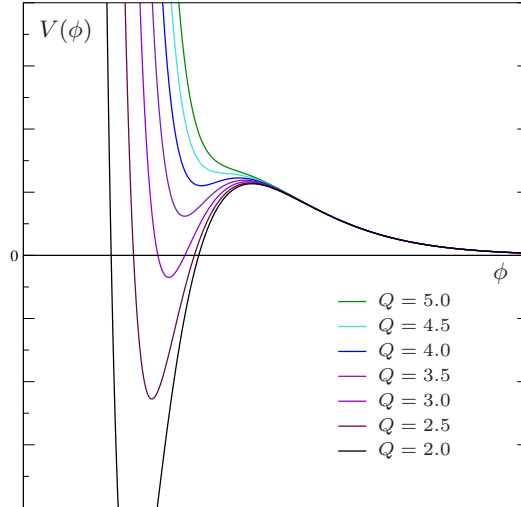
with

$$V(\phi) = \frac{V_q}{16\pi}\left[2\Lambda e^{-\sqrt{\frac{32\pi q}{(d-2)(D-2)V_q}}\phi} - q\left(q-1\right)e^{-\sqrt{\frac{32\pi(D-2)}{q(d-2)V_q}}\phi} + q!Q^2 e^{-\sqrt{\frac{32\pi q(d-1)^2}{(d-2)(D-2)V_q}}\phi}\right].$$

(3.9)

A plot of the effective potential $V(\phi)$ is shown in fig. 3.1 for an example where $D = 11$ and $q = 7$, such that the dimensionally reduced theory has $d = 4$. Independent of the choice of q or D, the potential has following qualitative structure. At very large ϕ, corresponding to large radius of the extra dimensions, the potential is always dominated by the Λ-term. For positive Λ, this term tends to inflate the extra dimensions. In fact, since the potential has an exponential shape, the d-dimensional effective theory has an asymptotic slow-roll attractor where the field ϕ rolls to infinity while the d-dimensional spacetime is subject to power-law inflation. One can show that this attractor solution, in the D-dimensional picture, corresponds to D-dimensional de Sitter space, which is an attractor whenever Λ dominates the energy density (no-hair conjecture).

At very small ϕ, corresponding to tiny radius of the extra dimensions, the flux term dominates, which is also repulsive. The only attractive term is the one associated with the curvature of the compact dimensions. It is relevant in an intermediate range of ϕ and leads to a dip in the potential. If the flux term is not too large, the dip gives rise to a local minimum at which the field ϕ, and thus the size of the compact dimensions, can be stabilized. This stable configuration is called a *compactification vacuum*. The value of the effective potential at the local minimum then corresponds to an effective vacuum energy in the compactification vacuum of the d-dimensional theory. Depending on the values of Λ and Q, this vacuum energy can be positive or negative. Note, however, that it is bounded from above for any fixed value of the fundamental cosmological constant Λ, because the local minimum disappears for large values of Q.

A positive value of the effective cosmological constant in the compactification vacuum leads to inflationary solutions in the d-dimensional theory. In particular, this means that the D-dimensional theory has a stable solution of the type $\mathrm{dS}_d \times \mathrm{S}_q$. A negative vacuum energy, on the other hand, leads to a Big Crunch in the d-dimensional spacetime.

It is noteworthy that the vacuum energy in the dimensionally reduced theory strongly depends on the "magnetic" charge Q. In a quantum theory of the field **F**, the flux will be quantized, such that Q has a discrete spectrum. It has been argued *e.g.* in [57] that, in a theory with many gauge fields with incommensurate elementary charges, the spectrum of available values for the effective cosmological constant in a compactification vacuum

is dense enough so that the observed value could be accommodated without further fine-tuning.

3.2   Transdimensional Tunneling

It is evident from the sketch in fig. 3.1 that the compactification vacuum, at least for the interesting case of non-negative effective vacuum energy, is metastable, because the field can tunnel through the potential barrier to the region where the potential tapers off to zero as ϕ becomes large. This "tapering off" for large sizes of the compact dimensions is actually a generic feature in compactification scenarios, see [69] for a detailed discussion. In this case, a tunneling event corresponds to the spontaneous nucleation of a bubble in which the radius of the compact dimensions lost its restraining force and starts to grow indefinitely. Therefore, the compact dimensions eventually become macroscopic, such that, for instance, particles can propagate freely in them. The lower-dimensional picture finally becomes obsolete, as the bubble-universe settles to a higher-dimensional vacuum. Consequently, this process has been termed *spontaneous decompactification*[6], *e.g.* in [70].

The inverse process, which corresponds to the spontaneous nucleation of a bubble containing a lower-dimensional compactification vacuum within a higher-dimensional ambient spacetime is also possible, and may be called *spontaneous compactification*. For a comprehensive overview and discussion of the various processes, in the context of the example presented in the previous section, see [66].

In the framework of a landscape of flux compactifications, where numerous gauge fields and a vast number of different compactification vacua are available, spontaneous compactification and decompactification represent elementary processes only. They describe transitions between configurations where either a certain number of macroscopic dimensions is spontaneously compactified or a certain number of microscopic dimensions spontaneously start to grow large. In any of the two cases, the remaining dimensions are left untouched as far as possible. It is, however, conceivable that also more complicated processes exist, where the configuration of macroscopic and microscopic dimensions is re-arranged in a more general way. The term *shapeshifting process* has been suggested in [2] for this general type of tunneling events. Schematically, these processes can be described with following diagrams:

$$
\begin{array}{ccc}
\mathcal{ST}_D & \mathcal{ST}_d \times \mathcal{M}_{D-d} & \mathcal{ST}_d \times \mathcal{M}_{D-d} \\
\downarrow \quad \searrow & \downarrow \quad \nearrow & \downarrow \quad \times \quad \downarrow \\
\mathcal{ST}'_d \times \mathcal{M}'_{D-d} & \mathcal{ST}'_D & \mathcal{ST}'_{d'} \times \mathcal{M}'_{D-d'} \\
\\
\text{compactification} & \text{decompactification} & \text{shapeshifting}
\end{array}
$$

Here, an arrow indicates how the spacelike directions are reassigned to the components of the new vacuum manifold. In the shapeshifting case it should be understood that any sensible subset of reassignments can be realized. The shapeshifting process therefore connects two arbitrary vacuum configurations in the landscape of compactification vacua[7].

The idea that the arrangement of macroscopic and compact microscopic directions can change in a tunneling process raises a number of new and interesting phenomenological questions. In particular, what are the consequences if some of our three macroscopic space dimensions have been microscopic prior to the most recent tunneling event in our cosmic history? If the amount of inflation which took place after the transition is not too large, then the compact nature of these directions could become apparent on the largest

---

[6]Note that the term "decompactification" does not refer to a topology change in this context. In fact, the compact topology is retained, but it is not apparent anymore because the compactification scale exceeds the Hubble radius.

[7]It should be noted that I have not presented a proof that these general processes exist, but I know of no reason why they should not. A simple setup is described in appendix A.

observable scales. Moreover, if only one or two directions are compact, it may be possible that they still play a special role and can therefore give rise to a preferred direction in our Universe. This would be seen as a breaking of statistical isotropy.

3.2.1   A Shapeshifting Universe

Let me discuss some of the simplest scenarios where our observable Universe is the result of a tunneling process in which at least some dimension(s) decompactified and became part of our macroscopic world. Since we are unable to probe the extra dimensions which are compact and microscopic in our present vacuum configuration, I will present the discussion entirely from our four-dimensional point of view. In a sense, I treat the extra dimensions merely as spectators – they give rise to some effective vacuum energy and other "constants of nature," but are otherwise dynamically irrelevant and have been integrated out.

As first example, consider the case where only one of our macroscopic dimensions was compact and microscopic in our parent vacuum. The only one-dimensional compact manifold is the circle S_1. Unfortunately, the mechanism of flux stabilization does not work in this particular case, because it requires some curvature on the compact manifold. In one dimension, curvature does not exist, as can also be seen from the vanishing of the corresponding term in eq. (3.9) for $q = 1$. However, other mechanisms to stabilize the radius of an S_1-factor are known, like *e.g.* the one used in [71]. Irrespectively of what happend to the extra dimensions of our present vacuum, the symmetries of the tunneling process guarantee that our macroscopic spacetime which is contained within the bubble can be written as the product of S_1 and a $2 + 1$-dimensional open FRW geometry. The homogeneous spatial slices therefore have topology $H_2 \times S_1$, where H_2 is the two-dimensional spacelike hyperboloid. The line element can be written as

$$ds^2 = -dt^2 + a_\perp^2(t)\left[\frac{dr^2}{1 - K_\perp r^2} + r^2 d\phi^2\right] + a_\parallel^2(t)dz^2 \; , \tag{3.10}$$

where $K_\perp < 0$ and z is a coordinate on the S_1-factor. This metric belongs to the Bianchi class III and describes a homogeneous and anisotropic cosmology. Some amount of inflation is required to take place in the bubble in order to dilute the *anisotropic* curvature and thus to obtain some convergence towards the ΛCDM concordance model. However, the spectrum of primordial perturbations may be affected by the anisotropy of the background geometry. This may leave some traces, *e.g.*, in the temperature anisotropies of the CMB. One expects that the effect is active on the largest scales because they are most sensitive to global properties of spacetime such as homogeneous curvature. A detailed analysis of the signatures in this scenario has been attempted in [71].

Going one step further, the next possibility is the case where two out of the three of our macroscopic dimensions decompactified in the latest tunneling event. Two-dimensional compact manifolds can be classified, and the simplest cases are the two-torus $S_1 \times S_1$ and the two-sphere S_2. Again, because of vanishing curvature, the flux compactification mechanism does not work for the torus, but there are other compactification mechanisms. An interesting example which may even work in the context of the standard model has been presented in [72]. The symmetry properties of the tunneling scenario lead to a bubble universe which contains a macroscopic spacetime which can be written as a product of the torus and a $1+1$-dimensional open FRW geometry. The homogeneous spatial hypersurfaces have topology $S_1 \times S_1 \times \mathbb{R}$, and the line element takes the form

$$ds^2 = -dt^2 + a_x^2(t)dx^2 + a_y^2(t)dy^2 + a_z^2(t)dz^2 \; . \tag{3.11}$$

Here, x and y are the two directions on the torus, and z is the noncompact direction. This metric falls into the Bianchi class I. In case the torus decompactifies isotropically, the two scale factors a_x and a_y can be identified, and the metric is of the form (3.10)

with $K_\perp = 0$. Primordial perturbations in a Bianchi I cosmology have been explored in [73, 74, 75]. However, the authors of these articles did not consider a tunneling scenario and were therefore unable to fix the initial conditions for the perturbations.

On the other hand, the possibility of the two-sphere is interesting, because the flux compactification mechanism is expected to be operative in principle. Furthermore, the flux is generated by a two-form in this case, for which a candidate exists in the standard model: electromagnetism. From our four-dimensional point of view, the spherical symmetric configurations of gravity and electromagnetism are well-known. The cosmological solutions correspond to Reissner-Nordström-de Sitter geometries, which describe magnetically charged black holes in a vacuum of non-negative vacuum energy density. The tunneling process, from the four-dimensional perspective, is completely analogous to pair creation of charged black holes [76, 77, 78]. This analogy actually runs very deep. It was already pointed out in [66] that dynamical compactification using magnetic fluxes is a generalization of charged black hole pair creation. The connection between the different interpretations was further elucidated in [68]. For the present context, the analogy has been reviewed in [2].

The symmetries of the four-dimensional one-bubble spacetime are such that the bubble-universe is the product of a two-sphere and a $1+1$-dimensional open FRW geometry. The homogeneous spatial hypersurfaces have topology $S_2 \times \mathbb{R}$, and the line element is that of eq. (3.10) with $K_\perp > 0$. This is a special type of homogeneous and anisotropic solution of Einstein's equations which does not correspond to any Bianchi class. It is known as the Kantowski-Sachs model [79]. The primordial power spectrum of a scalar "test field" for this model has been studied in [2] within the context of a transdimensional tunneling scenario. Some results will be reviewed in the next section.

The examples which I mentioned so far do of course not present a complete list of possibilities for the qualitative outcome of a shapeshifting process. However, they cover already the most simple options for homogeneous and anisotropic bubble-universes. The implications of the idea of transdimensional tunneling, or shapeshifting, have just begun to be explored, and there may be many new and interesting options ahead. It will be exciting to see how this field develops in the coming years.

3.3 Observability

In this section, I want to assess the phenomenological consequences of a tunneling scenario in some more detail. As mentioned before, it is assumed that some amount of slow-roll inflation has to take place inside the bubble-universe in order to make the scenario phenomenologically viable. It has been demonstrated in the context of open inflation [46, 80], and more recently also in the context of transdimensional tunneling [66], that inflation can be implemented in the model without much complication. Moreover, the "initial conditions" for inflation are unambiguously fixed by the tunneling scenario. The inflaton is just another field whose boundary conditions can be determined by constructing the instanton – at least in principle. For instance, with some appropriate coupling to fluxes and curvature of the extra dimensions, one can construct models where the tunneling event triggers slow-roll inflation by setting free the inflaton, which was trapped at a local minimum of its effective potential in the false vacuum configuration.

Due to inflation inside the bubble-universe, it is usually a good working hypothesis that the ΛCDM model is a suitable description of our Universe at *leading order*, and that the deviations are controlled by a *small parameter*. For instance, the open inflation scenario mentioned earlier comes with a non-vanishing spatial curvature, and Ω_K (today) can be assumed a small parameter. One can then try to understand the phenomenological deviations from the concordance model as perturbative effects.

The possible effects are numerous. In order to get some systematic overview, a rough distinction can be made between *early-type* and *late-type* effects. The early-type effects

are those which lead to a modification of the primordial perturbations, while the late-type effects lead to differences in the evolution long after the hot Big Bang. In terms of theoretical calculations, this distinction is reasonable and clean. However, from the observational point of view, the effects can be strongly entangled. For instance, the power spectrum of primordial perturbations for an open universe is modified compared to the flat ΛCDM model, which has an effect on the properties of CMB anisotropies. At the same time, the angular diameter distance to the surface of last scattering, and therefore the mapping of perturbations into the celestial sphere, also depends on the spatial curvature. Clearly, both effects are controlled by the same small parameter Ω_K and are therefore equally important.

In this section, I want to concentrate on the early-type effects which can appear in a tunneling scenario. Some late-type effects will be discussed in chapter 4. I will focus on two aspects. Firstly, I want to sketch how the computation of primordial perturbations in the tunneling scenario leads to modifications. Since the case of an isotropic open universe has been extensively studied in the context of open inflation, see *e.g.* [81], I will focus on the anisotropic case which can arise in a shapeshifting process. Due to the anisotropy in the background, one expects that the modifications will lead to a breaking of statistical isotropy, for instance in the CMB. Interestingly, there is a debate about some indications of such a breaking, see [17, 18, 19, 20]. I will present a calculation of the power spectrum in the Kantowski-Sachs model and discuss some implications for the CMB, with special attention on the reported "anomalies." Finally, as a second aspect, I will briefly comment on the subject of bubble collisions, which could give a completely different type of signature. There are, of course, also other aspects which can be studied, like *e.g.* the Grishchuk-Zel'dovich effect [82] or gravitational waves [83]. It would go beyond the purpose of this work to give a comprehensive review, and I will therefore leave it at a discussion of only the two aspects mentioned above.

3.3.1   Signatures of Global Anisotropy

The general procedure to obtain the perturbations around the $O(3,1)$-symmetric one-bubble solution is the following. First, one has to construct the $O(4)$-symmetric Euclidean solution corresponding to the instanton which describes the vacuum transition. Then, one introduces the fields which describe the perturbations. Their equations of motion follow from the second variation of the action evaluated on the instanton. Taking a maximal slice of the instanton (containing the two poles of the geometry) and using it as *initial Cauchy surface* at the classical turning point, the instanton solution *together with the perturbations* can be continued into the classically allowed domain by means of analytic continuation. The eigenfunctions of the Klein-Gordon operator yield a basis of solutions to the field equations, and can be used to define a vacuum state for the perturbations, once they have been quantized. To this end it is necessary to identify the "positive frequency" solutions which have to be associated with the creation operators of the modes. As has been argued in [84], a suitable selection criterion is to require regularity on the lower half of the Euclidean solution, *i.e.* the part of the instanton which is obtained by continuing the time coordinate through the classical turning point into the forbidden region. This particular construction of a vacuum will become more clear when I work out an explicit example below.

There are several levels of complication if one wants to carry out the program outlined above. Firstly, one has to take care that one only quantizes physical degrees of freedom. This is an issue in any theory with gauge freedom, like gravity. In order to bypass this problem, I will present a computation for a scalar "test field" only. This is not identical to the gauge-invariant scalar perturbation in cosmology, but the basic modifications of the power spectrum are more easily accessible in this example.

A second problem arises if one wants to carry out the mode decomposition. Since the

one-bubble spacetime does not have the full de Sitter symmetries, it is usually impossible to write down the decomposition explicitly. A numerical approach also cannot solve the problem entirely, because an infinite number of eigenfunctions would have to be computed. To my knowledge, no good way of solving this problem is known. One usually makes an approximation and assumes that the breaking of the full de Sitter symmetry only has negligible effects on the result of the computation. Therefore, one approximates the $O(3,1)$-symmetric solution by an $O(4,1)$-symmetric one. This is a very drastic measure since, for instance, the slow-roll evolution can no longer be taken into account, not to mention the interpolation between the two vacuum configurations. One might wonder why this approach should give any non-trivial results at all, because one is computing a power spectrum in de Sitter space, albeit in unfamiliar coordinates. However, it turns out that choosing a foliation which is adapted to the homogeneous foliation of the original one-bubble spacetime is a non-trivial step.

A calculation of the mode functions in the one-bubble open inflation scenario has been presented by Misao Sasaki, Takahiro Tanaka and Kazuhiro Yamamoto in [84] using the approximation outlined above. Following this approach, a similar calculation has been carried out for the Bianchi III model which arises in the decompactification of S_1 in [71]. I will now present the analysis for the Kantowski-Sachs model which arises in the decompactification of S_2. Major parts of this analysis have been published in [2].

The Primordial Power Spectrum in a Kantowski-Sachs Model

The first step is to find a coordinate system of de Sitter space which is adapted to the $S_2 \times \mathbb{R}$ topology of the homogeneous spatial foliation in the Kantowski-Sachs model. A suitable starting point is the static (Schwarzschild-type) coordinate system of de Sitter space, in which the line element reads

$$ds^2 = - \left(1 - \frac{\Lambda}{3} R^2 \right) dT^2 + \left(1 - \frac{\Lambda}{3} R^2 \right)^{-1} dR^2 + R^2 d\Omega^2 \ . \tag{3.12}$$

For the purpose of calculating an inflationary power spectrum, the vacuum energy Λ models the inflaton potential energy during the slow-roll phase. I want to approximate a bubble in which the radius of a two-sphere uniformly grows with time, *i.e.* which has a metric of the form (3.10). Such a situation is given if one extends the static coordinate system above into the region where $R > \sqrt{3/\Lambda}$. In this region, T becomes a spacelike coordinate while R becomes timelike, and the staticity of the metric translates to homogeneity. The line element can be rewritten as

$$ds^2 = H^{-2} \left[-d\tau^2 + \left(H^2 R^2(\tau) - 1 \right) dz^2 \right] + R^2(\tau) d\Omega^2 \ , \tag{3.13}$$

where I have introduced the inflationary Hubble parameter $H \equiv \sqrt{\Lambda/3}$. As can be seen from a comparison with eq. (3.12), the coordinate z is defined by $dz = H dT$, and the (dimensionless) time coordinate by $d\tau = H dR/\sqrt{H^2 R^2 - 1}$. This relation can be solved for R to yield $R(\tau) = H^{-1} \cosh \tau$. The patch covered by $0 < \tau < \infty$ and $-\infty < z < \infty$ indeed describes an inflationary bubble where a two-sphere uniformly inflates from an initial size of $R = H^{-1}$. This is illustrated in fig. 3.2, which shows the Penrose-Carter diagram of de Sitter space. Neglecting the dynamics of the inflaton (and the moduli fields of our extra dimensions), the patch can be used to approximate the interior of a bubble which arises in a shapeshifting process where a microscopic S_2 destabilizes and becomes large. Asymptotically, the scale factors for the S_2 and the third direction converge towards the same exponential behavior, as is expected by the cosmic no-hair conjecture.

Let me now consider a minimally coupled massless real scalar "test field" Φ on this background. Although I assume that Φ does not give rise to metric perturbations, it shall be used as a surrogate for real cosmological perturbations since one expects that they have

Figure 3.2: Causal diagram of de Sitter space. The dashed lines are lines of constant R. The *static patch* is the left (or right) triangular wedge where R grows in a spacelike direction. The diagonal straight lines are the locus of points where $R = H^{-1}$ and therefore mark the cosmological horizon of the static patch. Beyond the horizon, in the upper triangular wedge, lies a cosmological region which, by continuing the static coordinates, is foliated like a Kantowski-Sachs model. Here, the radius R grows uniformly in a timelike direction. The cosmological region looks very much like a bubble-universe as is created by the decompactification of a two-sphere in a shapeshifting process. The horizons mark the lightcone of the nucleation event, which is located at the central vertex. The horizontal dashed line indicates a global Cauchy surface of de Sitter space, and coincides with a maximal section through the Euclidean de Sitter.
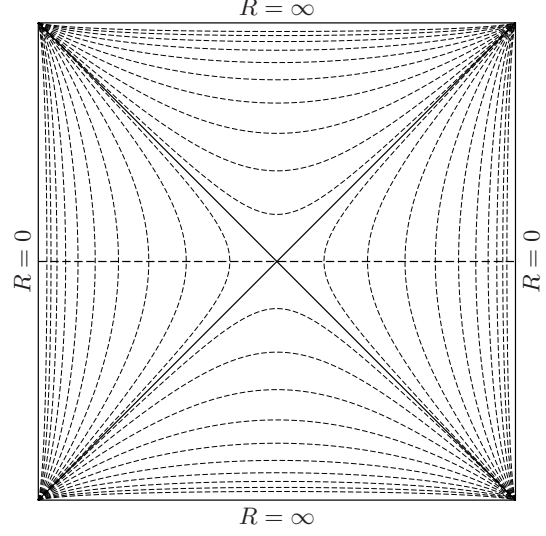
similar qualitative features in the primordial power spectrum. The action for Φ reads

$$\mathcal{S}_\Phi = -\frac{1}{2} \int d^4 x \sqrt{-g} \partial^\mu \Phi \partial_\mu \Phi \ . \tag{3.14}$$

The $S_2 \times \mathbb{R}$ structure of the spacelike hypersurfaces (in the bubble) suggests the mode-expansion

$$\Phi(\tau, z, \mathbf{n}) = \sum_{\ell, m} \int \frac{dk}{\sqrt{2\pi}} \Phi_{k\ell m}(\tau) e^{-ikz} Y_{\ell m}(\mathbf{n}) \ , \tag{3.15}$$

where $\mathbf{n}$ is a unit vector in $\mathbb{R}^3$ which specifies the point on the two-sphere, and $Y_{\ell m}$ is the usual spherical harmonic on S_2. Introducing the rescaled field $\Psi = \Phi H^{-1} \cosh \tau \sinh^{1/2} \tau$, the action reads

$$S_\Psi = \frac{1}{2} \sum_{\ell, m} \int dk d\tau \left\{ \partial_\tau \Psi_{k\ell m} \partial_\tau \Psi^*_{k\ell m} - \left[\frac{k^2 + 1/4}{\sinh^2 \tau} + \frac{\ell(\ell+1)}{\cosh^2 \tau} - \frac{9}{4} \right] \Psi_{k\ell m} \Psi^*_{k\ell m} \right\} \ , \tag{3.16}$$

where I dropped the boundary term of an integration by parts.

In analogy to the harmonic oscillator, the field is quantized by promoting the modes to operators which decompose into creation and annihilation operators as

$$\hat{\Psi}_{k\ell m}(\tau) = \frac{i^m}{\sqrt{2}} \hat{a}_{k\ell m} u_{k\ell}(\tau) + \frac{i^{-m}}{\sqrt{2}} \hat{a}^\dagger_{-k\ell-m} u^*_{k\ell}(\tau) \ . \tag{3.17}$$

The mode functions $u_{k\ell}$ satisfy the equation

$$\partial_\tau^2 u_{k\ell} + \left[\frac{k^2 + 1/4}{\sinh^2 \tau} + \frac{\ell(\ell+1)}{\cosh^2 \tau} - \frac{9}{4} \right] u_{k\ell} = 0 \ , \tag{3.18}$$

and are chosen such that they are independent of m and the sign of k. The numerical factors in eq. (3.17) are for convenience. The mode functions thus defined form a complete basis of solutions of the Klein-Gordon equation and are normalized by the condition

$$\text{Im}\left(u_{k\ell} \partial_\tau u^*_{k\ell}\right) = \frac{u_{k\ell} \partial_\tau u^*_{k\ell} - u^*_{k\ell} \partial_\tau u_{k\ell}}{2i} = 1 \ . \tag{3.19}$$

With this normalization, the equal time commutation relations

$$\left[\hat{\Psi}(\tau, z, \mathbf{n}), \partial_\tau \hat{\Psi}(\tau, z', \mathbf{n}')\right] = i\delta(z - z')\delta^{(\Omega)}(\mathbf{n} - \mathbf{n}') , \tag{3.20}$$

with the other commutators zero, are equivalent to

$$\left[\hat{a}_{k\ell m}, \hat{a}^\dagger_{k'\ell'm'}\right] = \delta(k - k')\delta_{\ell\ell'}\delta_{mm'} , \tag{3.21}$$

with all remaining commutators zero. Note that $\delta^{(\Omega)}(\mathbf{n} - \mathbf{n}')$ is the delta-function on the two-sphere which has the defining property

$$\int d\Omega f(\mathbf{n})\delta^{(\Omega)}(\mathbf{n} - \mathbf{n}') = f(\mathbf{n}') \tag{3.22}$$

for any test-function f defined on S_2.

The particular solution of eq. (3.18), that is, the positive-frequency mode, can be identified by demanding that the analytic continuation to the Euclidean half-sphere remains regular everywhere. This is the criterion which determines the choice of the vacuum in [84]. In the present case it is sufficient to require regularity on the Cauchy surface which is indicated as horizontal dashed line in the Penrose-Carter diagram shown in fig. 3.2. This surface – representing the classical turning point – coincides with a maximal slice through the Euclidean de Sitter space. For more details on this general prescription of defining the positive frequency solution, see [84].

An exact expression for $u_{k\ell}$ can be found by substituting $s \equiv \sinh^2\tau$, which casts eq. (3.18) into the form of Riemann's differential equation. Its general solution can be written in terms of the hypergeometric function $_2F_1$ as

$$u_{k\ell} = s^{1/4}s^{ik/2}\sqrt{(s+1)^{\ell+1}}\left[_2F_1\left(\frac{\ell + ik}{2}, \frac{\ell + 3 + ik}{2}; 1 + ik; -s\right)A_{k\ell}\right.$$
$$\left. + (-s)^{-ik}\,_2F_1\left(\frac{\ell - ik}{2}, \frac{\ell + 3 - ik}{2}; 1 - ik; -s\right)B_{k\ell}\right] \tag{3.23}$$

for $\ell > 0$. The case $\ell = 0$ has to be treated separately, the general solution here is

$$u_{k\ell} = s^{1/4}s^{ik/2}\left[_2F_1\left(\frac{ik-1}{2}, 1 + \frac{ik}{2}; 1 + ik; -s\right)A_{k0}\right.$$
$$\left. + (-s)^{-ik}\,_2F_1\left(\frac{-ik-1}{2}, 1 - \frac{ik}{2}; 1 - ik; -s\right)B_{k0}\right] . \tag{3.24}$$

For these solutions, I have placed the branch cuts such that all functions remain analytic in the entire upper half plane of complex s, including the real line up to isolated singular points. The constants of integration $A_{k\ell}$ and $B_{k\ell}$ are fixed by imposing the regularity and normalization conditions.

In order to implement the regularity condition on the Cauchy surface, the solution has to be continued into the static patches. This is achieved by integrating $d\tau = HdR/\sqrt{H^2R^2 - 1}$ to values $R < H^{-1}$, where τ acquires an imaginary part. The imaginary part of τ plays the role of a radial coordinate. A regular solution on the Cauchy surface in particular has to be regular at $R = 0$, $i.e.$ at the poles of the Euclidean de Sitter space. These are located at $\tau \to \pm i\pi/2$. As can be seen from inspection of eq. (3.18), for $\ell > 0$ the solutions near the poles asymptote to $u_{k\ell} \sim \epsilon^{\ell+1}$ or $u_{k\ell} \sim \epsilon^{-\ell}$ for $\tau = \pm i(\pi/2 - \epsilon)$ and $\epsilon \to 0^+$. The second solution is not normalizable and therefore has to be excluded from the physical spectrum. Expanding eq. (3.23) around $s = -1$, one can see that the regular branch fulfills the relation

$$B_{k\ell} = -A_{k\ell}\frac{\Gamma\left(1 + ik\right)\Gamma\left(\frac{\ell-ik}{2}\right)\Gamma\left(\frac{\ell+3-ik}{2}\right)}{\Gamma\left(1 - ik\right)\Gamma\left(\frac{\ell+ik}{2}\right)\Gamma\left(\frac{\ell+3+ik}{2}\right)} . \tag{3.25}$$

The case $\ell = 0$ has to be treated separately again, as it appears that both asymptotic solutions are normalizable. However, the derivative is only continuous at the poles if

$$\left.\frac{du_{k0}}{dR}\right|_{R=0} = 0 \; . \tag{3.26}$$

This condition leads to the following relation:

$$B_{k0} = -A_{k0}\frac{\Gamma\left(1+ik\right)\Gamma\left(\frac{-1-ik}{2}\right)\Gamma\left(1-\frac{ik}{2}\right)}{\Gamma\left(1-ik\right)\Gamma\left(\frac{-1+ik}{2}\right)\Gamma\left(1+\frac{ik}{2}\right)} \; . \tag{3.27}$$

Using the relations (3.25) and (3.27), the normalization of the Wronskian (3.19) implies

$$|A_{k\ell}|^2 = \frac{1}{k\left(e^{2\pi k} - 1\right)} \tag{3.28}$$

for any value of ℓ, including $\ell = 0$. This fixes the positive frequency mode functions up to irrelevant overall phase factors.

The two-point correlation at equal time can be expressed as

$$\left\langle \hat{\Phi}(\tau, z, \mathbf{n})\hat{\Phi}(\tau, z', \mathbf{n}') \right\rangle = \sum_\ell \frac{2\ell + 1}{16\pi^2} \int dk \frac{H^2 \left|u_{k\ell}(\tau)\right|^2}{\cosh^2\tau\,\sinh\tau} P_\ell(\mathbf{n}\cdot\mathbf{n}')e^{-ik\left(z-z'\right)} \; , \tag{3.29}$$

where P_ℓ denotes the Legendre polynomial of degree ℓ, and I have used the *addition theorem*[8] for spherical harmonics. In analogy to the convention in standard inflation, I call $H^2\left|u_{k\ell}(\tau)\right|^2 / \left(\cosh^2\tau\,\sinh\tau\right)$ the *power spectrum*. As usual, it asymptotes to a constant for $\tau \to \infty$, namely

$$\frac{H^2\left|u_{k\ell}(\tau)\right|^2}{\cosh^2\tau\,\sinh\tau} \to \frac{H^2\left|\Gamma\left(\frac{\ell+ik}{2}\right)\right|^2}{2\left(k^2 + (\ell+1)^2\right)\left|\Gamma\left(\frac{\ell+1+ik}{2}\right)\right|^2} \equiv \mathcal{P}_{k\ell} \tag{3.30}$$

for $\ell > 0$, and

$$\frac{H^2\left|u_{k0}(\tau)\right|^2}{\cosh^2\tau\,\sinh\tau} \to \frac{H^2\tanh\frac{\pi k}{2}}{k + k^3} \equiv \mathcal{P}_{k0} \tag{3.31}$$

for $\ell = 0$. These results are most conveniently obtained by taking the limit $s \to \infty$ of eqs. (3.23) and (3.24), noting that one divides by $\cosh^2\tau\,\sinh\tau = (s+1)s^{1/2}$.

Angular Power Spectrum and Map Distortions

The full two-point correlation function (at equal time) is not easily observed in cosmology. For instance, the primary anisotropies in the CMB can be used to probe[9] the correlation function (of cosmological perturbations, of course) on a two-dimensional surface only – the *surface of last scattering*. In order to parallel this situation, one can restrict the two-point correlation function to a two-dimensional submanifold of the spacelike hypersurface. This submanifold is thought to have the topology of a two-sphere, just as the surface of last scattering. For instance, one can consider the intersection of the past light cone of a

---

[8]The addition theorem for spherical harmonics is given by the identity

$$\sum_m Y_{\ell m}(\mathbf{n})Y_{\ell m}^*(\mathbf{n}') = \frac{2\ell + 1}{4\pi}P_\ell(\mathbf{n}\cdot\mathbf{n}') \; .$$

[9]The primary CMB anisotropies are only indirectly related to the primordial density perturbations, because they depend on the density field at redshift $z \approx 1100$. However, since structure evolution is still in a linear regime at that time, the transfer function which connects the observation to the primordial perturbations is well known. A clean measurement is impaired by secondary anisotropies such as CMB lensing, the Sunyaev-Zel'dovich and integrated Sachs-Wolfe effects or foreground contamination.

comoving observer with a certain equal-time hypersurface. This construction is very close to the idea that the CMB is a "snapshot" of the density field whose information traveled to us on our past light cone.

Because of the S_2-topology of the CMB sky map, it is convenient to make a multipole decomposition of the temperature field. I will apply this standard procedure to the restricted two-point correlation function. The information of the two-point function on the submanifold is encoded in the correlators between the multipole coefficients, $\langle a_{lm} a^*_{l'm'} \rangle$. These are given by

$$\langle a_{lm} a^*_{l'm'} \rangle = \int d\Omega d\Omega' Y_{lm}(\mathbf{n}) Y^*_{l'm'}(\mathbf{n}') \mathcal{C}(\mathbf{n}, \mathbf{n}') \ , \tag{3.32}$$

where the two-point function on the submanifold $\mathcal{C}$ is written as a function of $\mathbf{n}$, $\mathbf{n}'$, which are here coordinates on the S_2 onto which the submanifold is *mapped*. In order to relate this to the two-point function of eq. (3.29), one has first to specify the map. In analogy to CMB observations, the directions $\mathbf{n}$, $\mathbf{n}'$ shall denote the physical detector orientations with respect to a locally defined spherical coordinate system. For convenience, I will assume that the polar axis of this local coordinate frame is aligned with the z-direction. The correlation function $\mathcal{C}$ measures the correlation between the two points on the last scattering surface which are connected to the point of observation by the null rays passing through that point in directions $\mathbf{n}$ and $\mathbf{n}'$. The null rays can be obtained by integrating the null geodesic equation.

One can eliminate the affine parameter from the null geodesic equation in favor of the coordinate time. Adopting the notation of eq. (3.10) and using the condition for a null ray, $a_\parallel^2 (\partial_t z)^2 + a_\perp^2 (\partial_t \theta)^2 = 1$, one obtains the two decoupled ordinary differential equations

$$\partial_t^2 \theta + \partial_t \theta \left[\frac{\partial_t a_\perp}{a_\perp} + \left(\frac{\partial_t a_\perp}{a_\perp} - \frac{\partial_t a_\parallel}{a_\parallel} \right) \left(1 - a_\perp^2 (\partial_t \theta)^2 \right) \right] = 0 \ , \tag{3.33}$$

$$\partial_t^2 z + \partial_t z \left[\frac{\partial_t a_\parallel}{a_\parallel} + \left(\frac{\partial_t a_\parallel}{a_\parallel} - \frac{\partial_t a_\perp}{a_\perp} \right) \left(1 - a_\parallel^2 (\partial_t z)^2 \right) \right] = 0 \ . \tag{3.34}$$

Here, θ is the length of an arc on the expanding S_2 factor, which has been scaled such that $a_\perp = R$. Furthermore, a comparison between eqs. (3.13) and (3.10) shows that $t = \tau/H$ and $a_\parallel^2 = R^2 - H^{-2}$.

In order to solve the null geodesic equation, I will make the approximation that $a_\perp \simeq a_\parallel$. This is a good approximation at late time, after inflation has isotropized the Universe. Note, however, that one has to check that the error due to this approximation is not larger than the correction to the two-point correlation function which I want to compute. I will show in chapter 4 that both terms are in fact of the same order if one does not add some non-standard physical input.

In this approximation, the zeroth-order solutions to the above equations are

$$\partial_t z \propto \frac{1}{a_\parallel} \simeq \frac{1}{R} \ , \qquad \partial_t \theta \propto \frac{1}{a_\perp} = \frac{1}{R} \ . \tag{3.35}$$

I introduce

$$r \equiv \int_{t_*}^{t_0} \frac{dt}{R} \ , \tag{3.36}$$

which measures the zeroth-order comoving distance to the surface of last scattering. Since the comoving radius of the S_2 factor is 1 by definition, it is reasonable to assume that $r \ll 1$ for cosmological observations taken after the end of inflation. This suggests that r is a small parameter suitable for making a Taylor series expansion.

With the above results and definitions, a point observed on the surface of last scattering in direction $\mathbf{n}$ is located relative to the observer at

$$z_* - z_0 \;=\; r\,(\mathbf{n}\cdot\mathbf{z}) = r\cos\vartheta \;, \tag{3.37}$$

$$\theta_* - \theta_0 \;=\; r\sqrt{1 - (\mathbf{n}\cdot\mathbf{z})^2} = r\sin\vartheta \;, \tag{3.38}$$

where $\mathbf{z}$ is the unit vector pointing along the z-direction in the local spherical coordinate system, and ϑ is the corresponding polar angle. The azimuth of the direction $\mathbf{n}$ shall be denoted as φ.

In the limit of $\tau \to \infty$ (keeping r fixed), the two-point function on the surface of last scattering is obtained from eq. (3.29) as

$$\mathcal{C}(\mathbf{n}, \mathbf{n}') \equiv \mathcal{C}\left(\begin{array}{cc} \vartheta, & \vartheta' \\ \varphi, & \varphi' \end{array}\right) = \sum_{\ell m} \int \frac{dk}{4\pi} \mathcal{P}_{k\ell} Y_{\ell m}(r\sin\vartheta, \varphi) Y_{\ell m}^*(r\sin\vartheta', \varphi') e^{-ikr\left(\cos\vartheta - \cos\vartheta'\right)} \;, \tag{3.39}$$

where I have replaced the Legendre polynomial again in favor of the spherical harmonics using the addition theorem. This expression, together with the primordial power spectrum $\mathcal{P}_{k\ell}$ of eqs. (3.30) and (3.31), determines fully the correlation between the multipole coefficients $\langle a_{lm} a_{l'm'}^* \rangle$.

Unfortunately, I was unable to solve the integrals of eq. (3.32) analytically. However, one can see from the symmetries of the expression that some correlations have to vanish. For instance, because the two-point function above is even under parity, *i.e.* it is invariant under point-reflection, which is a symmetry of the Kantowski-Sachs model, any multipole coefficients of opposite parity (meaning that $l + l'$ odd) are uncorrelated. There is also an axisymmetry around the z-axis in the Kantowski-Sachs model. As a consequence, the correlation $\langle a_{lm} a_{l'm'}^* \rangle$ has to be proportional to $\delta_{mm'}$, as an integration over the azimuth angles alone demonstrates. One can therefore write

$$\langle a_{lm} a_{l'm'}^* \rangle = \frac{H^2}{2\pi} \delta_{mm'} \frac{2\left(\delta_{ll'} + \delta C_{ll'mm}\right)}{l(l+1) + l'(l'+1)} \;. \tag{3.40}$$

This choice is motivated by recalling the standard result in a statistically isotropic FRW model with a Harrison-Zel'dovich spectrum,

$$\langle a_{lm} a_{l'm'}^* \rangle_{\text{iso}} = \frac{H^2}{2\pi} \delta_{ll'} \delta_{mm'} \frac{1}{l(l+1)} \;, \tag{3.41}$$

which is obtained by computing the vacuum expectation value in the Bunch-Davies state using the flat foliation of de Sitter space. It is assumed that eq. (3.40) goes to the isotropic limit (3.41) for $r \to 0$, since the two-point function on the surface of last scattering then only probes length scales much below the curvature radius. The correction to the isotropic limit is carried by the parameters $\delta C_{ll'mm}$, which are functions of r that go to zero in the limit $r \to 0$.

In [2], some of the parameters $\delta C_{ll'mm}$ have been computed numerically (with a slightly differing normalization[10]). In order to get a deeper understanding of these results, let me do a thought experiment which might explain what actually happens. Coming from the flat limit $r \to 0$, where I expect that the isotropic result (3.41) holds, I assume that the *anisotropic curvature* in the Kantowski-Sachs geometry gives rise to a distortion of the map. More precisely, I assume that the distortion is such that the points on a statistically isotropic map are not mapped to their true positions on the $\mathcal{S}_2$ anymore, but are instead shifted a little bit[11]. The shifts can be described by the flow of a vector field $\mathbf{v}(\mathbf{n})$ defined

---

[10]In [2], the correction terms were normalized relative to the maximum of the two related diagonal elements (of the isotropic limit), while I choose here to normalize relative to the harmonic mean thereof.

[11]A similar effect is also expected in the late Universe if there is some differential expansion and has been analyzed in [85], although with very different methods from the ones I use here. In this case, however, there is an additional quadrupolar redshift signal in the modified map, see section 4.1 for details.

on the two-sphere. For infinitesimal shifts, the distorted random field[12] $f(\mathbf{n})$ is obtained from the undistorted (statistically isotropic) random field $f_0(\mathbf{n})$ by making a Taylor series expansion:

$$f(\mathbf{n}) = f_0(\mathbf{n} - \mathbf{v}) = f_0(\mathbf{n}) - \mathbf{v} \cdot \nabla f_0(\mathbf{n}) + \dots \tag{3.42}$$

For the statistically isotropic field f_0, the multipole coefficients have well-known statistical properties as given in eq. (3.41). The idea is therefore to express the multipole coefficients of the distorted field in terms of the original ones.

The multipole coefficients of f_0 are defined as

$$a_{lm} = \int d\Omega f_0(\mathbf{n}) Y_{lm}(\mathbf{n}) , \tag{3.43}$$

such that the real field f_0 can be written as

$$f_0(\mathbf{n}) = \sum_{lm} a_{lm} Y_{lm}^* = \sum_{lm} a_{lm}^* Y_{lm} . \tag{3.44}$$

Note that reality implies $a_{lm}^* = (-1)^m a_{l,-m}$.

The real vector field $\mathbf{v}$ also has a multipole expansion, which can be conveniently expressed if one writes the vector components in terms of the helicity basis

$$\mathbf{e}_+ = \frac{1}{\sqrt{2}} (\mathbf{e}_\vartheta - i\mathbf{e}_\varphi) , \qquad \mathbf{e}_- = \frac{1}{\sqrt{2}} (\mathbf{e}_\vartheta + i\mathbf{e}_\varphi) . \tag{3.45}$$

In this basis, the multipole expansion reads

$$\mathbf{v}(\mathbf{n}) = \mathbf{e}_+ \sum_{lm} {}_+v_{lm}^* {}_{+1}Y_{lm}(\mathbf{n}) + \mathbf{e}_- \sum_{lm} {}_-v_{lm}^* {}_{-1}Y_{lm}(\mathbf{n}) , \tag{3.46}$$

where ${}_sY_{lm}$ are the spherical harmonics of spin weight s, see *e.g.* appendix A4.2.4 of [9] for details. The spin-weighted spherical harmonics can be obtained from the usual (spin 0) spherical harmonics by applying spin raising and lowering operators $\eth$ and $\eth^*$, which are defined by

$$\begin{aligned}
\eth\, {}_sY_{lm} &= -\sin^s\vartheta \left(\partial_\vartheta + \frac{i}{\sin\vartheta} \partial_\phi \right) (\sin^{-s}\vartheta\, {}_sY_{lm}) = \sqrt{(l-s)(l+s+1)}\, {}_{s+1}Y_{lm} , \\
\eth^*\, {}_sY_{lm} &= -\sin^{-s}\vartheta \left(\partial_\vartheta - \frac{i}{\sin\vartheta} \partial_\phi \right) (\sin^s\vartheta\, {}_sY_{lm}) = -\sqrt{(l+s)(l-s+1)}\, {}_{s-1}Y_{lm} .
\end{aligned} \tag{3.47}$$

For any spin s, the spin-weighted spherical harmonics with $l \geq |s|$ form a complete and orthonormal basis for a spin-s field over the sphere. The phase convention follows from the definition above and reads

$${}_sY_{lm}^* = (-1)^{s+m}\, {}_{-s}Y_{l,-m} . \tag{3.48}$$

The coefficients in the expansion (3.46) are not completely independent. Reality of the vector field implies

$${}_\mp v_{lm}^* = -{}_\pm v_{l,-m}(-1)^m . \tag{3.49}$$

Since the Kantowski-Sachs model is axially symmetric under the subgroup of rotations around the z-axis, one expects that $\mathbf{v}$ has no component in the $\mathbf{e}_\varphi$-direction. Therefore, all coefficients vanish except for the ones with $m = 0$. Parity is another symmetry of

---

[12]In a real CMB measurement, one can replace f by the physical temperature field T, for which the angular two-point function can also be computed for a ΛCDM cosmological model. Instead of eq. (3.41), one has $\langle a_{lm} a_{l'm'}^* \rangle = C_l^{TT} \delta_{ll'} \delta_{mm'}$ with C_l^{TT} resembling the famous CMB curve.

the Kantowski-Sachs model, and one expects that $\mathbf{v}$ transforms accordingly under point-reflection $\mathbf{n} \rightarrow -\mathbf{n}$. This consideration yields the additional relation

$$
\begin{aligned}
{}_{\pm}v_{l0} &= {}_{\pm}v_{l0}^* && \text{for } l \text{ even} , \\
{}_{\pm}v_{l0} &= {}_{\pm}v_{l0}^* = 0 && \text{for } l \text{ odd} .
\end{aligned}
\tag{3.50}
$$

Another property of the expansion coefficients can be conjectured by drawing an analogy to electrodynamics. Consider, for instance, a localized charge distribution. It is a standard procedure to make a multipole expansion in order to obtain the field at some large distance R from the source. In the limit of $R \rightarrow \infty$, it is well-known that the contribution of each multipole l drops off as R^{-l}. A similar behavior is expected for the vector field $\mathbf{v}$. Its "source" is the anisotropic curvature, which is associated to a very remote scale. The smallness of $1/R$ in the electromagnetic example corresponds to the smallness of the parameter r defined in eq. (3.36). One therefore expects that ${}_{\pm}v_{l0} \sim r^l$ asymptotically for $r \rightarrow 0$. I write

$$
{}_{\pm}v_{l0} = {}_{\pm}v_{l0}^* \equiv {}_{\pm}v_l r^l \left[1 + \mathcal{O}(r) \right] ,
\tag{3.51}
$$

where v_l is now independent of r, and I have used the reality condition together with the parity relation.

The coefficients v_l give an expansion of $\mathbf{v}$ into parity-even, axially symmetric multipoles. Since I am interested in the limit of small r, it is sufficient to consider only the leading term,

$$
\mathbf{v}(\mathbf{n}) = \mathbf{e}_+ v_2 r^2 {}_{+1}Y_{20}(\mathbf{n}) - \mathbf{e}_- v_2 r^2 {}_{-1}Y_{20}(\mathbf{n}) + \mathcal{O}\left(r^4\right) ,
\tag{3.52}
$$

which is the quadrupole because the dipole has to vanish by parity.

In order to evaluate the scalar product $\mathbf{v} \cdot \nabla f_0$, it is useful to write the gradient field of f_0 in terms of the helicity basis, too. Using the multipole expansion of f_0, one finds

$$
-\nabla f_0(\mathbf{n}) = \frac{1}{\sqrt{2}} \left(\mathbf{e}_+ \sum_{lm} a_{lm}^* \eth Y_{lm}(\mathbf{n}) + \mathbf{e}_- \sum_{lm} a_{lm}^* \eth^* Y_{lm}(\mathbf{n}) \right) .
\tag{3.53}
$$

At order r^2, the scalar product hence evaluates to

$$
\mathbf{v} \cdot \nabla f_0(\mathbf{n}) = -\frac{1}{\sqrt{12}} \sum_{lm} a_{lm}^* v_2 r^2 \left(\eth Y_{20}(\mathbf{n}) \eth^* Y_{lm}(\mathbf{n}) + \eth^* Y_{20}(\mathbf{n}) \eth Y_{lm}(\mathbf{n}) \right) .
\tag{3.54}
$$

The expansion coefficients of the distorted map can now be related to the original coefficients by computing

$$
\begin{aligned}
\tilde{a}_{lm} &= \int d\Omega f(\mathbf{n}) Y_{lm}(\mathbf{n}) \\
&= a_{lm} + \frac{1}{\sqrt{12}} \sum_{l'm'} a_{l'm'}^* v_2 r^2 \int d\Omega \left(\eth Y_{20}(\mathbf{n}) \eth^* Y_{l'm'}(\mathbf{n}) + \eth^* Y_{20}(\mathbf{n}) \eth Y_{l'm'}(\mathbf{n}) \right) Y_{lm}(\mathbf{n}) \\
&= a_{lm} + \frac{1}{\sqrt{12}} \sum_{\substack{l'm' \\ l' \neq 0}} a_{l'm'}^* v_2 r^2 \left(l'(l'+1) - l(l+1) + 6 \right) \int d\Omega Y_{20}(\mathbf{n}) Y_{l'm'}(\mathbf{n}) Y_{lm}(\mathbf{n}) .
\end{aligned}
$$
$$
\tag{3.55}
$$

The last step follows from an identity which can be proven by repeated integration by parts until only angular momentum operators drop out. Note that the value $l' = 0$ has to be excluded – the monopole does not contribute to the gradient. One is finally left with a Gaunt's integral which gives the expansion coefficients of a product of spherical harmonics when expanded in terms of the spherical harmonics themselves. These coefficients are directly related to the Clebsch-Gordan coefficients which map the direct product of two angular momentum eigenstates into the total angular momentum representation.
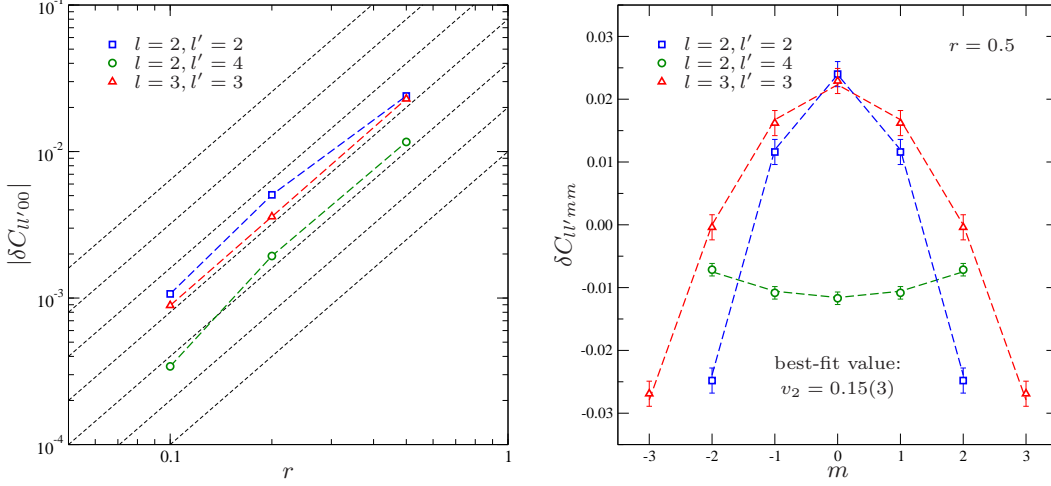
Figure 3.3: Numerical values for some correction terms $\delta C_{ll'mm}$ as a function of r (left panel) and as a function of m (right panel). The scaling with r appears to be compatible with an algebraic scaling $\sim r^2$, which is indicated by the dashed straight lines. As seen in the right panel, the values of the correction terms match the expected pattern (dashed lines) described by eq. (3.58), with a best-fit value for $v_2 = 0.15(3)$. Note that, despite the fact that the value of v_2 has not been predicted, it can be inferred numerically from a single point of the data. The hypothesis of a map distortion generated by the flux of a quadrupolar vector field is supported by the observation that all data points can be explained simultaneously.

Since one of the states in the product basis is fixed at values $l = 2$, $m = 0$, it is easy to see which values for the total angular momentum are allowed. The only non-vanishing coefficients have either $l = l'$ or $l = l' \pm 2$. The distortion generated by $\mathbf{v}$ to leading order produces correlations between coefficients which are separated by two units of angular momentum. The multipole coefficients of the distorted field are

$$\tilde{a}_{lm} = \left(1 + v_2 r^2 c_{lm}^0\right) a_{lm} + v_2 r^2 c_{lm}^+ a_{l+2,m} + v_2 r^2 c_{lm}^- a_{l-2,m} \,, \tag{3.56}$$

with deterministic real parameters c_{lm}^0, $c_{lm}^\pm$ which can be read off from eq. (3.55).

One can now compute the distorted multipole correlation by making use of the known statistical properties of the original coefficients. To order r^2, one finds

$$\langle \tilde{a}_{lm} \tilde{a}_{l'm'}^* \rangle = \frac{H^2}{2\pi} \delta_{mm'} \left[\left(1 + 2v_2 r^2 c_{lm}^0\right) \frac{\delta_{ll'}}{l(l+1)} \right.$$

$$\left. + v_2 r^2 \left(\frac{c_{l-2,m}^+}{l(l+1)} + \frac{c_{lm}^-}{(l-2)(l-1)} \right) \delta_{l-2,l'} + v_2 r^2 \left(\frac{c_{l+2,m}^-}{l(l+1)} + \frac{c_{lm}^+}{(l+2)(l+3)} \right) \delta_{l+2,l'} \right] \,, \tag{3.57}$$

where eq. (3.41) was used. Comparing with eq. (3.40), one can now read off the correction terms $\delta C_{ll'mm}$. Using Gaunt's formula and some tedious but straightforward algebra, one can obtain the following explicit expressions:

$$\delta C_{llmm} = v_2 r^2 \sqrt{\frac{15}{\pi}} \frac{l(l+1) - 3m^2}{4l(l+1) - 3} \,,$$

$$\delta C_{l,l-2,mm} = \delta C_{l-2,lmm} \underset{l>2}{=} -v_2 r^2 \sqrt{\frac{15}{\pi}} \frac{1 + l(l-1)}{2l - 6l^2 + 4l^3}$$

$$\times \sqrt{\frac{(l-m)(l+m)(l-1-m)(l-1+m)}{4l(l-1) - 3}} \,. \tag{3.58}$$

Figure 3.4: Mollweide projection of a simulated statistically isotropic random field on the sphere (solid contour lines). A quadrupolar distortion generated by a vector field with positive v_2 leads to a focussing effect towards the celestial equator (dashed contour lines). A negative v_2, on the other hand, would focus the map towards the celestial poles. The parameter v_2 characterizes the quadrupole amplitude of the vector field (see text for details).
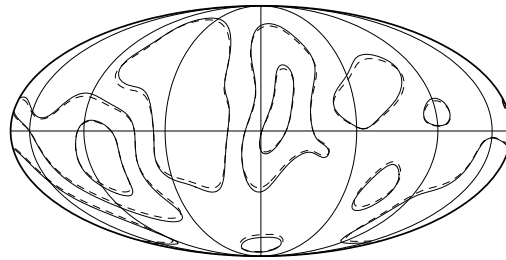
All other correction terms vanish up to order r^4.

If the correction to the multipole correlation is generated by an infinitesimal shift $\mathbf{v}$ in the map, one finds that in the limit $r \to 0$, the leading correction parameters $\delta C_{ll'mm}$ scale like r^2 and are governed by a single free parameter v_2, which characterizes the quadrupole amplitude of the shift field. In other words, if the hypothesis of a shift in the map is correct, then it should be possible to understand all the numerical results by fitting once a single global parameter.

Examining the numerical data, it appears that this is indeed the case. The left panel of fig. 3.3 shows the scaling of the numerical correction terms $\delta C_{ll'mm}$ with the parameter r for some examples. The results are in good agreement with an algebraic scaling $\sim r^2$. The right panel shows a plot of ten[13] different numerical correction terms at a fixed value $r = 0.5$. The values of $\delta C_{ll'mm}$ are in very good agreement with eq. (3.58), indicated as dashed lines, if the free parameter is fit to the value $v_2 = 0.15(3)$.

The fact that all data points can be explained simultaneously is a strong argument in support of the hypothesis regarding the nature of the effect. It seems that the geometry of the Kantowski-Sachs model leads to a distortion of the map which describes how information is distributed on the celestial sphere. In the nearly-isotropic limit, the corrections are compatible with a distortion generated by the flux of a quadrupolar, axisymmetric vector field. The positive sign of the parameter v_2, which characterizes the quadrupole amplitude of the vector field (modulo the expected r^2-scaling), implies that the map is focussed towards the celestial equator. The situation is illustrated in fig. 3.4.

It would be nice if the hypothesis could actually be proven, *e.g.* by finding an appropriate expansion of eq. (3.39). In principle, such an expansion would also determine the parameter v_2. However, I was unable to accomplish this formidable task because of the involved calculations it requires.

CMB Anomalies

Having established that the modifications of the angular two-point function in the nearly-isotropic Kantowski-Sachs model can be interpreted as a distortion which is generated by the flux of a quadrupolar, axisymmetric vector field, it is interesting to ask which implications such a distortion would have for the CMB. In particular, I want to discuss how the breaking of statistical isotropy manifests itself in the data, with special attention to the so-called *anomalies* which have already been reported [20]. The vector field distortion is a very useful tool in this respect, because it allows to study all the phenomenology based on the well-known properties of the CMB anisotropies in the statistically isotropic ΛCDM model and bypasses the cumbersome computation of cosmological perturbations in a non-standard background, for which numerical tools like CMBFAST [86] and CAMB [87] have not yet been developed. Of course, in order to check that no qualitative new modifications arise, a rigorous calculation would still be useful.

---

[13]Note that the correction terms $\delta C_{ll'mm}$ are invariant under $m \to -m$, such that of the 17 plotted values only 10 are independent.

In the statistically isotropic FRW limit, the multipole coefficients of the angular two-point correlation function on the CMB temperature map are

$$\langle a_{lm} a^*_{l'm'} \rangle_{\text{iso}} = C_l^{TT} \delta_{ll'} \delta_{mm'} \ . \tag{3.59}$$

Due to physical processes in the cosmic plasma taking place between the hot Big Bang and last scattering, the power spectrum C_l^{TT} has a more complicated structure than eq. (3.41), but since the physics is well understood and because the perturbations are in a linear regime, it can still be predicted with high accuracy[14]. Furthermore, it is not expected that these processes are affected by a small departure from the flat FRW limit, as long as the departure is associated with a length scale much larger than the Hubble radius at last scattering. Note that the comoving Hubble radius increases during radiation and matter domination, such that it is much larger today. Therefore, a distortion of the CMB (and thus, a breaking of the FRW symmetry) could be observable today although it did not play any significant role during the cosmological evolution up to last scattering.

The effect of a quadrupolar distortion can be calculated with the use of eq. (3.55). As in the test field case, it leads to additional off-diagonal correlations for multipole coefficients which are separated by two units of angular momentum, but also the diagonal correlations are modified. Let me examine the latter first. Keeping C_l^{TT} as the angular power spectrum in the isotropic limit, the diagonal correlations on the distorted CMB map read

$$\langle \tilde{a}_{lm} \tilde{a}^*_{lm} \rangle = C_l^{TT} \left(1 + v_2 r^2 \sqrt{\frac{15}{\pi}} \frac{l(l+1) - 3m^2}{4l(l+1) - 3} \right) \ . \tag{3.60}$$

It is noteworthy that this implies

$$\frac{1}{2l+1} \sum_m \langle \tilde{a}_{lm} \tilde{a}^*_{lm} \rangle = C_l^{TT} \ , \tag{3.61}$$

just as in the isotropic limit. This means that the estimator $\hat{C}_l^{TT} \equiv \sum_m |a_{lm}^{\text{obs}}|^2 / (2l+1)$ is still an unbiased estimator for the C_l^{TT} of the statistically isotropic model. Furthermore, the *cosmic variance* of the estimator is only modified at order r^4,

$$\text{Var}\left[\hat{C}_l^{TT} \right] = \frac{2C_l^2}{2l+1} \left(1 + \frac{3l(l+1)}{4l(l+1) - 3} \frac{v_2^2 r^4}{\pi} \right) \ . \tag{3.62}$$

In order to derive this expression, it has to be assumed as usual that the random fluctuations in the temperature field (in the statistically isotropic limit) are Gaussian.

The angular two-point correlation function can be characterized in an alternative way by representing it in terms of a total angular momentum basis. If I denote the "quantum numbers" associated with the total angular momentum as L and M, then the two-point correlation function can be written as

$$\mathcal{C}(\mathbf{n}, \mathbf{n}') \equiv \langle \mathbf{n}, \mathbf{n}' | \mathcal{C} \rangle = \sum_{l,l',L,M} N_{ll'}^L A_{ll'}^{LM} \langle \mathbf{n}, \mathbf{n}' | ll'; LM \rangle \ , \tag{3.63}$$

where the $A_{ll'}^{LM}$ are sometimes called *bipolar coefficients*, and I follow the normalization convention chosen by the WMAP team [20] in order to facilitate comparison. This convention has

$$N_{ll'}^L \equiv \sqrt{\frac{(2l+1)(2l'+1)}{2L+1}} \langle l, 0, l', 0 | ll'; L0 \rangle \ . \tag{3.64}$$

Other conventions can be found in the literature, for instance $N_{ll'}^L = 1$ as in [88].

---

[14]Of course, in order to calculate the angular power spectrum, a set of cosmological parameters is needed as physical input, some of which are usually inferred from CMB observations. One may thus prefer to call the result of the calculation a *postdiction* instead.

Figure 3.5: Bipolar power spectrum gener-
ated by a quadrupolar, axisymmetric distor-
tion of a simulated ΛCDM model. The plot
shows the two types of non-trivial coefficients,
A_{ll}^{20} and $A_{l-2,l}^{20}$, with the quadrupole ampli-
tude of the distortion field, $v_2 r^2$, divided out.
The angular power spectrum of the underlying
ΛCDM model was generated with CAMB us-
ing the default cosmological parameters which
produce a good fit to current CMB data.
The bipolar coefficients A_{ll}^{20} are simply pro-
portional to C_l^{TT} and therefore reproduce the
familiar angular power spectrum. The bipolar
coefficients $A_{l-2,l}^{20}$, on the other hand, depend
on two different C_l^{TT} which are separated by
two units of angular momentum. The shape of
the corresponding curve is more complicated
and appears very noisy.
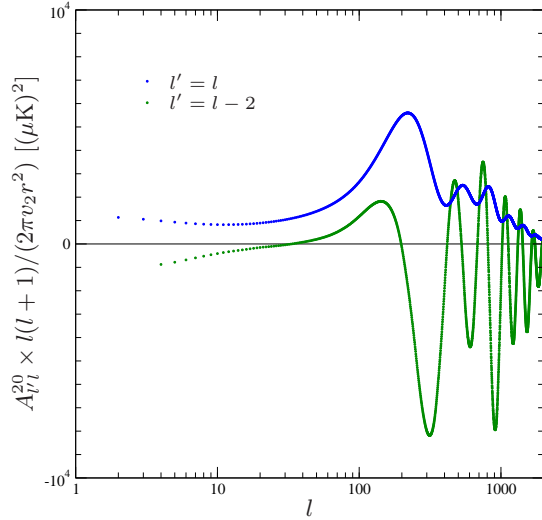
Because the total angular momentum eigenstates $|ll'; LM\rangle$ generate a $(2L+1)$-dimen-
sional representation of the rotation group, it is evident that $\mathcal{C}(\mathbf{n}, \mathbf{n}')$ is statistically isotropic
if and only if $A_{ll'}^{LM} = 0$ for all $L > 0$. The only non-vanishing coefficients therefore are the
A_{ll}^{00}, and the normalization (3.64) is chosen such that $A_{ll}^{00} = C_l^{TT}$.

The bipolar coefficients can be computed from the sum over the multipole correlations,
dressed with appropriate Clebsch-Gordan coefficients:

$$\sum_{mm'} \langle \tilde{a}_{lm} \tilde{a}_{l'm'} \rangle \langle l, m, l', m' | ll'; LM \rangle = N_{ll'}^L A_{ll'}^{LM} \ . \tag{3.65}$$

With the known properties of the multipole correlations which are the result of the axi-
symmetric and quadrupolar character of the distortion, one can see that only three types
of bipolar coefficients occur. These are

$$A_{ll}^{00} \ \ = \ \ C_l^{TT} \ , \tag{3.66}$$

$$A_{ll}^{20} \ \ = \ \ \frac{3 v_2 r^2}{\sqrt{3\pi}} C_l^{TT} \ , \tag{3.67}$$

$$A_{l-2,l}^{20} \ \ = \ \ \frac{v_2 r^2}{\sqrt{3\pi}} \left(C_l^{TT} (l+1) - C_{l-2}^{TT} (l-2) \right) \ , \tag{3.68}$$

where I used eq. (3.55) together with eq. (3.65) in order to obtain the explicit expressions.
All other bipolar coefficients vanish up to order r^4.

Evidently, the coefficients A_{ll}^{00} remain unchanged at order r^2, whereas the two new non-
vanishing types of coefficients, A_{ll}^{20} and $A_{l-2,l}^{20}$, carry the information about the diagonal
and off-diagonal corrections, respectively. Both are proportional to $v_2 r^2$, as expected. A
plot of their l-dependence is shown in fig. 3.5 for a simulated[15] ΛCDM model.

It should be noted that the bipolar coefficients depend on the choice of the quantization
axis for the total angular momentum. The results presented here are valid if this axis coin-
cides with the axis of symmetry of the distortion. A direct comparison with observational
data, from which estimators for the bipolar coefficients can be obtained, requires an *a pri-
ori* knowledge of the direction in the sky in which this axis is pointing. Unfortunately, we
are in the less comfortable situation that we have to infer this direction from observational
data too. If the distortion effect is very small, this can become arbitrarily difficult.

---

[15]I used the web-based CAMB interface of LAMBDA (http://lambda.gsfc.nasa.gov/toolbox/) with
the default parameters $t_0 = 13.738$ Gyr, $\Omega_b h^2 = 0.0226$, $\Omega_c h^2 = 0.114$, $\Omega_\Lambda = 0.7212$, $\Omega_K = \Omega_\nu = 0$,
$\tau_{rec} = 283.72$ Mpc, $\tau_0 = 14301.8$ Mpc.

The WMAP team has estimated the bipolar coefficients of the CMB temperature map for a certain choice of quantization axis, *cf.* [20]. A look at their figure 16 reveals that the coefficients A_{ll}^{20} are fairly compatible with the hypothesis that $A_{ll}^{20} \propto C_l^{TT}$, as in the case of a quadrupolar and axisymmetric map distortion. The coefficients $A_{l-2,l}^{20}$, however, do not seem to resemble the pattern shown in my fig. 3.5. Since it is uncertain if the choice of quantization axis made by the WMAP team was adequate, the comparison remains inconclusive[16]. On the other hand, the overall amplitude of the observed signal should at least give an upper bound on the amplitude of a possible distortion, determined by the parameter combination $v_2 r^2$. Comparing the observed amplitude of A_{ll}^{20} with my fig. 3.5 gives a very rough bound of $v_2 r^2 \lesssim \text{few} \times 10^{-2}$. I will show in chapter 4 that a much more stringent bound can be obtained from the CMB quadrupole once the corrections due to late-type effects are taken into account.

In several papers [17, 18, 19, 20] an exceptional alignment of the CMB temperature quadrupole with the octopole has been reported. Depending on the statistics used, the alignment has been claimed to be more or less highly significant. Due to the implementation of *a posteriori* statistics, the true significance is hard to judge, however, the issue has attracted a lot of interest in recent years. It is therefore interesting to study whether a quadrupolar and axisymmetric distortion of the temperature map could account for such an alignment. I have carried out a statistical test using the method of multipole vectors as outlined in [89]. The results, published in [2], show that the map distortion does indeed favor some alignment of the quadrupole and octopole. However, the effect remains so small that it is probably unable to account for an alignment at the observed level.

3.3.2 Bubble Collisions

In the final part of this chapter, I want to briefly discuss the signatures of *bubble collisions* as another class of observable effects in the tunneling scenario. A rigorous treatment would go beyond the intention of this work, so I will only give some heuristic results here, quoting the relevant literature on this interesting subject. The subject has a long history and was considered already in the context of "old inflation," see *e.g.* [53]. A more specific study of observational effects in cosmology has been initiated more recently *e.g.* in [90, 91]. Based on the new insights, a preliminary search for observational evidence in current CMB data has been attempted in [92].

If the premise holds that our observable Universe is located within a bubble which collided with other similar bubbles, it is commonly believed that the collisions may lead to perturbations which give rise to distinct observational signatures. Some presumed properties of these perturbations can be understood without studying the dynamics of bubble collisions in detail. For instance, the symmetries of a collision setup involving two bubbles strongly suggest that the perturbation is axisymmetric from the point of view of an observer inside one of the bubbles. One could imagine that each collision which is causally accessible to her leads to a disk-like disturbance of the CMB temperature field on her celestial sphere. Precisely such disturbances have been sought for in [92].

In the context of transdimensional tunneling events, the possibilities for bubble collisions are constrained by the additional requirement that the bubbles have to be separated along a direction which is macroscopic in the parent vacuum. This leads to interesting consequences if some of our observed macroscopic directions are the result of a decompactification. It has been pointed out in [93] that the collision events with other bubbles are seen on a great circle in the sky if only one of our dimensions was compact and microscopic prior to the tunneling event. This may be intuitively clear since the remaining two dimensions define a plane in which the different bubbles can be separated, the great circle marking the edge-on view into this plane. For the same reasons, in case of two dimensions

---

[16]One could try to rotate the quantization axis for the distortion model and see if a choice can be found for which the pattern of the bipolar power spectrum is compatible with the observed one.

being the result of decompactification, any collision events are expected to be seen on two single antipodal points on our celestial sphere. Therefore, if several collision events can be identified, their locations on our celestial sphere will give us some information about the type of tunneling event which occurred. Two collisions observed at antipodal locations would indicate a scenario where two of our macroscopic directions are the result of decompactification, while three collisions on a great circle would suggest decompactification of a single dimension. In both cases, the observation would also allow one to determine exactly in which directions the compact dimensions unfold. On the other hand, three collisions which are clearly not on a great circle would probably rule out the possibility that any of our dimensions decompactified in the most recent tunneling event.

Chapter 4

Phenomenology of Anisotropic Spacetime

In this final chapter of this work, I will shift the focus towards the cosmological era after the hot Big Bang and discuss some effects which a small global anisotropy may have on the evolution of our Universe. I have already shown in section 1.1 that curvature has an effect on the expansion history, since it gives rise to a term in Friedmann's equations. Furthermore, the angular diameter distance also depends on the spatial curvature, which has to be taken into account when interpreting observations. In the last chapter, I introduced some cosmological models with *anisotropic curvature*, known as the Bianchi III and Kantowski-Sachs models. The curvature in these models will also have an effect on the expansion history and angular diameter distance, with the additional complication that the effect is anisotropic. I will show in the next section that anisotropic curvature acts as an anisotropic source in Einstein's equations and leads to differential expansion. But also in spatially flat models there may be sources of anisotropy. As a particular example, I will discuss a homogeneous magnetic field in section 4.2.

Since cosmic redshift is the result of expansion integrated along the line of sight, any differential expansion will give rise to anisotropic redshift. This effect can be used to constrain any source of anisotropy which causes differential expansion. For instance, a very stringent constraint can be obtained from the quadrupole which an anisotropic redshift would produce in the CMB. It should be noted, however, that this only puts limits on the total amount of differential expansion between photon last scattering and today. This has to be considered carefully, since in some cases there are mechanisms which can dynamically isotropize the expansion. If this happens before last scattering, the differential expansion will not be seen in the CMB quadrupole – at least not at the expected level. In section 4.3 I will explain how dynamical isotropization can be achieved. Continuing the example of the homogeneous magnetic field I show that free-streaming particles, *e.g.* cosmic neutrinos, can give rise to considerable isotropization.

4.1 Anisotropic Curvature

The anisotropic geometries which I want to consider are characterized by the line element of eq. (3.10), with $K_\perp$ positive, negative or zero. I assume that the cosmic fluid respects the symmetries of this metric *ansatz*. In particular, this requires that the fluid is isotropic with respect to the residual $O(2)$-symmetry of rotations around the z-axis. The stress-energy tensor in the comoving frame still has diagonal form, but the pressure components parallel and perpendicular to the z-axis are in principle independent. Einstein's equations for such

a homogeneous but anisotropic *ansatz* reduce to following set of evolution equations,

$$\left(\frac{\partial_t a_\perp}{a_\perp}\right)^2 + 2\frac{\partial_t a_\perp}{a_\perp}\frac{\partial_t a_\parallel}{a_\parallel} = 8\pi\rho - \frac{K_\perp}{a_\perp^2} + \Lambda \ , \tag{4.1}$$

$$\frac{\partial_t^2 a_\perp}{a_\perp} + \frac{\partial_t^2 a_\parallel}{a_\parallel} + \frac{\partial_t a_\perp}{a_\perp}\frac{\partial_t a_\parallel}{a_\parallel} = -8\pi P_\perp + \Lambda \ , \tag{4.2}$$

$$2\frac{\partial_t^2 a_\perp}{a_\perp} + \left(\frac{\partial_t a_\perp}{a_\perp}\right)^2 = -8\pi P_\parallel - \frac{K_\perp}{a_\perp^2} + \Lambda \ , \tag{4.3}$$

see, *e.g.*, [85]. These are, in some sense, the generalized Friedmann's equations. It is useful to introduce the two expansion rates $H_\parallel \equiv \partial_t a_\parallel / a_\parallel$ and $H_\perp \equiv \partial_t a_\perp / a_\perp$. Differential expansion can then be characterized by the quantity $\Delta H \equiv H_\perp - H_\parallel$. The last two equations (4.2) and (4.3) can be combined to an evolution equation for ΔH,

$$\partial_t \Delta H + \left(2H_\perp + H_\parallel\right)\Delta H = 8\pi\left(P_\perp - P_\parallel\right) - \frac{K_\perp}{a_\perp^2} \ . \tag{4.4}$$

It is evident from this equation that differential expansion can be sourced by anisotropic stress $P_\parallel \neq P_\perp$ and by anisotropic curvature. On the other hand, anisotropic stress may be sourced by differential expansion, such that backreaction effects may become relevant. This mutual dependency is very important for any mechanism of dynamical isotropization, as I will explain in the corresponding section 4.3.

Since our observable Universe, to first approximation, can be described by the flat FRW model, it makes sense to treat ΔH and any source of anisotropy as small quantities suitable for a Taylor series expansion. One can then linearize all evolution equations and compute correction terms order by order in the small quantities. I will consider the leading order only.

In this section, I want to focus on the case where the differential expansion is sourced only by anisotropic curvature. Let me introduce the anisotropic curvature *density parameter*[1]

$$\Omega_{K_\perp} \equiv \frac{K_\perp}{a_\perp^2 H_\perp^2} \ , \tag{4.5}$$

cf. eq. (1.10). Furthermore, let me rescale the coordinates such that $K_\perp = \pm 1$, where the positive sign characterizes the Kantowski-Sachs model, while the negative sign belongs to the Bianchi III model. I want to estimate the effect of differential expansion, caused by the anisotropic curvature in these models, on the temperature map of the CMB. To this end I will solve the evolution equations to leading order in the matter dominated era. I assume that this is a good approximation for the cosmic evolution between photon last scattering and today, since radiation was subdominant already at last scattering and dark energy became dominant only very recently. I make this approximation only in order to get analytic results, since it would be no difficulty to solve the full evolution equation for a ΛCDM model with anisotropic curvature numerically. I will use the analytic results to estimate the CMB quadrupole resulting from the anisotropic redshift.

The temperature quadrupole, of course, also corresponds to a new source of anisotropic stress which is dynamically generated by differential expansion. However, since radiation is subdominant, I ignore any backreaction effects. I will show that the differential expansion, and therefore the temperature anisotropy, is proportional to $\Omega_{K_\perp}$. Thus, the backreaction term is expected to be suppressed by $\Omega_{K_\perp} \times \Omega_\gamma$, where Ω_γ is the density parameter of the CMB photons. Evidently, this term will be considerably smaller than the primary source

---

[1]The definition of a density parameter in an anisotropic background is a bit ambiguous. Furthermore, a look at eq. (4.1) suggests to add a factor of 1/3. However, I choose this definition as it is already used in the existing literature.

of differential expansion, which is $\Omega_{K_\perp}$. In section 4.3, I will discuss a different example where the backreaction term indeed becomes relevant.

Since I assume that the expansion rates $H_\parallel$ and $H_\perp$ differ only by an infinitesimal quantity, I can rescale the coordinates such that the scale factors themselves match at leading order, with their relative difference being just another infinitesimal number which I introduce now as

$$\delta \equiv \frac{a_\perp - a_\parallel}{a} \; . \tag{4.6}$$

The scale factor a in the denominator needs only to be defined at leading order, since corrections would change this definition only at order δ^2 and I am just interested in quantities linear in δ. For definiteness, I choose the geometric mean $a \equiv a_\perp^{2/3} a_\parallel^{1/3}$. At linear order, δ is just the integral of ΔH,

$$\int_{t_*}^{t_0} \Delta H(t)dt = \ln \frac{a_\perp(t_0)}{a_\parallel(t_0)} - \ln \frac{a_\perp(t_*)}{a_\parallel(t_*)} \simeq \delta(t_0) - \delta(t_*) \; . \tag{4.7}$$

At several places during the calculation, the expansion rate needs only be evaluated at zeroth order. I will use the symbol H in this case, and for definiteness, one can take $H \equiv \partial_t a/a$.

Let me now consider the following problem. A comoving element of cosmic plasma at the surface of last scattering emits photons with a spectrum of an ideal black body at temperature T_*. After a long time of free streaming, the photons are detected by a comoving ideal observer. Given that the geometry of spacetime is well approximated by a homogeneous and almost-isotropic model with line element as in eq. (3.10), what is the spectrum of those photons that she measures?

The spectrum at emission is given by Planck's law,

$$I_* = \frac{2p_*^3}{e^{p_*/T_*} - 1} \; , \tag{4.8}$$

where I_* is the intensity, *i.e.* the amount of energy per unit surface area (of the black body) per unit time interval per unit solid angle per infinitesimal wavenumber interval emitted at wavenumber p_*. The energy of a photon, however, is not a conserved quantity in an expanding universe. On the other hand, the number of photons per comoving volume element *is* a conserved quantity in the absence of interactions. Since each photon carries a quantum of energy which is proportional to its wavenumber, the intensity I_0 at the detector is related to I_* by

$$\frac{I_0}{p_0}dp_0 dA_0 dt_0 d\Omega_0 = \frac{I_*}{p_*}dp_* dA_* dt_* d\Omega_* \; , \tag{4.9}$$

where the quantities in this equation are related as follows. First, p_0 is related to p_* by a redshift factor, which has to be computed along the photon trajectory. Since spacetime is anisotropic, this redshift factor will depend on the orientation of the detector. If the observer chooses a local spherical coordinate system in her inertial frame whose polar axis is aligned with the z-direction, the redshift factor will be a function of the polar angle ϑ_0 only, due to the residual $O(2)$-symmetry of the model. The time intervals dt_0 and dt_* are related by the same redshift factor. The surface element dA_0 of the detector collects the photons which are emitted into the solid angle element $d\Omega_*$. *Vice versa*, the surface element dA_* on the black body source corresponds to a certain solid angle $d\Omega_0$ at the detector. A remarkable result of GR (see, for instance, [94]) is the so-called *reciprocity relation*

$$\frac{dA_0}{d\Omega_*} = \frac{p_*^2}{p_0^2} \frac{dA_*}{d\Omega_0} \; , \tag{4.10}$$

which holds in any spacetime and independently of the proper motions of the source and the observer. Note the important implication of this relation when applied to the present

problem:

$$I_0 = \frac{2p_0^3}{e^{p_*/T_*} - 1} \ . \tag{4.11}$$

The black body character of the source spectrum is preserved! The apparent temperature is simply $T_0 \equiv T_* p_0/p_*$. The important remark here is that the redshift factor p_0/p_* depends on the polar angle ϑ_0 at which the photon is received, but not on the wavenumber of the photon. I will now compute the redshift factor to linear order in δ.

In order to obtain the redshift factor of a photon which is received at a detector angle ϑ_0, one has to realize that the components of the wave vector parallel and perpendicular to the polar axis have been redshifted with the corresponding scale factors. The wavenumber at emission is therefore given as

$$p_* = p_0 \sqrt{\frac{a_\perp^2(t_0)}{a_\perp^2(t_*)} \sin^2\vartheta_0 + \frac{a_\parallel^2(t_0)}{a_\parallel^2(t_*)} \cos^2\vartheta_0} \ . \tag{4.12}$$

Since I want to compute the temperature anisotropy which is induced by differential expansion, let me assume that the temperature field at last scattering was uniform, *i.e.* the surface of last scattering emits at a uniform temperature T_*. The average temperature of the CMB as measured by the observer is given by an integral over the celestial sphere,

$$\bar{T}_0 \equiv \frac{1}{4\pi} \int d\Omega_0 T_0 = \frac{T_*}{2} \int_0^\pi \sin\vartheta_0 d\vartheta_0 \left(\frac{a_\perp^2(t_0)}{a_\perp^2(t_*)} \sin^2\vartheta_0 + \frac{a_\parallel^2(t_0)}{a_\parallel^2(t_*)} \cos^2\vartheta_0 \right)^{-1/2} \ . \tag{4.13}$$

The temperature anisotropy is finally given by

$$\frac{\delta T}{T}(\vartheta_0) = \frac{T_0(\vartheta_0) - \bar{T}_0}{\bar{T}_0} = \frac{\delta(t_0) - \delta(t_*)}{6} \left(1 + 3\cos 2\vartheta_0 \right) + \text{higher order terms} \ . \tag{4.14}$$

This expression can be found by making a Taylor series expansion in δ and noting that the integral expression which defines $\bar{T}_0$ reduces to elementary integrals at each order. Evidently, the temperature anisotropy has quadrupole character, and its amplitude is given by the total differential expansion accumulated between last scattering and detection. Since differential expansion, in the present model, is sourced by anisotropic curvature, one can put limits on the curvature parameter by relating it to the amplitude of the CMB quadrupole.

In order to establish this relation, one needs to solve the evolution equation (4.4) and integrate once to obtain $\delta(t_0) - \delta(t_*)$. At linear order, this can be done analytically if one assumes *e.g.* a purely matter dominated background. In this case, the zeroth order scale factor is proportional to $t^{2/3}$. Since $\Omega_{K_\perp} \propto (\partial_t a_\perp)^{-2}$, the leading order is given by $\Omega_{K_\perp} \propto t^{2/3}$. Note that $\Omega_{K_\perp}$ is a small quantity such that corrections to it are already of quadratic order. One can solve the linearized eq. (4.4) immediately and finds

$$\frac{\Delta H}{H} = -\frac{2}{5}\Omega_{K_\perp} + \frac{C}{t} \ , \qquad \text{(matter domination)} \tag{4.15}$$

where C is an integration constant for the homogeneous solution. Its value is fixed by the initial conditions at the onset of matter domination, but since the homogeneous solution decays quite rapidly, I will drop the entire term. Since the only source of anisotropy in the model is $\Omega_{K_\perp}$, which is a growing function of time in the entire post-Big-Bang era up to the point when dark energy begins to dominate, it is not expected that the homogeneous term will play any important role.

Integration of the inhomogeneous piece readily gives

$$\delta(t_0) - \delta(t_*) \simeq -\frac{2}{5}\left[\Omega_{K_\perp}(t_0) - \Omega_{K_\perp}(t_*)\right] \simeq -\frac{2}{5}\Omega_{K_\perp}(t_0) \ . \tag{4.16}$$

In the last approximation I drop the term coming from the lower bound since the integral is dominated by the upper bound due to the argument given above.

Putting everything together, the quadrupolar CMB anisotropy caused by the differential expansion in a background with anisotropic curvature is given roughly by

$$\frac{\delta T}{T}(\mathbf{n}) = -\frac{8}{15}\sqrt{\frac{\pi}{5}}\Omega_{K_\perp}(t_0)Y_{20}(\mathbf{n})\ , \tag{4.17}$$

where $\mathbf{n}$ is the direction of observation in the observer's frame. A similar result is given in [85], where a complete leading-order calculation of the null geodesics is presented. With this calculation, the authors attempt to study also the distortion of primary CMB anisotropies due to late-time effects. It turns out that the distortion leads to similar effects as in section 3.3.1, in particular to additional correlations in the multipoles which are separated by two units of angular momentum.

The important point about the late-time effects, however, is the differential redshift which occurs in addition to any distortion of the CMB anisotropy pattern. As I have demonstrated, this leads to a non-stochastic contribution to the CMB quadrupole with an amplitude which is proportional to $\Omega_{K_\perp}(t_0)$. Therefore, the observed CMB quadrupole can be used to put limits on models with anisotropic curvature. In particular, the CMB quadrupole observed by the WMAP space probe indicates that $\Omega_{K_\perp}(t_0) \lesssim 10^{-5}$. If this limit turns out to be robust, it will be very difficult to detect any signatures of anisotropic curvature in the higher multipoles. In this context, it should be noted that the parameter r introduced in section 3.3.1 is related to $\Omega_{K_\perp}$ approximately as

$$r \equiv \int_{t_*}^{t_0} \frac{dt}{a_\perp} \simeq 3\sqrt{\Omega_{K_\perp}(t_0)}\ . \qquad \text{(matter domination)} \tag{4.18}$$

Therefore, the previous limit $v_2 r^2 \lesssim \text{few} \times 10^{-2}$, with a best-fit value of $v_2 = 0.15(3)$ in the Kantowski-Sachs model, directly translates to a limit $\Omega_{K_\perp}(t_0) \lesssim \text{few} \times 10^{-2}$. Evidently, the limit obtained from the CMB quadrupole, taking into account differential expansion in the post-Big-Bang era, gives a much more stringent constraint.

The following conclusion seems inescapable. Since the amplitudes of the quadrupolar distortion field and the anisotropic redshift quadrupole are both controlled by the same small quantity $\Omega_{K_\perp}$, the possibility to observe the former is strongly limited by the non-observation of the latter. Note that the distortion acts upon another small quantity – the pattern of anisotropies which are of order 10^{-5} only. Therefore, it seems much harder to detect the distortion, despite the fact that the measurement of a large number of multipole correlations can help in terms of better statistics.

However, it should be noted that this statement can be mitigated if the anisotropic redshift is canceled somehow. Without fine-tuning, this can only be achieved if there is a mechanism of *dynamical isotropization* at work. The requirements for such a mechanism will be outlined in the corresponding section 4.3.

4.2 A Homogeneous Magnetic Field

The origin of cosmic magnetic fields with coherence lengths above the kiloparsec scale [95] is still being investigated, and both astrophysical and primordial origin is being considered a possibility. The astrophysical scenarios typically have problems to generate very large coherence lengths given the limited time which is available for cosmic structure formation. On the other hand, the primordial magnetogenesis scenarios can have exceedingly large coherence scales if the magnetic fields are produced during inflation but suffer from the drawback that adiabatic evolution typically tends to deplete the field strength too rapidly. Furthermore, the homogeneous limit can be used to put some simple constraints on the scenarios of primordial magnetic field origin. In this context the field strength on

coherence scales exceeding our Hubble radius is approximated by a homogeneous magnetic field mode. Similar to the case of anisotropic curvature, the magnetic field gives rise to a quadrupolar anisotropy in the CMB which has been used to put limits on the field strength in the homogeneous mode [96]. Other constraints include cross-correlations between CMB temperature and polarization anisotropies due to Faraday rotation [97]. In this section I want to examine only the quadrupolar CMB anisotropy caused by a homogeneous magnetic field. Following the approach of the previous section, this is a straightforward exercise.

Since the primary source of anisotropy is now in the cosmic fluid, I will consider a spatially flat background model. The line element is that of eq. (3.10) with $K_\perp = 0$, and I assume that the homogeneous magnetic field is aligned with the z-direction. The background is therefore given by an axisymmetric Bianchi I model, which is the simplest model compatible with a homogeneous magnetic field. Apart from the homogeneous magnetic field I assume that the cosmic fluid is given by the usual constituents present in the ΛCDM concordance model. Furthermore, for the time being, let me also assume that any anisotropy in the other constituents is irrelevant. The stress of the homogeneous magnetic field is intrinsically anisotropic and assumed to be the only anisotropic contribution to the stress-energy tensor. The components are related as

$$P_{B,\perp} = -P_{B,\parallel} = \rho_B = \frac{B^2}{8\pi} \; , \tag{4.19}$$

where ρ_B is the energy density in the homogeneous magnetic field, $P_{B,\perp}$ and $P_{B,\parallel}$ are, respectively, the pressure components perpendicular and parallel to the field direction, and B is the physical field strength. Note that B decays adiabatically as $a_\perp^{-2}$, which implies that ρ_B scales as $a_\perp^{-4} \sim a^{-4}$. Let me introduce a density parameter for the magnetic field as

$$\Omega_B \equiv \frac{8\pi\rho_B}{3H^2} \; . \tag{4.20}$$

With this definition, the linearized version of eq. (4.4) reads

$$\partial_t \Delta H + 3H\Delta H = 6H^2\Omega_B \; . \tag{4.21}$$

I assume that ΔH and Ω_B are small quantities and want to calculate the quadrupolar CMB anisotropy to leading order in them.

As in the last section, I use the approximation that the Universe is matter dominated between last scattering and today. In this case, $\Omega_B \sim t^{-2/3}$ to leading order, just as radiation. The above equation is readily solved,

$$\frac{\Delta H}{H} = 12\Omega_B + \frac{C}{t} \; , \qquad \text{(matter domination)} \tag{4.22}$$

where C is again the integration constant for the homogeneous solution. The latter decays faster than the inhomogeneous piece, and therefore I drop it as before. Integration yields

$$\delta(t_0) - \delta(t_*) \simeq 12\left[\Omega_B(t_*) - \Omega_B(t_0)\right] \simeq 12\Omega_B(t_*) \; . \tag{4.23}$$

In the last approximation, I dropped the term coming from the upper bound since the integral this time is dominated by the lower bound. The quadrupolar anisotropy is therefore roughly given by

$$\frac{\delta T}{T}(\mathbf{n}) = 16\sqrt{\frac{\pi}{5}}\Omega_B(t_*)Y_{20}(\mathbf{n}) \; . \tag{4.24}$$

Taking the magnitude of the CMB quadrupole as observed by the WMAP space probe as an upper limit, one can obtain a rough bound of $B \lesssim \text{few} \times 10^{-9}$ Gauss, scaled to today's value.

4.3   Dynamical Isotropization

The constraints on anisotropic models presented in the last two sections hold under the simplistic assumption that there is only a single source of anisotropy and there are no significant backreaction effects. In particular, it was assumed that the stress-energy tensor of the remaining constituents of the cosmic fluid is isotropic throughout. In this section I will show that differential expansion can in fact lead to a buildup of anisotropic stress in some initially isotropic component which can have a significant effect on the anisotropic expansion. Expanding the previous example of a homogeneous magnetic field, I will show that free-streaming radiation dynamically generates anisotropic stress which tends to isotropize the total stress-energy tensor. During radiation domination, this backreaction effect can evolve towards an equilibrium state where the anisotropic stress of the homogeneous magnetic field is completely compensated. Since the free-streaming radiation and the magnetic field scale in the same way with cosmic expansion, at least at leading order, this equilibrium can remain intact. These findings, which I will summarize in the following, have been published in [3], where more details can be found.

I want to consider a species of ultra-relativistic particles X which *initially*, *i.e.* at very high temperature, is in thermal equilibrium with the primordial plasma. Examples from the standard model of particles are photons and neutrinos. Gravitons are an interesting case for themselves, though they are never in thermal equilibrium unless the Universe is at some time hotter than the Planck temperature. A brief discussion can be found in [3]. In thermal equilibrium, the collision term in Boltzmann's equation continuously maintains the isotropy of the momentum space distribution such that the particle X can not generate any significant anisotropic stress. However, as the Universe expands and cools, the particle will eventually decouple from the thermal bath and start to free-stream. This happens typically when the temperature drops below some characteristic scale which is set by the strength of the interaction and can be estimated simply by equating the scattering rate with the expansion rate of the background. The decoupling temperature of cosmic neutrinos is roughly $T_{\nu,*} \simeq 1.4$ MeV, while photons decouple at roughly $T_{\gamma,*} \simeq 0.26$ eV.

For a homogeneous distribution of free-streaming particles, the momentum space distribution function in terms of the *comoving* momenta remains invariant. This, however, means that the *physical* momenta will give rise to anisotropic stress if the expansion rate is not isotropic. This can be seen by considering the components of the stress-energy tensor in the comoving frame,

$$\rho_X = n_X \int d^3 p f_X(t,p) p^0 \ , \tag{4.25}$$

$$P_{X,i} = n_X \int d^3 p f_X(t,p) \frac{\left(p^i\right)^2}{p^0} \ , \tag{4.26}$$

where p^μ is the physical four-momentum in the comoving frame, n_X is the number density of the species X, and $f_X(t,p)$ is the one-particle momentum space distribution function. Since f_X is invariant in the comoving picture, the time dependence comes entirely from the redshift of the physical momenta. By rewriting the integrals in terms of the comoving momenta, the anisotropic stress for an ultra-relativistic species X can therefore be calculated without a detailed knowledge of f_X. The only essential assumption is that f_X is isotropic at the time of decoupling. Making an expansion to first order in δ, one finds that the anisotropic stress is given by

$$P_{X,\perp} - P_{X,\parallel} = -\frac{8}{15} \rho_X \left[\delta(t) - \delta(t_{X,*})\right] + \text{higher order terms} \ , \tag{4.27}$$

where I introduced the time of decoupling $t_{X,*}$. This equation holds as long as the species X is ultra-relativistic, *i.e.* $p^\mu p_\mu = 0$. For massive neutrinos which eventually become non-relativistic, the anisotropic stress will quickly decay once their kinetic energy drops below

their mass scale. The mass ranges currently favored by measurements of neutrino flavor oscillations suggest that this may have happened quite recently in cosmic history.

With the above result, I can now take into account the backreaction effect of a free-streaming species X on the evolution of anisotropic expansion. If the primary source of anisotropy is a homogeneous magnetic field, the linearized evolution equation for δ reads

$$\partial_t^2 \delta + 3H \partial_t \delta + \frac{8}{5} H^2 \Omega_X \left[\delta - \delta(t_{X,*}) \right] = 6H^2 \Omega_B \ , \tag{4.28}$$

where I have used eq. (4.4) and identified $\partial_t \delta \simeq \Delta H$ by virtue of eq. (4.7). By introducing the new variable $N \equiv \ln a$, this equation can be transformed to the equation of a damped oscillator,

$$\partial_N^2 \delta + \frac{3}{2} \left(1 - w \right) \partial_N \delta + \frac{8}{5} \Omega_X \left[\delta - \delta(t_{X,*}) \right] = 6 \Omega_B \ . \tag{4.29}$$

I have used Friedmann's equations together with the barotropic equation of state (1.6), which are assumed to be valid zeroth order approximations.

In the radiation dominated era ($w = 1/3$), both Ω_X and Ω_B are constant at leading order. The solution therefore reads

$$\delta - \delta(t_{X,*}) = \frac{15}{4} \frac{\Omega_B}{\Omega_X} + e^{-N/2} \left(C_+ e^{iN\sqrt{8\Omega_X/5 - 1/4}} + C_- e^{-iN\sqrt{8\Omega_X/5 - 1/4}} \right) \ . \tag{4.30}$$

The constants of integration C_+ and C_- are fixed by the initial conditions at decoupling. Since the contribution of species X to eq. (4.29) vanishes before decoupling, the dominant solution there is simply $\delta \simeq 6N\Omega_B + C$, such that the matching conditions at $t_{X,*}$ are $\delta = \delta(t_{X,*})$ and $\partial_N \delta = 6\Omega_B$.

The system is that of a damped oscillator with constant mass and damping whose equilibrium position is given by $\delta = \delta(t_{X,*}) + (15/4)\Omega_B/\Omega_X$. The mass, however, is determined by the density parameter of species X. For $\Omega_X > 5/32$, the system is underdamped and oscillates around the equilibrium position with a damping envelope of $e^{-N/2}$. The damping timescale is therefore set by roughly one Hubble time. For the case of cosmic neutrinos, which are commonly assumed to have a density parameter comparable to the one of photons as long as they remain ultra-relativistic, this means that $\Delta H/H \simeq \partial_N \delta$ will decay within a few seconds after the temperature has dropped below 1.4 MeV. After that, δ will remain constant at its equilibrium value all the way until the neutrinos eventually become non-relativistic. During this time, $\Delta H/H \simeq 0$ and there is no differential expansion. The free-streaming particles have dynamically isotropized the Universe.

This mechanism of dynamical isotropization relies upon two important conditions. Firstly, the species X redshifts exactly in the same way as the primary source of anisotropy, which is the homogeneous magnetic field. Therefore, once the anisotropic stress in the free-streaming component has adjusted to the value of the magnetic field, the total stress-energy tensor remains isotropic irrespectively of the cosmic evolution, which is now in a Friedmann phase. Secondly, the damping can only be efficient if the species X contributes appreciably to the total energy density of the Universe. Good efficiency is guaranteed if $\Omega_X \gtrsim 5/32$, otherwise the system will be overdamped with detrimental effects on the damping timescale. In particular, if $\Omega_X \ll 5/32$ one can see that there is a mode which decays extremely slowly, roughly as $e^{-8N\Omega_X/5}$.

If neutrinos were massless, one would conclude that the backreaction effect completely spoils the constraint on a homogeneous magnetic field derived from the CMB quadrupole in the last section. However, it is expected that cosmic neutrinos, or at least some flavors thereof, became non-relativistic already. This happens when their physical momentum becomes redshifted below their mass scale[2]. When the cosmic neutrinos become non-

---

[2] Naively one might think that this happens precisely when the temperature of the Universe drops below the neutrino mass. However, one should keep in mind that the cosmic neutrinos dropped out of thermal equilibrium at roughly $T = 1.4$ MeV and that they then retain their extremely relativistic Fermi-Dirac distribution. Furthermore, electron-positron annihilation takes place *after* neutrino decoupling, which leads to additional heating of the photons.

relativistic, their pressure begins to decay more rapidly and can therefore be neglected later on. The compensation effect which isotropized the total stress-energy tensor is lost and some differential expansion can again begin to develop. The quadrupolar temperature effect in the CMB then depends on the neutrino mass scale, because it determines the total amount of differential expansion between photon last scattering and today. The situation is illustrated in fig. 4.1, which shows numerical results for $\Delta H/H$ and δ for different neutrino mass scales. The anisotropic stress which is dynamically generated by the neutrinos is computed by numerically solving the momentum integrals with the true out-of-equilibrium Fermi-Dirac distribution of massive fermions, which is expanded to first order in δ. The underlying zeroth-order cosmological model is based on a realistic ΛCDM cosmology. The cosmological parameters were chosen as $\Omega_\Lambda = 0.73$, $\Omega_m = 0.27$ today, where Ω_m includes a contribution of massive neutrinos which is approximated by $\Omega_\nu h^2 = N_\nu m_\nu/94$ eV with $N_\nu \simeq 3$. For some details how massive neutrinos can be handled in the ΛCDM model, see *e.g.* [98]. In order to simplify the analysis, the different neutrino flavors have not been distinguished. It is expected that taking into account different mass scales for different flavors will change the overall result at most by a numerical factor of order unity. A more explicit account of the numerical study from which the results presented here are taken can be found in [3].

One may also wonder if the backreaction of the CMB photons themselves is important, since they are as well a species of free-streaming relativistic particles. However, they decouple when the Universe is already matter dominated. This means that Ω_γ is already small and keeps decaying, and there is basically no time for the backreaction effect to build up. In order to check this analytically[3], one can solve eq. (4.29) in the matter dominated era ($w = 0$), noting that $\Omega_X \sim \Omega_B \sim e^{-N}$. The (not so obvious) solution in this case is

$$\delta - \delta(t_{X,*}) = \frac{15}{4}\frac{\Omega_B}{\Omega_X} + C\left[f\cos f - \sin f\right] + D\left[f\sin f + \cos f\right] \;, \qquad (4.31)$$

where I have introduced the shorthand $f \equiv 4\sqrt{2\Omega_X/5}$. As f decays, the solution asymptotes to $\delta = \delta(t_{X,*}) + (15/4)\Omega_B/\Omega_X + D$. Due to the appearance of the constant of integration D in the asymptotic result, it is evident that the isotropization of the total energy momentum tensor of all relativistic components is not achieved. Yet, the Universe isotropizes eventually because the primary source of anisotropy itself decays. This, however, happens without the backreaction effect playing a major role.

To summarize, I have established that differential expansion can lead to backreaction effects in the cosmic fluid. Under certain conditions, the buildup of anisotropic stress in different components can even dynamically restore the isotropy of the total stress-energy tensor, such that the Universe enters a phase of quasi-Friedmann expansion. In order to have the mechanism of dynamical isotropization operate properly, two important conditions have to be met. Firstly, the component of the cosmic fluid which generates the backreaction effect has to scale in the same way as the primary source of anisotropy. Loosely speaking this means that both should obey a similar equation of state. Secondly, the component in question must contribute an appreciable fraction to the total energy density, and should do so for at least several decades of redshift. This is necessary because the dynamical timescale is typically set by the Hubble time. All these conditions are met by cosmic neutrinos in case the primary source of anisotropy is a homogeneous magnetic field. It is also possible that a background of gravitational waves could play this role, or some other relativistic particle species outside the spectrum of the standard model, see [3] for a discussion.

In [99], the effect of free-streaming massive neutrinos on the full spectrum of cosmological perturbations, including magnetic fields, has been studied. The above discussion can be understood as referring to the infinite-wavelength limit of this effect. However, the way

---

[3]In addition, I have done a numerical check where I have computed the plots of fig. 4.1 with and without taking the small effect of free-streaming CMB photons into account and found no significant difference.
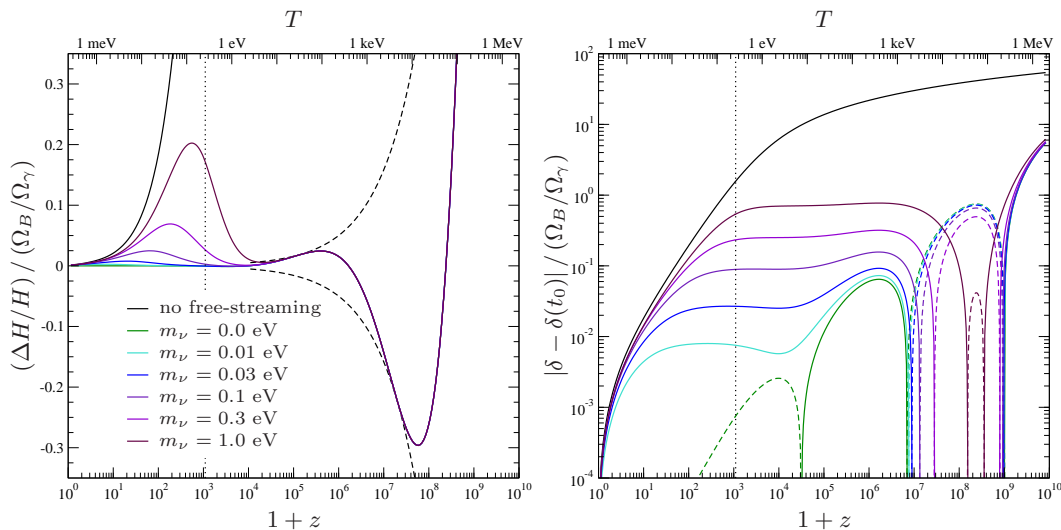
Figure 4.1: Evolution of the differential expansion rate $\Delta H/H$ (left panel) and its integral δ, which characterizes the relative anisotropic redshift (right panel). The quantities are normalized to Ω_B/Ω_γ, which to leading order is a time-independent small quantity that characterizes the amplitude of the homogeneous magnetic field, *i.e.* the primary source of anisotropy. The black line shows the evolution without taking into account the backreaction effect of free-streaming cosmic neutrinos. As evident from the colored lines, the backreaction is significant also for large neutrino mass scales $m_\nu \gtrsim 1$ eV. As long as the neutrinos are ultra-relativistic, the buildup of anisotropic stress in their stress-energy tensor leads to dynamical isotropization. In particular, this leads to an oscillatory decay of differential expansion – the predicted damping envelope in the radiation dominated era is indicated with dashed lines in the left panel. The effect ends when neutrinos become non-relativistic, and the magnetic field then gives rise to some amount of subsequent differential expansion. This can be seen by the appearance of the peak in $\Delta H/H$ which occurs when the temperature drops below m_ν. However, since the Universe becomes matter dominated, there is only little time available in which the magnetic field can source differential expansion. The vertical dotted line (both panels) indicates the time of photon last scattering. The amplitude of the temperature quadrupole in the CMB caused by anisotropic redshift can therefore be read off from the intercept of the curves in the right panel. The backreaction effect of free-streaming neutrinos reduces the quadrupole, the suppression being larger for smaller neutrino mass scales.

it is presented here is much simpler and easier accessible, owing to the reduced complexity of the setup.

Let me finally return to the first example, where anisotropic curvature was the primary source of differential expansion. Is it possible to have a mechanism of dynamical isotropization here as well? The conditions for a positive answer are listed above. One needs a component which scales like curvature and therefore should have an effective barotropic index of $w \simeq -1/3$. Furthermore, one needs to have a period where its contribution to the energy density is relatively large. It is easy to see that this condition can hardly be met in the post-Big-Bang era, because such a component would quickly start to dominate over radiation and even matter, so that the standard cosmological evolution would be spoiled. However, it is not inconceivable that such a period could have existed before the hot Big Bang. For instance, an early phase transition to a cosmic string dominated era followed by a second stage of inflation which ends with reheating and paves the way for standard cosmology could amount to a viable (yet speculative) scenario. It has been argued that a frustrated network of cosmic strings has an effective equation of state parameter $w = -1/3$, see *e.g.* [100]. Note that here it is not required to have a density of strings which contributes significantly to the total energy density any time after the Big

Bang, because I have assumed that the isotropization takes place already before radiation domination. However, in order to see if this idea can work one needs to calculate the effect of differential expansion on the stress of a cosmic string network. Some investigations in this direction may be a worthwile exercise, but shall not be part of this work.

Outlook

The ΛCDM concordance model provides us with a fairly simple description of our Universe which is consistent with most observed phenomena, at least within the experimental uncertainties. However, it leaves open a number of pressing questions, like the one about the true nature of the force driving accelerated expansion or the one about the progenitor of the inflationary phase in the early Universe. Seeking for answers to these fundamental questions, cosmologists will continue their efforts in going beyond the standard model from both the observational and theoretical side. In this work I tried to contribute to these efforts by hopefully giving some new insights on anisotropic models of the Universe, how they may arise from a quantum process and what their observational prospects may be.

On the observational side, it will be interesting to see whether the next generation of precision measurements and improved methods of data analysis will corroborate the indications on a breaking of statistical isotropy of the Universe mentioned in section 1.3. Notable in this context are two European space experiments. The PLANCK space probe is the next generation CMB experiment and is already taking data. It will measure the all-sky pattern of the CMB temperature and polarization to unprecedented precision. The spacecraft EUCLID, which is currently still in its definition phase with final decision on implementation expected[1] in mid-2011, will fly on a dedicated mission to observe and reconstruct the full $3D$ distribution of matter in a huge cosmological volume. A primary aim of this mission is to obtain a better understanding of the dynamics which govern the present accelerated expansion of our Universe. Since the survey will cover over half of the celestial sphere, one may also hope to obtain new independent tests of statistical isotropy. These and other advances in technology will sharpen the view on this issue considerably in the coming years and will pave the way from vague indications to solid evidence.

The observational efforts have to be accompanied by further developments in the understanding of the theoretical models. To this end, a lot of work remains to be done on the field of anisotropic cosmology. For instance, the assessment of primordial signatures presented here is still very preliminary. In particular, cosmological perturbations were not treated in a fully realistic and self-consistent way. It should be noted that a proper treatment will have to overcome several additional complications compared to the case of an isotropic background. As pointed out by the authors of [74, 75], not only are the equations more complicated, the anisotropy of the background can also couple the scalar, vector and tensor modes of perturbations such that they can no longer be treated as independent. In individual cases, like the Bianchi I model explored in [73, 74, 75], this problem has been solved. However, a more general assessment would certainly be useful, though technically challenging. As the example of the mechanism of dynamical isotropization discussed in section 4.3 shows, a consistent treatment should also take into account interactions and backreaction effects as they may well be important and have interesting consequences. After all, any new pieces of evidence for a breaking of statistical isotropy in our Universe can only be properly interpreted if the phenomenology at least of weakly anisotropic cosmological solutions is well understood also from the theoretical side.

---

[1]Note added in proof: by October 2011, ESA's Science Programme Committee has approved the implementation of EUCLID, with a launch planned for 2019.

However, despite these promising prospects one should not forget that the large scale structure of our Universe only carries a finite amount of information and that all this information will essentially be exhausted at some point in the forseeable future. In the end, data could remain inconclusive concerning deviations from the concordance model and the inflationary progenitor would not reveal itself. However, this would not mean that early Universe cosmology is at an end, but that certain questions one still hopes to answer one day are in fact inaccessible to empirical evidence. On the other hand, as I have tried to establish in this work, a positive detection of significant deviations from the statistical symmetries of the cosmological standard model would bear the opportunity to learn something fundamentally new about the origin of our Universe. Based on all the evidence available today and taking into account all the anomalies which are still not fully understood, this yet remains a credible and exciting possibility. Exciting, I say, because it comes with the promise to reveal some new answers to one of the oldest questions of humanity: *how did it all begin?*

Appendix A

Shapeshifting: A Simple Model

In this appendix, I want to consider a particularly simple setup which may be able to support a genuine *shapeshifting* process. I start out with a D-dimensional theory with Einstein gravity and *two* generalized Maxwell fields, called $\mathbf{F}$ and $\bar{\mathbf{F}}$. For definiteness, let $\mathbf{F}$ be a two-form field and $\bar{\mathbf{F}}$ be a d-form field where $d \equiv D-4 > 1$. With the mechanism of flux compactification as in [66], two different types of lower-dimensional compactification vacua can be constructed – one is $(\mathrm{A})\mathrm{dS}_{D-2} \times \mathrm{S}_2$ and the other is $(\mathrm{A})\mathrm{dS}_4 \times \mathrm{S}_d$. I have chosen d such that the latter can be a suitable vacuum for our effectively four-dimensional Universe if the effective cosmological constant resulting from the compactification lies within the anthropic range.

The shapeshifting transition I want to put forward here is the transition between these two vacua such that, starting from $\mathrm{dS}_{D-2} \times \mathrm{S}_2$, d of the macroscopic directions spontaneously compactify on an S_d, while the compact S_2 simultaneously opens up and becomes macroscopic. Although the $\mathrm{dS}_4 \times \mathrm{S}_d$ vacuum configuration is reached asymptotically, the natural foliation of the new vacuum will be of the Kantowski-Sachs type, owing to the de-compactification of the S_2 involved in the process. Schematically, this particular shapeshifting process has following structure:

$$\mathrm{dS}_{d+2} \times \mathrm{S}_2$$
$$\downarrow \;\; \times$$
$$\mathrm{dS}_4 \times \mathrm{S}_d$$

A causal diagram of the classical spacetime resulting from this type of process is shown in fig. A.1.

The D-dimensional Einstein-Maxwell theory with two generalized Maxwell fields has following action, *cf.* eq. (3.1),

$$\mathcal{S}^{(D)} = \frac{1}{16\pi} \int d^D x \sqrt{-g} \left[\mathcal{R} - 2\Lambda - \mathbf{F}^2 - \bar{\mathbf{F}}^2 \right] \;, \tag{A.1}$$

where Λ and $\mathcal{R}$ are, as usual, the cosmological constant and the (Ricci) curvature scalar in D dimensions, respectively. In order to obtain the desired compactification solutions, I make following *ansatz* for the line element,

$$ds^2 = g_{AB}dx^A dx^B = \gamma_{AB}dy^A dy^B + R^2(y^A)d\Omega_2^2 + \bar{R}^2(y^A)d\bar{\Omega}_d^2 \;. \tag{A.2}$$

In this expression, γ_{AB} is a $1+1$-dimensional metric field, *i.e.* the indices A, B take values 0 and 1 only. With this *ansatz*, all the metric components of the full D-dimensional spacetime only depend on the coordinates y^A. As shown in section 3.1, a compatible *ansatz* for the generalized Maxwell fields is given by

$$\mathbf{F} = Q \sin\theta_1 d\theta_1 \wedge d\theta_2 \;, \tag{A.3}$$
$$\bar{\mathbf{F}} = \bar{Q} \sin^{d-1}\bar{\theta}_1 \ldots \sin\bar{\theta}_{d-1} d\bar{\theta}_1 \wedge \ldots d\bar{\theta}_d \;. \tag{A.4}$$
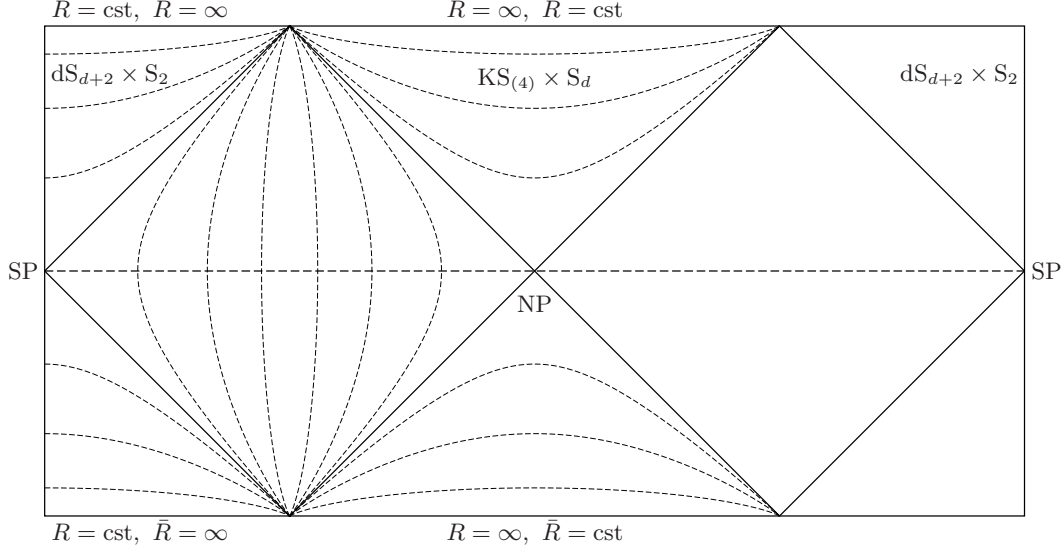
Figure A.1: Penrose-Carter diagram of the classical spacetime corresponding to a hypothetical shapeshifting transition between an effectively $d+2$-dimensional and an effectively 4-dimensional compactification vacuum (left and right edge can be identified). In the former configuration, the two extra dimensions are compactified on a two-sphere with radius R. This S_2 decompactifies in the process, while d macroscopic dimensions are simultaneously compactified on an S_d with radius $\bar{R}$. The dashed curves show lines of constant R and $\bar{R}$. Owing to the decompactification of the S_2 involved in the process, the resulting four-dimensional spacetime (labeled as $KS_{(4)} \times S_d$) is naturally of the Kantowski-Sachs type. The horizontal dashed line indicates the turning-point geometry, which can be obtained from a maximal section of the relevant instanton. It runs through the *south pole* (SP) and *north pole* (NP) of the Euclidean geometry and smoothly interpolates between the two vacuum configurations.

After integrating out the compact dimensions, one arrives at following effective action:

$$\mathcal{S}_{\text{eff}} = \frac{V_d}{4} \int d^2 y \sqrt{-\gamma} R^2 \bar{R}^d \left[\mathcal{R}_2 + \frac{2}{R^2} \left(1 + \gamma^{AB} \partial_A R \partial_B R \right) \right.$$
$$\left. + \frac{d(d-1)}{\bar{R}^2} \left(1 + \gamma^{AB} \partial_A \bar{R} \partial_B \bar{R} \right) + \frac{4d}{R\bar{R}} \gamma^{AB} \partial_A \bar{R} \partial_B R - 2\Lambda - \frac{2Q^2}{R^4} - \frac{d!\bar{Q}^2}{\bar{R}^{2d}} \right] \quad \text{(A.5)}$$

Here, $\mathcal{R}_2$ is the (Ricci) curvature scalar of the $1+1$-dimensional metric γ_{AB} alone. From the variation of this action, one can obtain the equation of motion for R, the radius of the S_2,

$$\frac{1}{2}\mathcal{R}_2 + \frac{d(d-1)}{2\bar{R}^2} - \Lambda - \frac{d!\bar{Q}^2}{2\bar{R}^{2d}} + \frac{Q^2}{R^4} - \frac{d}{R\bar{R}} \gamma^{AB} \partial_A R \partial_B \bar{R}$$
$$- \frac{1}{R}\Box R - \frac{d}{R}\Box \bar{R} - \frac{d(d-1)}{2\bar{R}^2} \gamma^{AB} \partial_A \bar{R} \partial_B \bar{R} = 0 \ , \quad \text{(A.6)}$$

where I have introduced the covariant box-operator associated with the metric γ_{AB}. Similarly, the equation of motion for $\bar{R}$ (the radius of the S_d) reads

$$\frac{1}{2}\mathcal{R}_2 + \frac{1}{R^2} + \frac{(d-1)(d-2)}{2\bar{R}^2} - \Lambda + \frac{d!\bar{Q}^2}{2\bar{R}^{2d}} - \frac{Q^2}{R^4} - \frac{2(d-1)}{R\bar{R}} \gamma^{AB} \partial_A R \partial_B \bar{R}$$
$$- \frac{2}{R}\Box R - \frac{d-1}{\bar{R}}\Box \bar{R} - \frac{(d-1)(d-2)}{2\bar{R}^2} \gamma^{AB} \partial_A \bar{R} \partial_B \bar{R} - \frac{1}{R^2} \gamma^{AB} \partial_A R \partial_B R = 0 \ . \quad \text{(A.7)}$$

Finally, the variation with respect to γ^{AB} yields

$$
\frac{d}{\bar{R}}\nabla_A\nabla_B\bar{R} + \frac{2}{R}\nabla_A\nabla_B R - \gamma_{AB}\left(\frac{d(d-1)}{2\bar{R}^2}\partial^C\bar{R}\partial_C\bar{R} + \frac{2d}{R\bar{R}}\partial^C R\partial_C\bar{R}\right.
$$
$$
\left. +\frac{1}{R^2}\partial^C R\partial_C R + \frac{d}{\bar{R}}\Box\bar{R} + \frac{2}{R}\Box R - \frac{1}{R^2} - \frac{d(d-1)}{2\bar{R}^2} + \Lambda + \frac{Q^2}{R^4} + \frac{d!\bar{Q}^2}{2\bar{R}^{2d}}\right) = 0 \ . \quad \text{(A.8)}
$$

Here, ∇_A denotes the covariant derivative associated with γ^{AB}.

In order to find the Euclidean solutions (instantons), I now make a formal analytic continuation to imaginary time. The equations above remain formally identical, however, the metric signature of γ^{AB} is now $(++)$. The instantons which describe bubble nucleation are found among the $O(2)$-symmetric solutions. I therefore make the *ansatz*

$$
\begin{aligned}
\gamma_{AB}dy_{\mathrm{E}}^A dy_{\mathrm{E}}^B &= d\chi^2 + \rho^2(\chi)d\varphi^2 \ , \\
R(\chi,\varphi) &= R(\chi) \equiv e^{\phi(\chi)} \ , \qquad \text{(Euclidean)} \\
\bar{R}(\chi,\varphi) &= \bar{R}(\chi) \equiv e^{\bar{\phi}(\chi)} \ .
\end{aligned} \qquad \text{(A.9)}
$$

Up to a constant normalization, the logarithms ϕ and $\bar{\phi}$ are analogous to the scalar field defined in eq. (3.7). With the above definitions, the equations (A.6) – (A.8) read, respectively,

$$
\frac{\partial_\chi^2\rho}{\rho} + d\partial_\chi\phi\partial_\chi\bar{\phi} + \partial_\chi^2\phi + (\partial_\chi\phi)^2 + \frac{\partial_\chi\rho}{\rho}\partial_\chi\phi + \frac{d(d+1)}{2}\left(\partial_\chi\bar{\phi}\right)^2 + d\partial_\chi^2\bar{\phi} + d\frac{\partial_\chi\rho}{\rho}\partial_\chi\bar{\phi}
$$
$$
- \frac{d(d-1)}{2}e^{-2\bar{\phi}} + \Lambda + \frac{d!}{2}\bar{Q}^2 e^{-2d\bar{\phi}} - Q^2 e^{-4\phi} = 0 \ , \quad \text{(A.10)}
$$

$$
\frac{\partial_\chi^2\rho}{\rho} + 3\left(\partial_\chi\phi\right)^2 + \frac{d(d-1)}{2}\left(\partial_\chi\bar{\phi}\right)^2 + 2(d-1)\partial_\chi\phi\partial_\chi\bar{\phi} + (d-1)\partial_\chi^2\bar{\phi} + (d-1)\frac{\partial_\chi\rho}{\rho}\partial_\chi\bar{\phi}
$$
$$
+ 2\partial_\chi^2\phi + 2\frac{\partial_\chi\rho}{\rho}\partial_\chi\phi - e^{-2\phi} - \frac{(d-1)(d-2)}{2}e^{-2\bar{\phi}} + \Lambda - \frac{d!}{2}\bar{Q}^2 e^{-2d\bar{\phi}} + Q^2 e^{-4\phi} = 0 \ ,
$$
$$
\text{(A.11)}
$$

and

$$
\frac{d(d-1)}{2}\left(\partial_\chi\bar{\phi}\right)^2 + 2d\partial_\chi\phi\partial_\chi\bar{\phi} + (\partial_\chi\phi)^2 + d\frac{\partial_\chi\rho}{\rho}\partial_\chi\bar{\phi} + 2\frac{\partial_\chi\rho}{\rho}\partial_\chi\phi
$$
$$
- e^{-2\phi} - \frac{d(d-1)}{2}e^{-2\bar{\phi}} + \Lambda + Q^2 e^{-4\phi} + \frac{d!}{2}\bar{Q}^2 e^{-2d\bar{\phi}} = 0 \ . \quad \text{(A.12)}
$$

This system of coupled equations looks very complicated, however, amazingly one can in fact eliminate the scale factor ρ completely. By combining the equations in the right way, one obtains the relation

$$
\frac{\partial_\chi\rho}{\rho} = \frac{d\left(\partial_\chi\bar{\phi}\right)^2 + 2\left(\partial_\chi\phi\right)^2 + d\partial_\chi^2\bar{\phi} + 2\partial_\chi^2\phi}{d\partial_\chi\bar{\phi} + 2\partial_\chi\phi} \ . \qquad \text{(A.13)}
$$

Taking only the third equation and the difference of the first two equations, one can replace $\partial_\chi\rho/\rho$ everywhere and is left with two coupled second order equations for ϕ and $\bar{\phi}$. These, however, appear too complicated to be solved analytically except for trivial cases. A numerical study, on the other hand, is straightforward.

A strategy to find the numerical solutions corresponding to the various instantons can be sketched as follows. First, one fixes the local value of ϕ and $\bar{\phi}$ at the *south pole* of the

Euclidean geometry. At this initial boundary, regularity requires $\partial_\chi \phi = \partial_\chi \bar{\phi} = 0$. One then numerically solves the coupled system for ϕ and $\bar{\phi}$. In general, for some arbitrary local values ϕ_0, $\bar{\phi}_0$ at the south pole one will find $\phi, \bar{\phi} \to \pm\infty$. More specifically, one can imagine the ϕ_0-$\bar{\phi}_0$-plane to be partitioned into two types of domains – ones where the solutions tend to $+\infty$ and ones where they tend to $-\infty$. The boundaries between these domains can easily be found numerically using recursive bisections on a dense enough grid.

On these boundaries, which are one-dimensional curves in the ϕ_0-$\bar{\phi}_0$-plane, the solutions for ϕ and $\bar{\phi}$ by continuity tend to a constant at some finite $\chi = \chi_{\max}$ where the Euclidean scale factor ρ becomes zero and the geometry closes. However, in general one will have $\partial_\chi \rho \neq -1$ at $\chi_{\max}$, which means that there will be a conical singularity at the *north pole* and the geometry is not regular. But one can again partition the curves into two types of segments – one where $\partial_\chi \rho > -1$ and one where $\partial_\chi \rho < -1$ at $\chi_{\max}$. Using once more the method of recursive bisections, one can identify the points with $\partial_\chi \rho = -1$. These mark the regular instanton solutions.

This, however, is not really the end of the story. The procedure outlined above can only be applied once all the model parameters have been fixed. In this simple setup, these are the four parameters d, Λ, Q and $\bar{Q}$. Note that Q and $\bar{Q}$ measure the strength of the magnetic fluxes and that the existence of certain solutions depends crucially on their values. The interesting range of these parameters for the purpose of constructing a shapeshifting transition is the range where both the $\mathrm{dS}_{D-2} \times \mathrm{S}_2$ and the $\mathrm{dS}_4 \times \mathrm{S}_d$ compactification vacua exist and have a positive effective cosmological constant for the lower-dimensional de Sitter factor. The relevant parameter range can therefore be found by analyzing the effective potentials obtained from the fluxes, see eq. (3.9). It should also be noted that it is by no means guaranteed that all possible types of instantons exist for the entire range of Q, $\bar{Q}$, even if restricted according to the above requirement. The theory may even support different types of instantons depending on the number of extra dimensions d.

Bibliography

[1] D. Simon, J. Adamek, A. Rakić, and J. C. Niemeyer, "Tunneling and propagation of vacuum bubbles on dynamical backgrounds," *JCAP* **0911** (2009) 008.

[2] J. Adamek, D. Campo, and J. C. Niemeyer, "Anisotropic Kantowski-Sachs Universe from Gravitational Tunneling and its Observational Signatures," *Phys. Rev.* **D82** (2010) 086006.

[3] J. Adamek, R. Durrer, E. Fenu, and M. Vonlanthen, "A large scale coherent magnetic field: interactions with free streaming particles and limits from the CMB," *JCAP* **1106** (2011) 017.

[4] E. P. Hubble, "A relation between distance and radial velocity among extra–galactic nebulae," *Proc. Nat. Acad. Sci.* **15** (1929) 168–173.

[5] A. A. Penzias and R. W. Wilson, "A Measurement of Excess Antenna Temperature at 4080 Mc/s," *Astrophys. J.* **142** (1965) 419–421.

[6] **COBE** Collaboration, C. L. Bennett *et al.*, "4-Year COBE DMR Cosmic Microwave Background Observations: Maps and Basic Results," *Astrophys. J.* **464** (1996) L1–L4.

[7] **WMAP** Collaboration, E. Komatsu *et al.*, "Seven-Year Wilkinson Microwave Anisotropy Probe (WMAP) Observations: Cosmological Interpretation," *Astrophys. J. Supp.* **192** (2011) 18.

[8] S. Dodelson, *Modern Cosmology*. Acad. Press, San Diego, 2003.

[9] R. Durrer, *The Cosmic Microwave Background*. Cambridge Univ. Press, Cambridge, 2008.

[10] **HST** Collaboration, W. L. Freedman *et al.*, "Final Results from the Hubble Space Telescope Key Project to Measure the Hubble Constant," *Astrophys. J.* **553** (2001) 47–72.

[11] G. Bertone, D. Hooper, and J. Silk, "Particle dark matter: Evidence, candidates and constraints," *Phys. Rept.* **405** (2005) 279–390.

[12] **Supernova Search Team** Collaboration, A. G. Riess *et al.*, "Observational Evidence from Supernovae for an Accelerating Universe and a Cosmological Constant," *Astron. J.* **116** (1998) 1009–1038.

[13] **Supernova Cosmology Project** Collaboration, S. Perlmutter *et al.*, "Measurements of Omega and Lambda from 42 High-Redshift Supernovae," *Astrophys. J.* **517** (1999) 565–586.

[14] S. Weinberg, "The cosmological constant problem," *Rev. Mod. Phys.* **61** (1989) 1–23.

[15] A. H. Guth, "The Inflationary Universe: A Possible Solution to the Horizon and Flatness Problems," *Phys. Rev.* **D23** (1981) 347–356.

[16] D. S. Goldwirth and T. Piran, "Initial conditions for inflation," *Phys. Rept.* **214** (1992) 223–291.

[17] A. de Oliveira-Costa, M. Tegmark, M. Zaldarriaga, and A. Hamilton, "The significance of the largest scale CMB fluctuations in WMAP," *Phys. Rev.* **D69** (2004) 063516.

[18] K. Land and J. Magueijo, "The axis of evil," *Phys. Rev. Lett.* **95** (2005) 071301.

[19] C. J. Copi, D. Huterer, D. J. Schwarz, and G. D. Starkman, "Large-angle anomalies in the CMB," *Adv. Astron.* **2010** (2010) 847541.

[20] **WMAP** Collaboration, C. L. Bennett *et al.*, "Seven-Year Wilkinson Microwave Anisotropy Probe (WMAP) Observations: Are There Cosmic Microwave Background Anomalies?," *Astrophys. J. Supp.* **192** (2011) 17.

[21] M. Schlosshauer, *Decoherence and the quantum-to-classical transition.* Springer, Berlin, 2007.

[22] B. S. DeWitt, "Quantum Theory of Gravity. 1. The Canonical Theory," *Phys. Rev.* **160** (1967) 1113–1148.

[23] C. Kiefer, *Quantum Gravity.* Oxford Univ. Press, Oxford, 2004.

[24] R. L. Arnowitt, S. Deser, and C. W. Misner, "The Dynamics of General Relativity," in *Gravitation: an introduction to current research*, L. Witten, ed., pp. 227–264. Wiley, New York, 1962.

[25] C. W. Misner, K. S. Thorne, and J. A. Wheeler, *Gravitation.* Freeman, San Francisco, 1973.

[26] J. J. Halliwell, "Introductory Lectures on Quantum Cosmology, 9. No-Boundary vs. Tunneling," in *Quantum Cosmology and Baby Universes*, S. R. Coleman, J. B. Hartle, T. Piran, and S. Weinberg, eds., vol. 7, pp. 204–208. World Scientific, Singapore, 1991.

[27] J. B. Hartle and S. W. Hawking, "Wave Function of the Universe," *Phys. Rev.* **D28** (1983) 2960–2975.

[28] R. P. Feynman, "Space-Time Approach to Non-Relativistic Quantum Mechanics," *Rev. Mod. Phys.* **20** (1948) 367–387.

[29] J. J. Halliwell and J. B. Hartle, "Integration Contours for the No Boundary Wave Function of the Universe," *Phys. Rev.* **D41** (1990) 1815.

[30] J. B. Hartle, S. W. Hawking, and T. Hertog, "The Classical Universes of the No-Boundary Quantum State," *Phys. Rev.* **D77** (2008) 123537.

[31] S. R. Coleman, "The Fate of the False Vacuum. 1. Semiclassical Theory," *Phys. Rev.* **D15** (1977) 2929–2936.

[32] C. G. Callan, Jr. and S. R. Coleman, "The Fate of the False Vacuum. 2. First Quantum Corrections," *Phys. Rev.* **D16** (1977) 1762–1768.

[33] S. R. Coleman and F. De Luccia, "Gravitational Effects on and of Vacuum Decay," *Phys. Rev.* **D21** (1980) 3305.

[34] E. Farhi, A. H. Guth, and J. Guven, "Is it Possible to Create a Universe in the Laboratory by Quantum Tunneling?," *Nucl. Phys.* **B339** (1990) 417–490.

[35] A. Aguirre and M. C. Johnson, "Two tunnels to inflation," *Phys. Rev.* **D73** (2006) 123529.

[36] K. Becker, M. Becker, and J. H. Schwarz, *String theory and M-theory, a modern introduction.* Cambridge Univ. Press, Cambridge, 2007.

[37] M. Abramowitz and I. A. Stegun, *Handbook of mathematical functions with formulas, graphs, and mathematical tables.* Dover, New York, 1972.

[38] E. Keski-Vakkuri and P. Kraus, "Tunneling in a Time-dependent Setting," *Phys. Rev.* **D54** (1996) 7407–7420.

[39] L. F. Abbott, D. Harari, and Q.-H. Park, "Vacuum Decay in Curved Backgrounds," *Class. Quant. Grav.* **4** (1987) L201–L204.

[40] R. Basu, A. H. Guth, and A. Vilenkin, "Quantum creation of topological defects during inflation," *Phys. Rev.* **D44** (1991) 340–351.

[41] S. K. Blau, E. I. Guendelman, and A. H. Guth, "The Dynamics of False Vacuum Bubbles," *Phys. Rev.* **D35** (1987) 1747.

[42] V. A. Berezin, V. A. Kuzmin, and I. I. Tkachev, "Dynamics of Bubbles in General Relativity," *Phys. Rev.* **D36** (1987) 2919.

[43] W. Israel, "Singular hypersurfaces and thin shells in general relativity," *Nuovo Cim.* **B44S10** (1966) 1.

[44] Ø. Grøn and S. Hervik, *Einstein's general theory of relativity with modern applications in cosmology.* Springer, Berlin, 2007.

[45] W. Fischler, D. Morgan, and J. Polchinski, "Quantization of false-vacuum bubbles: A Hamiltonian treatment of gravitational tunneling," *Phys. Rev.* **D42** (1990) 4042–4055.

[46] M. Bucher, A. S. Goldhaber, and N. Turok, "An open universe from inflation," *Phys. Rev.* **D52** (1995) 3314–3337.

[47] S. R. Coleman, "The uses of instantons," *Subnucl. Ser.* **15** (1979) 805.

[48] R. P. Feynman and A. R. Hibbs, *Quantum Mechanics and Path Integrals*, ch. 3. McGraw-Hill, New York, 1965.

[49] S. R. Coleman, V. Glaser, and A. Martin, "Action Minima Among Solutions to a Class of Euclidean Scalar Field Equations," *Commun. Math. Phys.* **58** (1978) 211.

[50] S. W. Hawking and I. G. Moss, "Supercooled Phase Transitions in the Very Early Universe," *Phys. Lett.* **B110** (1982) 35.

[51] G. W. Gibbons and S. W. Hawking, "Cosmological Event Horizons, Thermodynamics, and Particle Creation," *Phys. Rev.* **D15** (1977) 2738–2751.

[52] U. Gen and M. Sasaki, "False vacuum decay with gravity in non-thin-wall limit," *Phys. Rev.* **D61** (2000) 103508.

[53] A. H. Guth and E. J. Weinberg, "Could the Universe Have Recovered from a Slow First Order Phase Transition?," *Nucl. Phys.* **B212** (1983) 321.

[54] A. Vilenkin, "The Interpretation of the Wavefunction of the Universe," *Phys. Rev.* **D39** (1989) 1116.

[55] L. Susskind, "The anthropic landscape of string theory," `arXiv:hep-th/0302219`.

[56] J. D. Brown and C. Teitelboim, "Dynamical Neutralization of the Cosmological Constant," *Phys. Lett.* **B195** (1987) 177–182.

[57] R. Bousso and J. Polchinski, "Quantization of four-form fluxes and dynamical neutralization of the cosmological constant," *JHEP* **06** (2000) 006.

[58] S. Weinberg, "Anthropic Bound on the Cosmological Constant," *Phys. Rev. Lett.* **59** (1987) 2607.

[59] S. Weinberg, "Living in the Multiverse," in *Universe or Multiverse?*, B. Carr, ed., pp. 29–42. Cambridge Univ. Press, Cambridge, 2007.

[60] A. D. Linde, "Sinks in the Landscape, Boltzmann Brains, and the Cosmological Constant Problem," *JCAP* **0701** (2007) 022.

[61] A. D. Linde, "Eternally Existing Selfreproducing Chaotic Inflationary Universe," *Phys. Lett.* **B175** (1986) 395–400.

[62] A. H. Guth, "Eternal inflation and its implications," *J. Phys.* **A40** (2007) 6811–6826.

[63] A. De Simone and M. P. Salem, "The distribution of Ω_k from the scale-factor cutoff measure," *Phys. Rev.* **D81** (2010) 083527.

[64] P. G. O. Freund and M. A. Rubin, "Dynamics of Dimensional Reduction," *Phys. Lett.* **B97** (1980) 233–235.

[65] M. Graña, "Flux compactifications in string theory: A comprehensive review," *Phys. Rept.* **423** (2006) 91–158.

[66] S. M. Carroll, M. C. Johnson, and L. Randall, "Dynamical compactification from de Sitter space," *JHEP* **11** (2009) 094.

[67] J. J. Blanco-Pillado, D. Schwartz-Perlov, and A. Vilenkin, "Quantum Tunneling in Flux Compactifications," *JCAP* **0912** (2009) 006.

[68] J. J. Blanco-Pillado, D. Schwartz-Perlov, and A. Vilenkin, "Transdimensional Tunneling in the Multiverse," *JCAP* **1005** (2010) 005.

[69] S. B. Giddings, "The fate of four dimensions," *Phys. Rev.* **D68** (2003) 026006.

[70] S. B. Giddings and R. C. Myers, "Spontaneous decompactification," *Phys. Rev.* **D70** (2004) 046005.

[71] J. J. Blanco-Pillado and M. P. Salem, "Observable effects of anisotropic bubble nucleation," *JCAP* **1007** (2010) 007.

[72] J. M. Arnold, B. Fornal, and M. B. Wise, "Standard Model Vacua for Two-dimensional Compactifications," *JHEP* **12** (2010) 083.

[73] A. E. Gümrükçüoğlu, C. R. Contaldi, and M. Peloso, "Inflationary perturbations in anisotropic backgrounds and their imprint on the CMB," *JCAP* **0711** (2007) 005.

[74] T. S. Pereira, C. Pitrou, and J.-P. Uzan, "Theory of cosmological perturbations in an anisotropic universe," *JCAP* **0709** (2007) 006.

[75] C. Pitrou, T. S. Pereira, and J.-P. Uzan, "Predictions from an anisotropic inflationary era," *JCAP* **0804** (2008) 004.

[76] R. B. Mann and S. F. Ross, "Cosmological production of charged black hole pairs," *Phys. Rev.* **D52** (1995) 2254–2265.

[77] R. Bousso and S. W. Hawking, "Pair creation of black holes during inflation," *Phys. Rev.* **D54** (1996) 6312–6322.

[78] R. Bousso and S. W. Hawking, "Primordial black holes: Pair creation, Lorentzian condition, and evaporation," *Int. J. Theor. Phys.* **38** (1999) 1227–1252.

[79] R. Kantowski and R. K. Sachs, "Some spatially homogeneous anisotropic relativistic cosmological models," *J. Math. Phys.* **7** (1966) 443.

[80] J. García-Bellido, J. Garriga, and X. Montes, "Quasi-open inflation," *Phys. Rev.* **D57** (1998) 4669–4685.

[81] J. Garriga, X. Montes, M. Sasaki, and T. Tanaka, "Spectrum of cosmological perturbations in the one-bubble open universe," *Nucl. Phys.* **B551** (1999) 317–373.

[82] J. García-Bellido, A. R. Liddle, D. H. Lyth, and D. Wands, "The Open Universe Grishchuk-Zel'dovich Effect," *Phys. Rev.* **D52** (1995) 6750–6759.

[83] T. Tanaka and M. Sasaki, "The spectrum of gravitational wave perturbations in the one-bubble open inflationary universe," *Prog. Theor. Phys.* **97** (1997) 243–262.

[84] M. Sasaki, T. Tanaka, and K. Yamamoto, "Euclidean vacuum mode functions for a scalar field on open de Sitter space," *Phys. Rev.* **D51** (1995) 2979–2995.

[85] P. W. Graham, R. Harnik, and S. Rajendran, "Observing the Dimensionality of Our Parent Vacuum," *Phys. Rev.* **D82** (2010) 063524.

[86] U. Seljak and M. Zaldarriaga, "A Line of Sight Approach to Cosmic Microwave Background Anisotropies," *Astrophys. J.* **469** (1996) 437–444.

[87] A. Lewis, A. Challinor, and A. Lasenby, "Efficient Computation of CMB anisotropies in closed FRW models," *Astrophys. J.* **538** (2000) 473–476.

[88] A. Hajian and T. Souradeep, "Measuring the Statistical Isotropy of the Cosmic Microwave Background Anisotropy," *Astrophys. J.* **597** (2003) L5–L8.

[89] C. J. Copi, D. Huterer, and G. D. Starkman, "Multipole Vectors – a new representation of the CMB sky and evidence for statistical anisotropy or non-Gaussianity at $2 \le l \le 8$," *Phys. Rev.* **D70** (2004) 043515.

[90] A. Aguirre, M. C. Johnson, and A. Shomer, "Towards observable signatures of other bubble universes," *Phys. Rev.* **D76** (2007) 063509.

[91] A. Aguirre, M. C. Johnson, and M. Tysanner, "Surviving the crash: assessing the aftermath of cosmic bubble collisions," *Phys. Rev.* **D79** (2009) 123514.

[92] S. M. Feeney, M. C. Johnson, D. J. Mortlock, and H. V. Peiris, "First Observational Tests of Eternal Inflation," *Phys. Rev. Lett.* **107** (2011) 071301.

[93] M. P. Salem, "A Signature of anisotropic bubble collisions," *Phys. Rev.* **D82** (2010) 063530.

[94] P. Schneider, J. Ehlers, and E. E. Falco, *Gravitational lenses*, ch. 3.5. Springer, Berlin, 1992.

[95] T. Clarke, P. Kronberg, and H. Böhringer, "A New Radio - X-ray Probe of Galaxy
     Cluster Magnetic Fields," *Astrophys. J.* **547** (2001) L111–L114.

[96] J. D. Barrow, P. G. Ferreira, and J. Silk, "Constraints on a Primordial Magnetic
     Field," *Phys. Rev. Lett.* **78** (1997) 3610–3613.

[97] E. S. Scannapieco and P. G. Ferreira, "Polarization-Temperature Correlation from
     Primordial Magnetic Field," *Phys. Rev.* **D56** (1997) 7493–7497.

[98] **WMAP** Collaboration, E. Komatsu *et al.*, "Five-Year Wilkinson Microwave
     Anisotropy Probe (WMAP) Observations: Cosmological Interpretation,"
     Astrophys. J. Suppl. **180** (2009) 330–376.

[99] J. R. Shaw and A. Lewis, "Massive Neutrinos and Magnetic Fields in the Early
     Universe," *Phys. Rev.* **D81** (2010) 043517.

[100] D. Spergel and U.-L. Pen, "Cosmology in a string-dominated universe," *Astrophys.
      J.* **491** (1997) L67–L71.

Lebenslauf – Curriculum Vitae

Angaben zur Person

Vollständiger Name:	Julian Adamek
Geboren:	20. Oktober 1981 in Würzburg
Staatsangehörigkeit:	Deutsch

Hochschulausbildung

seit 05/2008 — Doktorand an der Julius-Maximilians-Universität Würzburg
Mitglied des Graduiertenkollegs GRK1147
"Theoretische Astrophysik und Teilchenphysik"

Themenfelder der wissenschaftlichen Tätigkeit:

- Quantenkosmologie / Physik des frühen Universums
- Anisotrope kosmologische Lösungen der allgemeinen Relativitätstheorie
- Phänomenologie der kosmischen Hintergrundstrahlung

04/2004-04/2008 — Diplom in Physik an der Julius-Maximilians-Universität Würzburg
Titel der Diplomarbeit: "Inflationary Perturbation Spectra from Lorentz Violating Dissipative Models"

04/2002-04/2004 — Vordiplom in Informatik an der Julius-Maximilians-Universität Würzburg

Schulausbildung

09/1993-06/2001 — Abitur am Röntgen-Gymnasium Würzburg

04/1990-07/1993 — International School of Zanzibar

01/1990-03/1990 — Grundschule in Berlin-Kladow

09/1988-12/1989 — Grundschule in Reichenberg

Forschungsaufenthalte

04/2008 — Université Paris-Sud 11, Orsay, Frankreich
Gastgeber: Prof. Dr. Renaud Parentani

10-12/2010 — Université de Genève, Genf, Schweiz
Gastgeber: Prof. Dr. Ruth Durrer und Prof. Dr. Claudia de Rham

04/2011 — Université de Genève, Genf, Schweiz
Gastgeber: Prof. Dr. Claudia de Rham

Konferenzen und Workshops

10/2010	*2nd Bethe Center Workshop: Cosmology meets Particle Physics*, PBH, Bad Honnef
05/2010	*5. Kosmologietag*, IBZ Bielefeld, Bielefeld
03/2010	*DPG Frühjahrstagung*, Universität Bonn, Bonn
06/2009	*7th PI Summer School: Exploring the Cosmological Frontiers*, Perimeter Institute for Theoretical Physics, Waterloo, ON, Kanada
05/2009	*4. Kosmologietag*, IBZ Bielefeld, Bielefeld
03/2009	*DPG Frühjahrstagung*, LMU, München
09/2008	*CMB mini-workshop des Graduiertenkollegs 1147*, ITA Universität Heidelberg, Heidelberg
09/2008	*DPG-School on Foundations of Quantum Physics*, PBH, Bad Honnef
08/2008	*NORDITA Summer School on de Sitter Cosmology*, Nordic Institute for Theoretical Physics, Stockholm, Schweden
05/2008	*3. Kosmologietag*, IBZ Bielefeld, Bielefeld
09/2007	*Initial Conditions in Cosmology*, Universität Würzburg, Würzburg

Publikationen

- J. Adamek, R. Durrer, E. Fenu & M. Vonlanthen, *A large scale coherent magnetic field: interactions with free streaming particles and limits from the CMB*, J. Cosmol. Astropart. Phys. 06 (2011) 017

- J. Adamek, D. Campo & J.C. Niemeyer, *Anisotropic Kantowski-Sachs universe from gravitational tunneling and its observational signatures*, Phys. Rev. D 82, 086006 (2010)

- D. Simon, J. Adamek, A. Rakić & J.C. Niemeyer, *Tunneling and propagation of vacuum bubbles on dynamical backgrounds*, J. Cosmol. Astropart. Phys. 11 (2009) 008

- J. Adamek, D. Campo, J.C. Niemeyer & R. Parentani, *Inflationary spectra from Lorentz violating dissipative models*, Phys. Rev. D 78, 103507 (2008)

- L. Iapichino, J. Adamek, W. Schmidt & J.C. Niemeyer, *Hydrodynamical adaptive mesh refinement simulations of turbulent flows – I. Substructure in a wind*, Mon. Not. R. Astron. Soc. 388, 1079-1088 (2008)

- J. Adamek, M. Keller, A. Senftleben & H. Hinrichsen, *Epidemic spreading with long-range infections and incubation times*, J. Stat. Mech. P09002 (2005)